

**FRET Reveals Substantial Reorientation of the Cytoplasmic Interface
of the Skeletal Muscle DHPR in the Presence of RyR1**

**Von der Naturwissenschaftlichen Fakultät
der Gottfried Wilhelm Leibniz Universität Hannover
zur Erlangung des Grades**

Doktor der Naturwissenschaften

Dr. rer. nat.

genehmigte Dissertation

von

M.Sc. Alexander Polster

geboren am 20.12.1978 in Georgsmarienhütte

2011

Referent: Prof. Dr. Gerolf Gros

Korreferent: Prof. Dr. Symeon Papadopoulos

Tag der Promotion: 26.01.2011

“Whether I shall turn out to be the hero of my own life? I do not know.”

Zusammenfassung

Im Skelettmuskel führt die kontrollierte intrazelluläre Freisetzung von Kalziumionen aus dem sarkoplasmatischen Retikulum (sR) zur Kontraktion. Die Einleitung dieses Prozess wird über das Membranpotential gesteuert (elektromechanische Kopplung, EMK). Ein spezialisierter Kalziumkanal der transversal-tubulären Membran des Skelettmuskels, Dihydropyridinrezeptor (DHPR), hat hierbei eine Schlüsselstellung als Spannungssensor. Er gibt die während der Membrandepolarisation erfahrene Konformationsänderung seiner α_{1S} Untereinheit weiter an einen weiteren Kalziumkanal, den in der Membran des sR verankerten Ryanodin Rezeptor Typ 1 (RyR1). Daraufhin öffnet sich dieser und entlässt Kalziumionen in das Sarkoplasma. Voraussetzung für diese spezielle Art der DHPR-RyR1 Kommunikation ist eine hoch geordnete Positionierung von DHP-Rezeptoren in Form von „Tetraden“ an den elektronenmikroskopisch nachweisbaren Annäherungen von t-tubulärer und sR Membran ("junctions"). Die am Zusammenspiel von DHPR und RyR1 während der EMK beteiligten Strukturen sind weitgehend unbekannt, doch aufgrund ihrer topographischen Lage involviert sein könnten die zytoplasmatischen Domänen der DHPR-Hauptuntereinheit α_{1S} : Die intrazellulären Verbindungsschleifen (I-II, II-III, III-IV), sowie der N- und C-terminus der Untereinheit. Zur Identifizierung molekularer α_{1S} Bereiche, welche bei der Kommunikation mit dem RyR1 Änderungen ihrer räumlichen Anordnung erfahren, wurden Messungen von Fluoreszenz Resonanz Energietransfer (FRET) an fluoreszenzmarkierten und innerhalb lebender Muskelzellen in Kultur exprimierten α_{1S} -Untereinheiten durchgeführt. Dabei wurden verschiedene Kombinationen von an jeweils zwei unterschiedlichen zytoplasmatischen Domänen markierter α_{1S} vermessen. Hierbei diente CyPet als FRET-Donor und YPet als FRET-Akzeptor. Die Untersuchungen wurden an zwei Zellmodellen durchgeführt, nach Expression in sog. „dyspedic“ Myotuben (RyR1-knock-out) und in sog. „dysgenic“ Myotuben (keine endogene α_{1S}). Zunahme oder Abnahme von FRET Signalen zeigten, ob sich markierte α_{1S} Schleifen bei Anwesenheit von - und bei Interaktion mit - RyR1 annähern oder entfernen. Für alle Markierungskombinationen wurde, unabhängig davon ob RyR1 anwesend war oder nicht, FRET nachgewiesen. Dieser Befund zeigt, dass die markierten Domänen unter beiden Bedingungen in Abständen < 10 nm angeordnet sind.

Bis auf eine Ausnahme - N-/C-terminal doppelt markierte α_{1S} – führte die Anwesenheit des RyR1 zu einer signifikanten Änderung des FRET-Signals, was auf eine RyR1-induzierte Neuordnung der gesamten intrazellulären α_{1S} -Schnittstelle schließen lässt. Basierend auf diesen Daten wird ein Modell vorgeschlagen, das zum ersten Mal die durch die Anwesenheit des RyR1 generierte, mögliche molekulare Ausgangslage darlegt, an die die dynamischen Vorgänge bei der EMK anknüpfen. Zu den weiteren wichtigen Befunden dieser Arbeit gehört, dass die Markierung an der relativ kurzen III-IV Schleife mit der Zielsteuerung des Kanals interferiert, so dass diese Schleife eine wichtige Rolle bei diesem Prozess spielen könnte. Weiterhin wurde erstmals gezeigt, dass eine distale Verkürzung des α_{1S} C-terminus um 237 Aminosäurereste keinen Einfluss auf die Zielsteuerungsfunktion oder die Funktionalität des DHPR als Kalziumkanal hat.

Schlüsselwörter: Dihydropyridinrezeptor, elektromechanische Kopplung, Fluoreszenz Resonanz Energietransfer

Abstract

In skeletal muscle, the dihydropyridine receptor (DHPR) in the t-tubular membrane serves as a Ca^{2+} channel and as the voltage sensor for excitation-contraction (EC) coupling, triggering Ca^{2+} release via a physical / conformational coupling to the type 1 ryanodine receptor (RyR1) in the sarcoplasmic reticulum (SR) membrane. The particulars of the structural and functional links between these two proteins are widely unknown. The putative intracellular portions of the DHPR α_{1S} subunit, namely the N-terminus, the C-terminus, and the loops connecting the four intra-membrane domains (I-IV), play important roles in the communication with the RyR1. Examples are the β -subunit recruiting function of the I-II loop, the bi-directional signalling function of the II-III loop with the RyR1 during EC-coupling, the influence of the III-IV loop on RyR1 mediated Ca^{2+} delivery, and the α_{1S} carboxyl terminus. These channel parts are believed to either directly or indirectly interact with the RyR1, and the close spatial proximity between the two channels at t-tubule/SR 'junctions' constitutes the structural prerequisite for this linkage. The central goal of the present work was to provide for the first time a structural insight into the arrangement of the crucial molecular components of the DHPR-RyR1 interaction, by using the extremely sensitive method of fluorescence resonance energy transfer (FRET) measurements, conducted within the intact cellular environment of myotubes. For this purpose, a plethora of mammalian expression vectors were engineered, encoding fluorescently double-labelled α_{1S} constructs where a defined cytoplasmic α_{1S} domain was tagged with the FRET donor CyPet and one other with the FRET acceptor YPet. Upon expression in myotubes, the degree of FRET was determined for every combination of labelled cytoplasmic α_{1S} domains using the non-bleaching, sensitized emission variant of the FRET technique. Confocal fluorescence microscopy was applied to check for correct targeting and for function of the constructs upon expression in dyspedic (RyR1 null) and dysgenic (α_{1S} null) myotubes. All doubly tagged α_{1S} constructs, except for those which were tagged within the III-IV loop, were able to target to the junctions and to restore EC coupling in dysgenic myotubes. An astonishing observation was that a massive truncation of the α_{1S} C-terminus at residue E¹⁶³⁶, ablating regions previously implicated in targeting and function of the channel, does not interfere with

either process. Significant FRET occurred between the intracellular loops of the DHPR α_{1S} in absence and in presence of the RyR1, indicating that these domains under both conditions are arranged in distances < 10 nm. The presence of RyR1 altered significantly the intramolecular energy transfer signal for every double tagged α_{1S} construct with the exception of the N-/C-terminally double-tagged α_{1S} . Thus, this study reveals that virtually the complete cytoplasmic α_{1S} architecture is significantly rearranged by the presence of the RyR1. Thus, it is very likely that multiple contacts between these two channels constitute the link which underlies the unique mode of EC coupling in skeletal muscle. On the basis of the gathered data a model is defined for the first time, describing how the interaction with the RyR1 might change the molecular architecture of the cytoplasmic DHPR interface. This model might serve as basis for further refinements of the mode of skeletal muscle-type EC coupling, given the ongoing improvements in resolution of ultrastructural and imaging techniques.

Keywords: Dihydropyridine receptor, excitation-contraction coupling, fluorescence resonance energy transfer

Table of contents

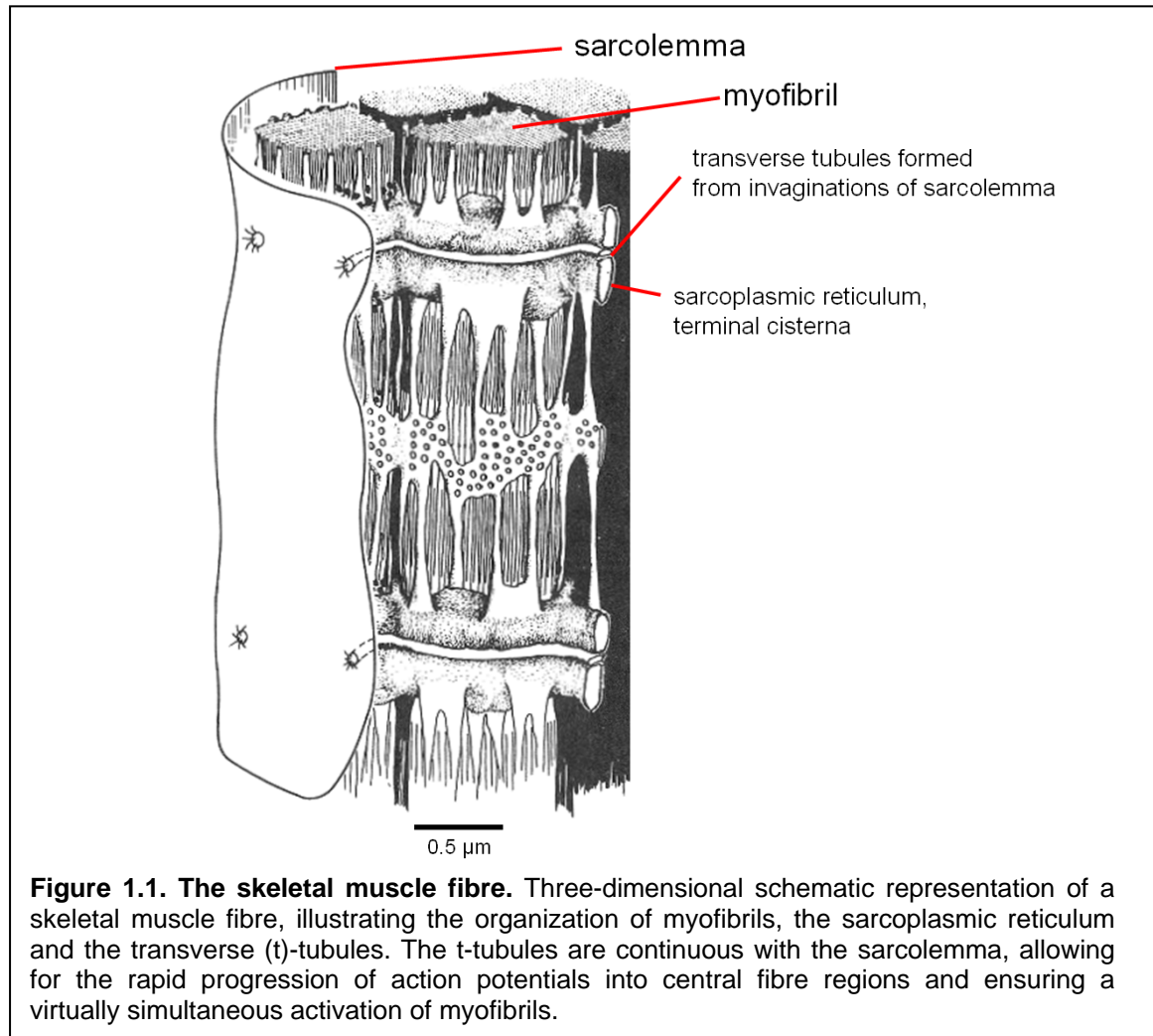
	Page
1. INTRODUCTION	1
1.1 Skeletal muscle: basic structural features and principle of operation.....	1
1.2 DHPRs and RyRs are calcium channels	2
1.2.1 Voltage-gated calcium channels.....	2
1.2.2 Ryanodine receptors.....	6
1.3 The structural basis and the mode of EC-coupling in skeletal muscle.....	7
1.4 The DHPR:RyR1 communication in skeletal muscle - state of the art and open questions	11
1.5 Aims of the present work and description of the experimental approach	18
2. MATERIAL & METHODS	24
2.1 Materials and chemicals	24
2.1.1 Consumables and kits.....	24
2.1.2 Restriction enzymes.....	25
2.1.3 Oligonucleotides.....	26
2.1.4 Bacterial strain and plasmids.....	27
2.2 Molecular biological techniques.....	27
2.2.1 PCR	27
2.2.2 Site-directed mutagenesis.....	28
2.2.3 Restriction digest.....	29
2.2.4 Dephosphorylation of DNA.....	30
2.2.5 Agarose gel electrophoresis.....	31
2.2.6 Purification of DNA fragments	31
2.2.7 Ligation of DNA fragments.....	31
2.2.8 Culture growth.....	32
2.2.9 Preparation of chemically competent <i>E. coli</i>	32
2.2.10 Transformation of chemically competent <i>E. coli</i>	33
2.2.11 Preparation of Plasmid DNA.....	34
2.2.12 Restriction digests	34
2.2.13 Determination of DNA concentration in aqueous solution.....	35
2.3 Generation of cDNA constructs for cellular expression	35
2.3.1 Generation of fluorescent protein vectors.....	35
2.3.2 Generation of fluorescently tagged rabbit skeletal muscle α_{1S}	37
2.3.2.1 N-terminal labelled α_{1S}	37
2.3.2.2 C-terminal labelled α_{1S}	37
2.3.2.3 Insertion of CyPet or YPet into cytoplasmic α_{1S} loops	40
2.3.2.4 Generation of 'no-FRET' control constructs.....	43
2.4 Cell culture & plasmid-DNA injection.....	44
2.4.1 tsA-201 cell culture and transfection procedure	44
2.4.2 Primary skeletal muscle cell culture	45
2.4.2.1 Mouse models.....	45
2.4.2.2 Genotyping	45
2.4.2.3 Preparation of primary skeletal muscle cultures.....	47
2.4.3 Transfection of myotubes via intranuclear plasmid-DNA microinjection.....	48
2.5 Electrophysiology	49
2.5.1 Electrically evoked contractions.....	49
2.5.2 Measurement of L-type Ca^{2+} currents	49

	Page
2.6 Confocal laser-scanning microscopy	50
2.7 Measurements of Fluorescence / Förster Resonance Energy Transfer (FRET) ratio.....	54
2.7.1 Donor to acceptor stoichiometry	54
2.7.2 Measurement of sensitized emission for the calculation of the degree of FRET.....	54
2.7.3 Background correction	55
2.7.4 Detection of cellular autofluorescence	56
2.7.5 Estimating the degree of FRET within fluorescent foci by using a binary mask	56
2.8 Statistical analysis	60
3. RESULTS	61
3.1 Tagged α_{1S} constructs restore EC coupling	61
3.2 Quantification of FRET in fluorescent spots	71
3.2.1 Significant FRET occurs between the intracellular loops of the DHPR α_{1S}	72
3.2.2 Quantifying differences in FRET ratio associated with absence or presence of RyR1	75
4. DISCUSSION	77
4.1 Significant FRET between cytoplasmic loops of the DHPR α_{1S} subunit.....	77
4.2 Rearrangements of cytoplasmic α_{1S} domains in the presence of RyR1	79
4.3 On the molecular basis of RyR1-caused rearrangement of cytoplasmic α_{1S} domains	81
4.4 Concluding remarks	91
4.5 Outlook	92
5. REFERENCES	94
6. ABBREVIATIONS	105
7. LIST OF FIGURES AND TABLES	110
8. ACKNOWLEDGEMENT	112
9. DECLARATION	113
10. CURRICULUM VITAE	114
11. LIST OF PUBLICATIONS	115

Introduction

1.1 Skeletal muscle: basic structural features and principle of operation

Skeletal muscle fibres are longitudinally extended cylindrical structures which at their outer surface are bound by a plasma membrane, the sarcolemma, as well as an overlying basal lamina. They group into bundles to form fascicles, which themselves group to form individual muscles. The sarcolemma forms a physical barrier against the external environment and also mediates signals between the extracellular space and the muscle cell interior. The sarcoplasm is the specialized cytoplasm of muscle cells, containing the regular subcellular elements along with abundant myofibrils, as well as a modified endoplasmic reticulum known as the sarcoplasmic reticulum (SR). The SR forms a network around the myofibrils, storing and providing the calcium (Ca^{2+}) required for muscle contraction. Transverse (t)-tubules are plasma membrane invaginations emanating from the sarcolemma (Figure 1.1), allowing action potentials transmitted by motor neurons to propagate rapidly into deeper parts of the fibre. A sarcolemmal / t-tubular voltage 'sensor', the Dihydropyridine receptor (DHPR), is responsive to depolarization and - most probably by a direct mechanical / conformational link, details below - activates the skeletal muscle Ca^{2+} release channel, the type 1 Ryanodine receptor (RyR1), which spans the < 20 nm cytoplasmic gap between the t-tubule and the SR. This direct mechanism of RyR1 activation by the DHPR is - in contrast to cardiac muscle - independent of Ca^{2+} influx from the extracellular space and normally ensures rapid and effective SR Ca^{2+} release for the activation of the myofilaments. This process of plasma membrane depolarization resulting in muscle contraction is known as excitation-contraction (EC) coupling (Schneider & Chandler 1973; Melzer *et al.* 1995).



1.2 DHPRs and RyRs are calcium channels

The two main players in EC coupling, DHPR and RyR1, both are Ca^{2+} ion channels. However, whereas the DHPR is gated by depolarising changes in voltage, like for instance during an action potential, RyRs are gated by ligand binding, which normally is Ca^{2+} .

1.2.1 Voltage-gated calcium channels

DHPRs belong to the group of voltage-gated Ca^{2+} channels (VGCCs), which are widely expressed and found in many different cell types. Interestingly, their expression is not confined to excitable cells (VGCCs of lymphocytes, for instance). The different VGCCs are characterized mainly by their isoform-specific depolarisation threshold for opening, their ion conductance and their inactivation kinetics. Their different electrophysiological

properties are reflected by the diverse processes VGCCs are involved in, contraction, secretion, synaptic transmission, and gene expression. VGCCs consist of multiple subunits. Purification studies on skeletal muscle t-tubule membrane preparations identified α_1 , β , γ , and $\alpha_2\delta$ as subunits (Figure 1.2) of the skeletal muscle VGCC isoform (DHPR) (Curtis & Catterall 1984; Hosey *et al.* 1987). Analysis of the biochemical properties, glycosylation and hydrophobicity of these five components led to a model comprising a principal, pore-forming α_1 subunit of 190 kDa (Figure 1.2). The latter is associated with the $\alpha_2\delta$ dimer of 170 kDa, the intracellular β subunit of 55 kDa, and a transmembrane γ subunit of 33 kDa (Takahashi *et al.* 1987). Ten different genes have been identified so far, encoding α_1 subunits with discrete types of Ca^{2+} currents (Table 1.1). Four genes have been described for the $\alpha_2\delta$ subunit, four for the β subunit, and γ subunits are encoded by eight different genes (Catterall 2000; Arikath & Campbell 2003). Protein biochemistry in combination with cDNA cloning and sequencing allowed to predict the membrane topology of the five channel subunits. α_1 subunits are proteins of about 2,000 amino acid residues, organized in four repeated domains (I to IV), each of

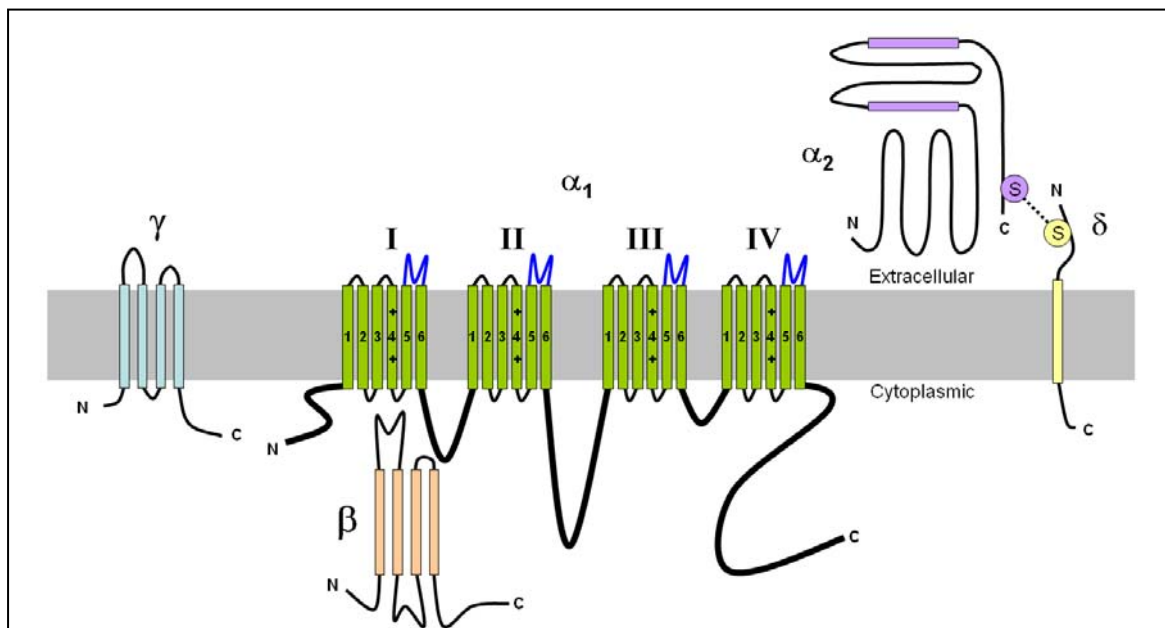


Figure 1.2. Topography of voltage-gated Ca^{2+} channels (VGCCs). Shown is the subunit composition (α_1 , α_2 , β , γ , and δ) and the putative transmembrane regions, the model is updated from the original description of the subunit structure of skeletal muscle Ca^{2+} channels (Takahashi *et al.* 1987). The α_1 subunit is composed of four homologous repeats (I-IV), each consisting of six transmembrane segments (1-6). The fourth transmembrane segment in all four repeats contains positively charged residues (+) and serves as the voltage sensing structure, which is important for the initiation of EC coupling. The loop connecting the fifth and sixth transmembrane segments (blue) is important for the ion selectivity of VGCCs. VGCCs also contain large cytoplasmic regions, serving as interaction sites for a variety of regulatory molecules of the intracellular milieu.

which contains six transmembrane segments (S_1 to S_6), and a membrane-associated loop between transmembrane segments S_5 and S_6 (Figure 1.2). The domains I to IV are thought to be arranged around the central ion conducting pore (Huber *et al.* 2000). Important in the context of the present work, the α_1 N- and C-terminus, as well as the sequence regions connecting domains I to II, II to III, and III to IV ('loops'), are located at the cytoplasmic site of the subunit. As to the β subunit, biochemical analysis and expression in cellular systems suggests that this protein is membrane-associated but that it lacks transmembrane segments (Ruth *et al.* 1989), whereas the γ subunit is a glycoprotein with four transmembrane domains (Jay *et al.* 1990) (Figure 1.2). The α_2 subunit has numerous glycosylation sites and several hydrophobic sequences (Ellis *et al.* 1988), but biochemical studies indicate that it is an extracellular protein attached to the membrane through the δ subunit (Gurnett *et al.* 1996). The δ subunit is encoded by the 3' end of the coding sequence of the same gene as the α_2 subunit, and the mature forms of these two subunits are produced by post-translational proteolytic processing and disulfide linkage (Figure 1.2) (De Jongh *et al.* 1991; Jay *et al.* 1991).

Intensive studies of the structure and function of the pore-forming α_1 subunits of Ca^{2+} channels have led to identification of their principal functional domains (Catterall 1995; Hofmann *et al.* 1999; Catterall 2000). The S_4 segments of the four homologous domains serve as the voltage sensors for activation, moving outward and rotating under the influence of the electric field, causing a conformational change that opens the pore (Figure 1.2). The S_5 and S_6 segments, together with their connecting loop, form the pore lining for Ca^{2+} influx (Figure 1.2). All voltage-gated Ca^{2+} channels share these general structural features (Catterall 2000).

Since the first recordings of Ca^{2+} currents in cardiac myocytes (Reuter 1967; Reuter *et al.* 1979; Reuter 1979), it has become apparent that there are five types of Ca^{2+} currents as defined by electrophysiological and pharmacological criteria and they have been assigned to cloned Ca^{2+} channel α_1 subunits (Table 1.1) (Tsien *et al.* 1988; Bean 1989; Hess 1990; Llinas *et al.* 1992). In cardiac, smooth, and skeletal muscle, the major Ca^{2+} currents are characterized by their high voltage of activation (i.e., relatively strong depolarisations are required for opening), large single-channel conductance, slow voltage-dependent inactivation, marked regulation by cAMP-dependent protein phosphorylation, and specific inhibition by Ca^{2+} antagonist drugs including dihydropyridines, phenylalkylamines, and benzothiazepines (Reuter 1983). These Ca^{2+} currents are typical of the Ca_v1 gene family

of voltage-gated Ca^{2+} channels and have been designated L-type, as they are long lasting when Ba^{2+} is the current carrier (Nowycky *et al.* 1985). The other current types, N-, P/Q- and R-type are mainly found in neuronal cells (e.g., presynaptic membranes), whereas T-type currents, which activate at relatively hyperpolarized potentials, comprise a Ca^{2+} current component in cardiac and skeletal muscle. Intriguingly however, whereas L-type Ca^{2+} currents through Ca_v1 channels are essential for excitation contraction coupling in cardiac muscle, they are not a prerequisite for this process in skeletal muscle. This principal independence of the activation of intracellular Ca^{2+} release from extracellular Ca^{2+} inflow is referred to when the term *skeletal muscle-type EC coupling* is used.

Table 1.1. Subunit composition and function of VGCC sub-types (Catterall 2000). The ten genes encoding VGCCs are expressed in a variety of tissues and are classified into three groups (Ca_v1 , Ca_v2 , and Ca_v3). To carry out a variety of important processes Ca^{2+} channels are subjected to differential splicing and thus possess multiple biophysical traits (the different splice variants are not listed here). Channels of the Ca_v1 group are sensitive to dihydropyridines and have been termed dihydropyridine receptors.

Ca^{2+} channel	Ca^{2+} current type	α_1 main subunit	Primary localizations	Functions
$\text{Ca}_v1.1$	L	α_{1S}	Skeletal muscle	EC coupling Calcium homeostasis Gene regulation
$\text{Ca}_v1.2$	L	α_{1C}	Cardiac muscle Endocrine cells Neurons	EC coupling coupling Hormone secretion Gene regulation
$\text{Ca}_v1.3$	L	α_{1D}	Endocrine cells Neurons	Hormone secretion Gene regulation
$\text{Ca}_v1.4$	L	α_{1F}	Retina	Tonic neurotransmitter release
$\text{Ca}_v2.1$	P/Q	α_{1A}	Nerve terminals Dendrites	Neurotransmitter release Dendritic Ca^{2+} transients
$\text{Ca}_v2.2$	N	α_{1B}	Nerve terminals Dendrites	Neurotransmitter release Dendritic Ca^{2+} transients
$\text{Ca}_v2.3$	R	α_{1E}	Cell bodies Dendrites Nerve Terminals	Ca^{2+} -dependent action potentials Neurotransmitter release
$\text{Ca}_v3.1$	T	α_{1G}	Cardiac muscle Skeletal muscle Neurons	Repetitive firing
$\text{Ca}_v3.2$	T	α_{1H}	Cardiac muscle Neurons	Repetitive firing
$\text{Ca}_v3.3$	T	α_{1I}	Neurons	Repetitive firing

1.2.2 Ryanodine receptors

The conformational changes of the skeletal muscle DHPR control the intracellular release of Ca^{2+} via the type 1 ryanodine receptor (RyR1), a ligand-gated Ca^{2+} channel of the SR membrane. In general, RyRs are high-conductance, intracellular Ca^{2+} channels regulated by both exogenous and intracellular mediators, releasing Ca^{2+} stored in the SR. RyRs are the largest ion channels known. They consist of four identical subunits (homotetramers), each with a molecular mass of ~ 560 kDa, and with an average molecular weight of the complete channel of about 2.3 MDa (Meissner 2002). About nine-tenth of this mass are cytoplasmic, forming the 'foot' structures visible in thin section electron micrographs (Figure 1.3). Only one-tenth of the protein sequence, the carboxy-terminal part, contributes to the formation of the pore. Three isoforms, or types, of RyRs have been described in mammals, RyR1, RyR2, and RyR3 (Takeshima 1993). Whereas RyR1 is the essential isoform for EC coupling in skeletal muscle, RyR2 has this role in cardiac muscle, but also serves Ca^{2+} release in other tissues, like, for instance, smooth muscle or in neurons of the central nervous system. In contrast, RyR3 is not required for EC coupling and RyR3 knock-out mice are viable and breed. RyR3 has been suggested to play transient roles in skeletal muscle development (Takeshima *et al.* 1995).

Despite being a ligand-gated Ca^{2+} channel, the skeletal muscle RyR1 is believed to be activated directly by mechanical coupling to the DHPR. This is an exclusive feature of RyR1, since skeletal muscle-type EC coupling can not be established when RyR1 is replaced by either of the two other RyR isoforms (Takeshima *et al.* 1994; Bertocchini *et al.* 1997). This fact has initiated a number of studies aiming to identify the RyR1 regions capable of direct interaction with the DHPR (Protasi *et al.* 2002; Sheridan *et al.* 2006). In the latter studies, chimeras of RyR1 and RyR2 have been constructed and their potential to restore skeletal muscle-type EC coupling has been investigated upon their expression in myotube cultures prepared from RyR1 knock-out mice. The conclusion from these studies is that multiple - more or less extended - regions of the RyR1-type sequence are required for the restoration of Ca^{2+} -independent activation of Ca^{2+} release in skeletal muscle. However, whether or not these sequence regions actually participate in direct interactions with the DHPR remains to be seen.

1.3 The structural basis and the mode of EC-coupling in skeletal muscle

The two major players in the process of skeletal muscle-type EC coupling described above, the sarcolemmal/t-tubular DHPR and the RyR1 of the SR membrane, obviously belong to separate membrane systems. However, in skeletal muscle, there appears to be an intricate linkage between the two channels, not only functionally, but also mechanically. According to the current view, the DHPR is the transducer of the electrical signal to RyR1 via physical (also termed conformational) coupling between the two proteins (Tanabe *et al.* 1988). However, as stated above, the molecular identities of the interacting regions as well as the mode of operation of this critical step in EC coupling remain unknown.

Obviously, it is a prerequisite for conformational coupling that the DHPR must be in close proximity to RyR1. Actually, ultrastructural studies show that there is only a narrow gap of < 20 nm between the sarcolemmal/t-tubular and the SR membrane of terminal cisternae, which has led to the introduction of the term *junction* for these structures. Electron microscopy (EM) approaches have furthermore established that DHPRs and RyRs reside in these junctions and that the huge electron-dense mass bridging the junctional gap is the cytoplasmic part of RyR1, a structure also called ‘foot’ (Figure 1.3) (Franzini-Armstrong 1970; Block *et al.* 1988; Protasi *et al.* 1998; Takekura & Franzini-Armstrong 1999; Protasi *et al.* 2000; Felder *et al.* 2002; Protasi *et al.* 2002). Together with a number of associated proteins, DHPRs and RyR1s of the junctions form so called calcium release units (CRUs) (Flucher & Franzini-Armstrong 1996). CRUs can either persist at junctions located at the cell surface, formed between a SR cistern and the sarcolemma, a configuration which has been termed *peripheral coupling*. Or, as is the case in mature skeletal muscle with presence of a t-tubule system, two opposed cisternae develop a junction with a centrally located t-tubule, forming a triad (Figure 1.3). Despite this variety of shape, junctions of either type are functionally equivalent to each other with respect to molecular composition and functional mode of EC coupling (Flucher & Franzini-Armstrong 1996). The meticulous work of Franzini-Armstrong and colleagues, using freeze-fracture replicas and thin section EM analysis, has provided a detailed insight into the relative disposition of RyRs and DHPRs within junctions (Figure 1.3).

DHPRs and RyRs in junctions of skeletal muscle display a highly ordered disposition. The DHPRs are organized in groups of four (‘tetrads’). Within an individual tetrad, every DHPR is opposed to one of the 4 subunits of the underlying RyR1 homotetramer

(Figure 1.4) (Block *et al.* 1988; Takekura *et al.* 1994; Protasi *et al.* 1998; Protasi *et al.* 2000; Protasi *et al.* 2002) Interestingly, not every RyR1 is associated with a tetrad, only every second RyR1 is undergoing such association. The reason for this is not known but it has been speculated there might be a lack of sufficient space for the continuous deposition of tetrads (Block *et al.* 1988; Franzini-Armstrong & Kish 1995). In support of the direct link-hypothesis, the formation of DHPR tetrads absolutely requires the presence of the RyR1, since tetrads are not formed in skeletal muscle devoid of RyR1 ('dyspedic' muscle, see below; (Takekura *et al.* 1995; Protasi *et al.* 2000). It should be added that the regular arrangement of DHPRs and RyR1s in junctions of skeletal muscle is not a significant contributor to the formation of junctions, since the latter are still formed in the absence of

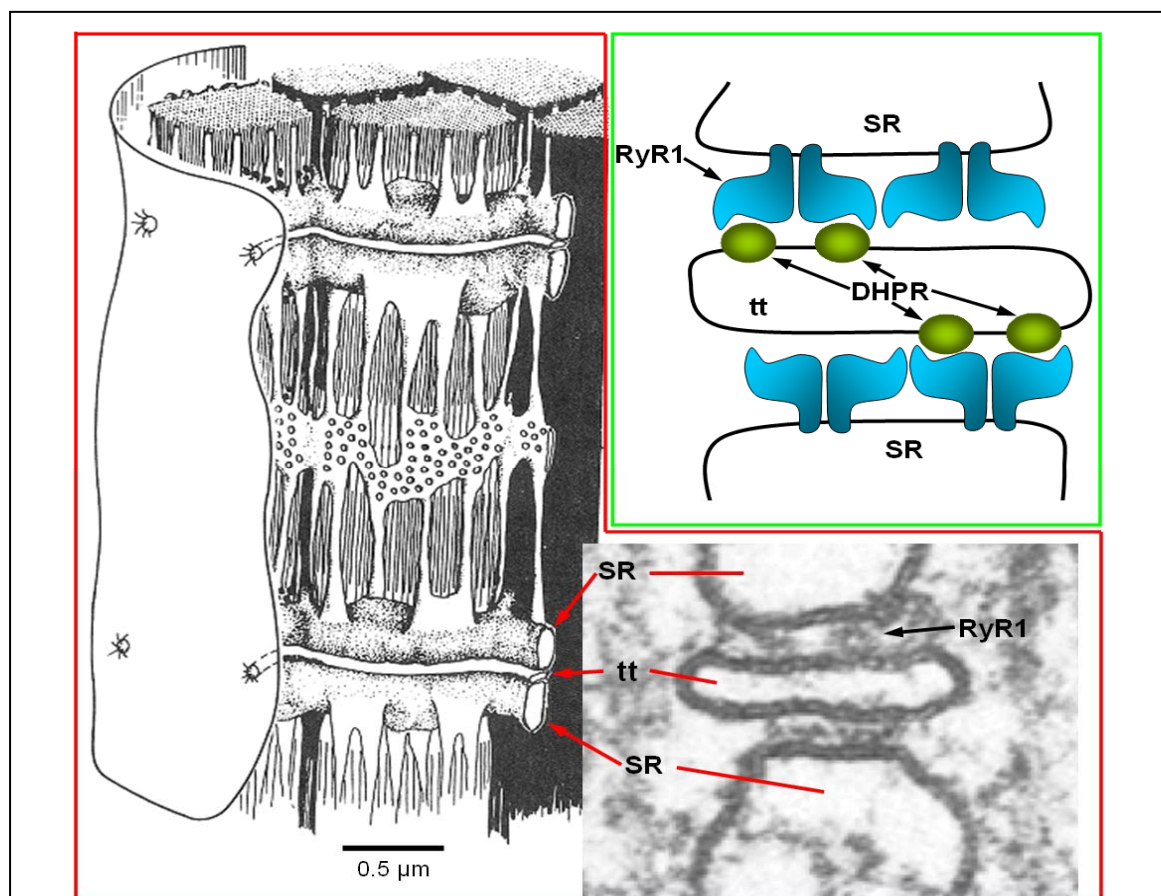


Figure 1.3. Location of calcium release units in skeletal muscle. Red Frame: A skeletal muscle fibre (as seen in Figure 1.1) and an electron micrograph showing a triad structure in cross-section (bottom right). Two SR terminal cisternae dock on a t-tubule (tt). Calcium release units (CRUs) are macromolecular complexes of numerous proteins, with the DHPR and the RyR1 forming the essential, central components. CRUs localize to the junctional region of the two compartments (Franzini-Armstrong & Nunzi 1983). The cytoplasmic domains of RyR1, also termed 'feet' are visible as electron dense mass in the cleft. Green frame: A triad with the major CRU components, the RyR1 (blue) and the DHPR (green). The schematic cross-sections show only two of the four subunits of each RyR1 homotetramer. RyR1s are closely associated with DHPRs, and this association exhibits a unique, characteristic architecture (details shown in subsequent figures).

DHPRs (Flucher *et al.* 1993; Powell *et al.* 1996), and also in the absence of the RyR1 (Takekura *et al.* 1995; Takekura & Franzini-Armstrong 1999).

It has been shown that the distance between DHPRs within tetrads is decreased by exposure of myotubes to the RyR ligand ryanodine, a finding which further supports the idea that skeletal DHPRs are linked (directly or indirectly) to RyR1s (Paolini *et al.* 2004). Thus, the tetradic structure might very likely represent the visible correlate of a direct link between α_{1S} and the RyR1. In support of this view, tetrads are never seen in cardiac preparations (Sun *et al.* 1995; Protasi *et al.* 1996), indicating the absence of mechanical linkage and reflecting the different mode of EC coupling in heart, where Ca^{2+} influx through the cardiac DHPR is required to activate the RyR2, a process which has been termed Ca^{2+} induced Ca^{2+} release (Tanabe *et al.* 1990b).

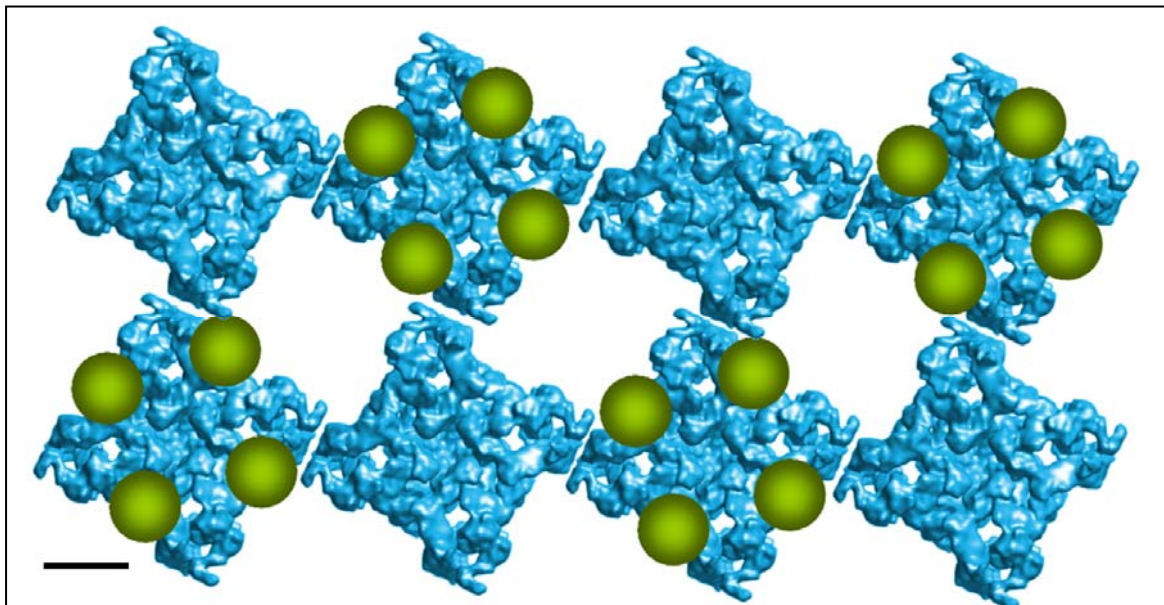


Figure 1.4. Ordered arrangement of DHPR and RyR1 in junctions of skeletal muscle. The relationship between RyR1 homotetramer clusters (blue) and DHPRs (green) is shown schematically, as viewed from the t-tubular luminal site. A characteristic feature of skeletal muscle is the regular arrangement of DHPRs in groups of four, 'tetrads'. Freeze-fracture studies revealed that tetrads are in register with every other RyR1, which could be explained by steric hindrance, not allowing DHPRs to interlock on subunits of adjacent RyRs. This specific arrangement supports the widely accepted view that in skeletal muscle there very likely is a mechanical link between the cytoplasmic RyR1 domain and yet to be identified domains of the DHPR. It has been shown that presence of the RyR1 is essential for tetrad formation (Franzini-Armstrong 2004). The geometry of the DHPR-RyR1 association in skeletal muscle has been extensively studied (Block *et al.* 1988; Franzini-Armstrong & Kish 1995; Protasi *et al.* 1997). The RyR1 structure used in this figure is from a 3D reconstruction by Samso *et al.* (2009, and is based on single particle analysis in combination with cryo electron microscopy. Bar represents 10 nm and refers to RyR1.

It has long been known that RyRs and DHPRs are essential components of EC coupling in both cardiac and skeletal muscle. Skeletal muscle is completely incapable of EC coupling after ablation of the RyR1 gene (*dyspedic* muscle, no visible ‘foot’ in EM preparations, Takeshima *et al.* 1994). As to the DHPR however, not all subunits are of equal importance with respect to EC coupling. EC coupling fails completely in muscle cells genetically null for the principal subunit, α_{1S} (as represented by *dysgenic* muscle from the *muscular dysgenesis* mouse strain, *mdg*, Tanabe *et al.* 1988). Furthermore, EC coupling is also abolished by knocking out the gene encoding the β_1 subunit of the DHPR (Gregg *et al.* 1996). This is not surprising, since the β_1 subunit, in addition to influencing the gating properties of α_{1S} , is essential for effective targeting of the principal subunit to junctions and for its arrangement as tetrads (Strube *et al.* 1996; Neuhuber *et al.* 1998a; Schredelseker *et al.* 2005). In contrast, the γ subunit does not appear to play a major role during EC coupling since only minor functional alterations occur as a consequence of knocking out the gene encoding the γ subunit in mouse skeletal muscle (Freise *et al.* 2000). Also, silencing the $\alpha_{2\delta}$ expression in skeletal muscle cells does not interfere with targeting of the α_{1S} subunit or with skeletal muscle-type EC coupling (Obermair *et al.* 2005; Garcia *et al.* 2008), although complete ablation of the $\alpha_{2\delta}$ gene resulted in mice which were reduced in size and which failed to survive beyond day 35.

Despite the eminent importance of DHPR and RyR1 for EC coupling, a number of additional junctional proteins with important accessory roles have been identified, among them triadin, junctophilin-1, Homer, AKAP15, Ca^{2+} -CaM, JP-45, and junctate/humbug. Of those, junctophilin has been found to be critical for the development of normal junctions (Ito *et al.* 2001; Komazaki *et al.* 2002). However, unlike the DHPR and the RyR1, none of these associated proteins appears to be absolutely required for EC coupling in skeletal muscle (Treves *et al.* 2009).

1.4 The DHPR:RyR1 communication in skeletal muscle - state of the art and open questions

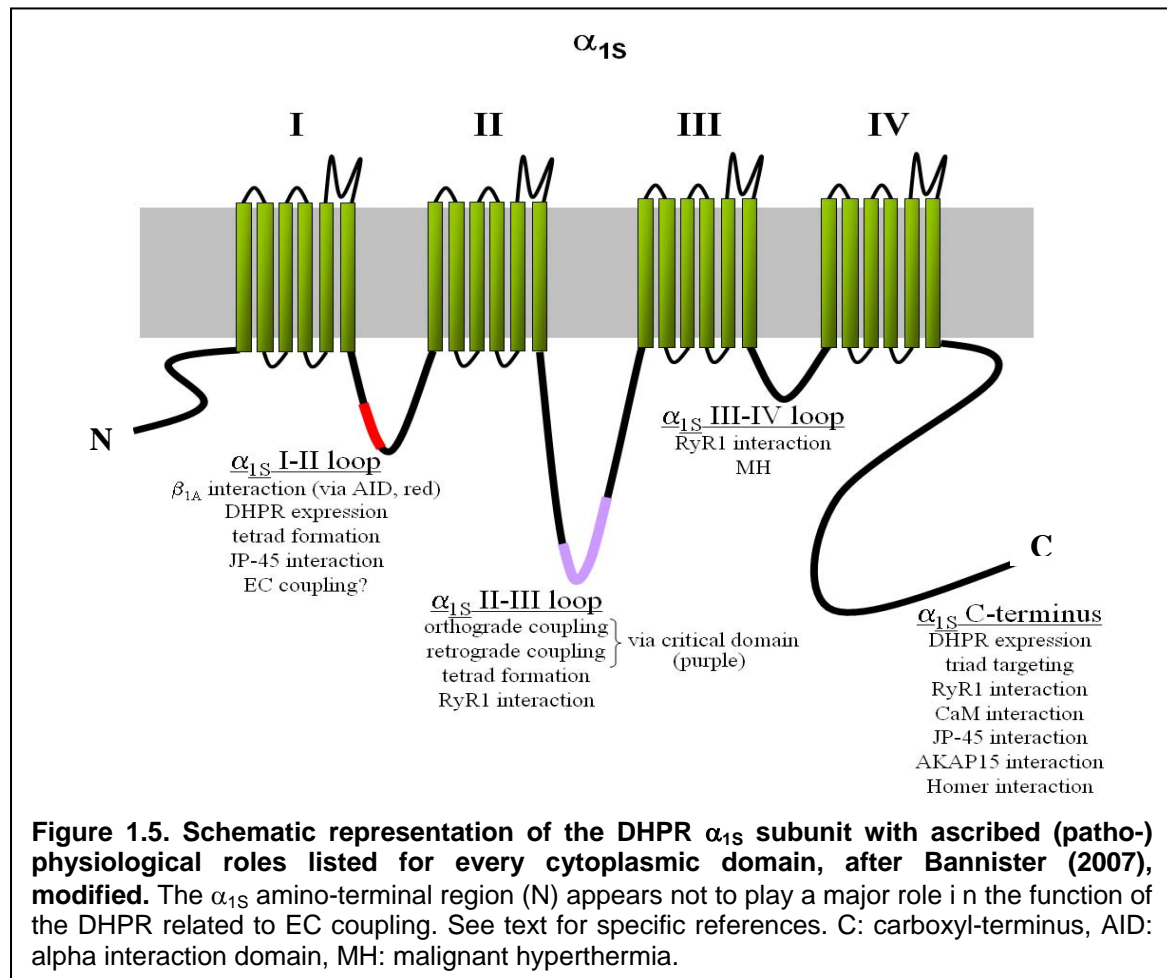
The usage of two mouse models for cellular studies has proven invaluable for the advancement of the EC coupling field. A model representing the complete cellular equipment of a skeletal muscle cell, except for the α_{1S} subunit of the DHPR, is the so called *muscular dysgenesis* mouse (Tanabe *et al.* 1988). In this model, a single base deletion within the α_{1S} gene in the coding sequence for the fourth repeat domain creates a premature stop codon. In the homozygous condition, in the so called dysgenic muscle, levels of the mutated α_{1S} mRNA are significantly reduced and the prematurely truncated α_{1S} polypeptide cannot be detected by Western blots (Knudson *et al.* 1989). Thus, the homozygous mice are incapable of endogenous α_{1S} expression, resulting in perinatal death due to asphyxia (Chaudhari 1992). The second mouse model is the so called *dyspedic* mouse (see above) and is a conventional knock-out for the RyR1 gene via genetic engineering (Takeshima *et al.* 1994). Absence of RyR1 also is lethal at birth, due to complete paralysis of skeletal muscle. Since heterozygous animals from both models have no phenotype, conventional breeding is possible, whereby the mating of two mice heterozygous for either condition provides homozygous offspring with a 1:4 frequency, obeying Mendelian rules. Primary skeletal muscle cultures from such animals have been used in numerous studies for the expression of genetically modified α_{1S} and/or RyR1 cDNAs, to decipher the role of defined protein regions in EC coupling.

In the pursuit of answers, one experimental approach undertaken was the expression and analysis of chimeric DHPR subunits and/or chimeric RyRs (chimeric refers to usage of fusion proteins generated from different isoforms of the same channel family, e.g., fusing the α_{1S} sequence encoding the first two repeats with the α_{1C} sequence encoding the two remaining repeats of the subunit). Another frequently used approach was the *in vitro* application of peptides representing defined, short α_{1S} regions to isolated, lipid bilayer-reconstituted RyR1s. However, despite the wealth of knowledge that such studies generated about possible structural and functional requirements for normal DHPR-RyR1 interaction (detailed below), the precise mechanism and the molecular regions involved remain elusive. Thus, the same mechanistic questions facing investigators 15 years ago still persist today: What parts of the DHPR α_{1S} subunit trigger EC coupling? How is the EC coupling signal transmitted from the voltage-sensing regions of the α_{1S} to RyR1?

What is known so far?

Referring to the direction of signal procession, the activation of the RyR1 by the activated voltage-sensor, the DHPR, has been termed orthograde signalling. This term has been introduced after discovery that DHPR-RyR1 signalling also occurs in the opposite direction, retrograde (Nakai *et al.* 1998b). The presence of such a retrograde signal was revealed by the observation that L-type currents of dyspedic myotubes were substantially smaller than L-type currents of wild-type myotubes, despite similar membrane expression of the DHPR. Just as orthograde DHPR-RyR1 coupling does not depend upon Ca^{2+} influx through the skeletal muscle DHPR, the retrograde, RyR1-dependent enhancement of skeletal L-type current does not depend upon Ca^{2+} movements via RyR1 (Nakai *et al.* 1996; Nakai *et al.* 1998a; Avila & Dirksen 2000). Moreover, both orthograde and retrograde coupling depend on the integrity of some of the same structural elements of the DHPR α_{1S} subunit and RyR1 (Grabner *et al.* 1999). Neither of these interactions depends on any obvious diffusible messenger (such as entry of external Ca^{2+}), which has led to the idea that there is bidirectional conformational coupling between these two proteins (Tanabe *et al.* 1988; Garcia *et al.* 1994; Garcia & Beam 1994; Nakai *et al.* 1998b). Collectively, these observations suggest that retrograde coupling, like orthograde coupling, is supported by direct protein-protein contacts linking RyR1 and the DHPR channel complex (Beam and Horowicz, 2004).

Introduction of Fluorescence resonance energy transfer (FRET) (Papadopoulos *et al.* 2004; Leuranguer *et al.* 2006) and the usage of other optical approaches (Lorenzon *et al.* 2004) has given new insights into the spatial orientation of the DHPR within intact tetrads as well as putative α_{1S} domains involved in interactions with the RyR1. From these and from additional studies it has become clear that the cytoplasmic interface of the pore forming α_{1S} subunit - in addition to its critical role in functional membrane expression - also represents an essential determinant for interactions with the RyR1. Multiple cytoplasmic α_{1S} domains have been implicated in these interactions. However, as has been stated above, a conclusive picture, about the mechanistic details and the relative contribution of each domain does not exist. The structures referred to here as cytoplasmic α_{1S} domains include the amino- and carboxyl-terminal peptide sequences as well as the three cytoplasmic loops connecting the four homologous α_{1S} repeats, I–II, II–III, and III–IV (Figure 1.5). In principle, their cytoplasmic location makes all of them candidates for interactions with the RyR1, either directly, or via bridging proteins.



The **amino-terminus** of α_{1S} (residues 1–51) appears not to play a significant role in EC coupling. The ability of the DHPR to support evoked contractions or myoplasmic Ca^{2+} transients was not hindered by substitution of α_{1C} amino-terminus for that of α_{1S} (Tanabe *et al.* 1990b; Carbonneau *et al.* 2005). In accordance with these findings, it has been demonstrated that deletion of the bulk of the α_{1S} amino-terminus (residues 2–37) has essentially no effect on either L-type currents or myoplasmic Ca^{2+} transients (Bannister & Beam 2005).

In skeletal muscle, the **carboxyl-terminus** of α_{1S} is subject to proteolytic cleavage at residue A¹⁶⁶⁴ or thereabouts (De Jongh *et al.* 1989; Hulme *et al.* 2005). However, as demonstrated by Beam *et al.* (1992) by the expression of an α_{1S} variant with shortened carboxyl terminal sequence (terminating at residue N¹⁶⁶²), this truncation does not appear to affect the ability of α_{1S} to target to junctions and to couple functionally to RyR1. However, more proximal deletions of the α_{1S} carboxyl-terminus beyond the site of cleavage progressively diminish DHPR surface expression (Proenza *et al.* 2000; Flucher

et al. 2000). Recent data obtained with optical techniques have shown that the proximal α_{1S} carboxyl-terminus may interact with the RyR1. Papadopoulos *et al.* (2004) observed that a cyan/yellow fluorescent protein tandem (CFP-YFP) reporter fused to a truncated α_{1S} carboxyl-terminus (α_{1S} residues 1–1667) produced a substantially reduced FRET efficiency when expressed in dysgenic myotubes (i.e., in the presence of RyR1) relative to the same construct expressed in dyspedic myotubes (i.e., in the absence of RyR1), indicating that conformational influence is exerted on the α_{1S} carboxyl-terminus by RyR1. Lorenzon and co-workers (2004) showed that the C-terminus of α_{1S} appears to be accessible for streptavidin in dyspedic myotubes but not in dysgenic myotubes, indicating an interaction between the α_{1S} C-terminus and the RyR1, either directly or via some other tightly associated molecule.

The α_{1S} **I-II loop** is essential for EC coupling because it is the site for interaction with the equally essential DHPR β_{1A} subunit (Chen *et al.* 2004; Opatowsky *et al.* 2004; Van Petegem *et al.* 2004). The primary binding region for all β subunits on α_1 subunits is the alpha interaction domain (AID), an 18 amino acid region in the I–II loop of α_1 subunits, beginning ~ 23 amino acids from the end of the sixth transmembrane segment (S_6) of domain I (Pragnell *et al.* 1994). The requirement for the β_{1A} subunit underscores the importance of the α_{1S} I–II loop for EC coupling and junctional targeting. The functional nature of the α_{1S} - β_{1A} interaction is an enigma that will require further experiments to unfold.

The short α_{1S} **III-IV loop** does not appear to play a direct role in EC coupling, but it participates indirectly in the process by influencing DHPR gating transitions important both for EC coupling and activation of L-type conductance (Bannister *et al.* 2008).

For several years, there has been general agreement among investigators that the **II-III loop** of the α_{1S} subunit plays a key role in transmitting the EC coupling signal to RyR1 (Tanabe *et al.* 1990a; Garcia *et al.* 1994; Nakai *et al.* 1998b). Numa and colleagues first identified the α_{1S} II–III loop as a major contributor to skeletal muscle-type EC coupling by examining the functional properties of chimeric DHPRs consisting of the individual α_{1S} cytoplasmic domains within the highly-conserved background of the cardiac α_{1C} subunit (Tanabe *et al.* 1990b). The α_{1S} II–III loop substituted into the corresponding region of the cardiac DHPR α_{1C} subunit conferred skeletal muscle-type EC coupling (Tanabe *et al.* 1990b; Carbonneau *et al.* 2005) and, conversely, substitution into

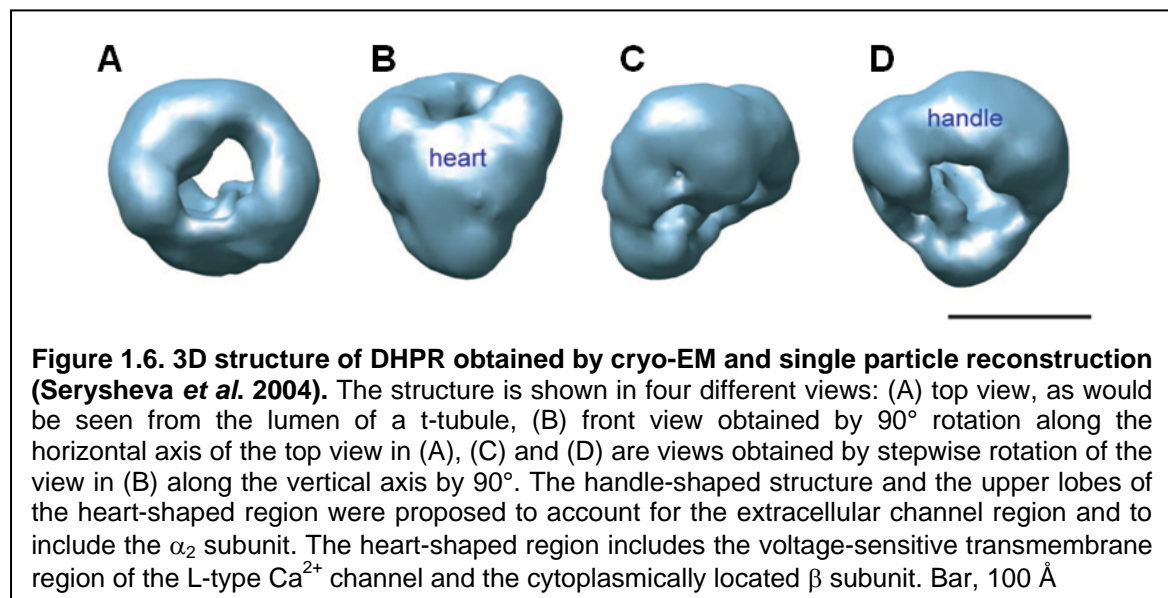
an α_{1S} backbone with the II–III loop of α_{1C} (SkLC; (Grabner *et al.* 1999) or the α_1 subunit of the housefly, α_{1M} (SkLM; (Wilkens *et al.* 2001a; Kugler *et al.* 2004b), abolished skeletal muscle-type EC coupling. However, proper DHPR-RyR1 communication could be restored when a defined region of the α_{1S} II–III loop (residues 720–765, nowadays referred to as *critical domain* (Nakai *et al.* 1998b), was reintroduced within SkLC or SkLM (Grabner *et al.* 1999; Wilkens *et al.* 2001a; Kugler *et al.* 2004b).

In contrast, a synthetic peptide corresponding to an α -helical domain (roughly α_{1S} residues 671–690; or ‘peptide A’) in the amino-terminal portion of the α_{1S} II–III loop activates RyR1 in reconstituted lipid bilayers, which has given rise to the idea that this portion of the α_{1S} II–III loop may interact directly with RyR1. Indeed, recent studies showed binding between peptide A and a fragment of RyR1 *in vitro* (Cui *et al.* 2009; Tae *et al.* 2009). However, the physiological implications of this interaction are unclear because several studies have shown that EC coupling can be restored in dysgenic myotubes expressing α_{1S} constructs in which the peptide A domain has been disrupted or even deleted (El Hayek & Ikemoto 1998; Ahern *et al.* 2001a; Ahern *et al.* 2001b; Flucher *et al.* 2002). Most recently, Bannister *et al.* (2009) have demonstrated that both orthograde and retrograde coupling are supported by four different α_{1S} constructs in which a 56-kDa CFP-YFP tandem replaced the peptide A region. Thus, it seems unlikely that the peptide A region or immediately adjacent segments of the α_{1S} II–III loop directly participate in protein-protein interactions necessary for bidirectional coupling. But these results do not exclude a modulatory role for this amino-terminal segment of the α_{1S} II–III loop.

Bannister and co-workers (2009) used YFP insertions as a means to probe the importance of the carboxyl-terminal region of the α_{1S} II–III loop, which links the critical domain to repeat III. In this particular experiment, introduction of a single YFP between residues 785 and 786 in the carboxyl-terminal portion of the loop ablated bidirectional coupling without affecting membrane expression of the channel or significantly distorting the conformation of the critical domain. The disruption of EC coupling by YFP insertion in the conserved carboxyl-terminal region of the α_{1S} II–III loop suggests that it may be an important site of protein–protein interaction required for signaling. Thus, although the importance of the α_{1S} II–III loop for skeletal-type EC coupling is almost universally accepted, muscle physiologists consider a more inclusive idea of DHPR-RyR1 coupling. This broader view of multiple contacts is consistent with corresponding work indicating

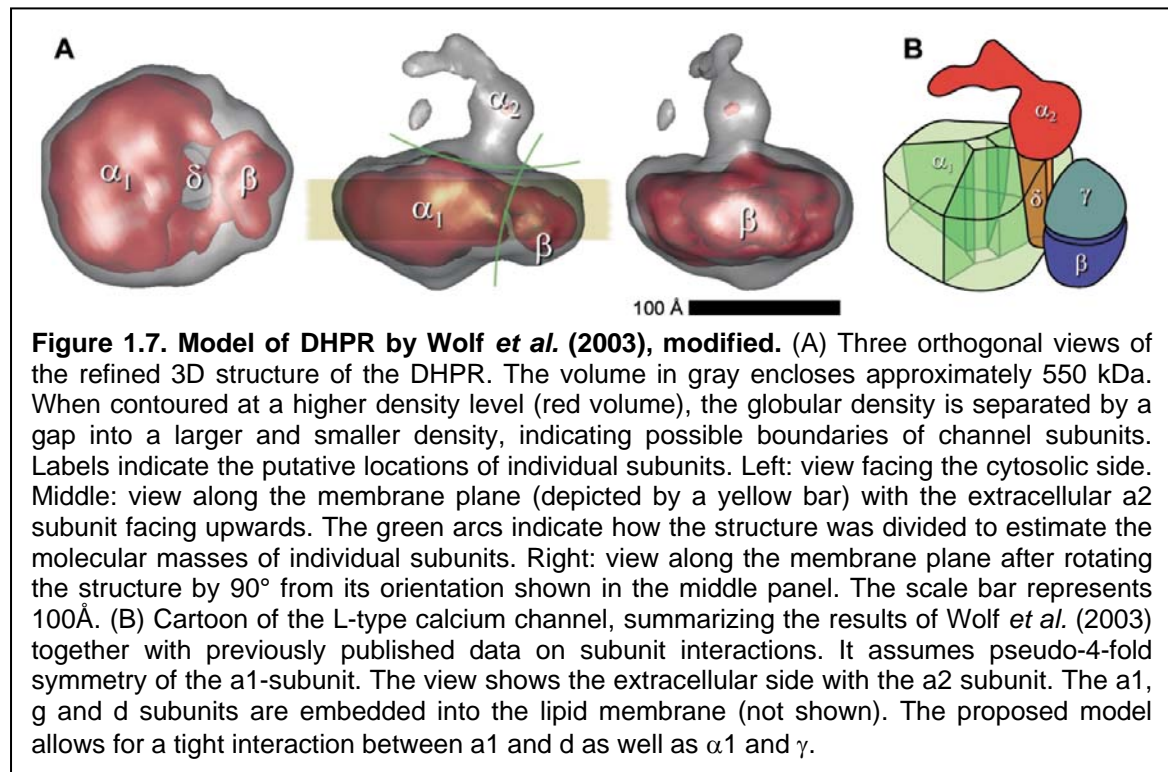
that multiple regions of RyR1 are probably involved in bi-directional coupling with the DHPR (Nakai *et al.* 1998b; Proenza *et al.* 2002; Protasi *et al.* 2002; Perez *et al.* 2003; Sheridan *et al.* 2006).

A better knowledge of the 3D architecture of DHPR complexes would be basic to understanding the channel function and how the EC coupling signal may be transmitted. Since the generation of DHPR protein crystals is not feasible yet, research groups with focus on structure are working on revealing and improving DHPR structures using cryo-EM and single-particle analysis. The most recent studies present 3D structures of skeletal muscle DHPRs with a resolution maximum of $\sim 20 \text{ \AA}$ (Wolf *et al.* 2003; Serysheva 2004; Murata *et al.* 2009), which is still ~ 10 fold lower than the resolving power of crystal structure studies and which does not allow the identification of discrete subregions. Yet, the molecular dimensions determined for single DHPRs (and for individual RyR1 tetramers) using cryo EM suggest that the two channels very likely are in physical contact. The 3D structure presented by Serysheva (2004) comprises two domains, a so called heart region and a handle region, tilted with respect to each other and forming a cavity between them (Figure 1.6). The heart-shaped portion of the complex is proposed to span the membrane and house the α_1 , β and γ subunits, the handle-shaped domain and upper portion of the heart region is predicted to be formed by the $\alpha_2\delta$ subunit (Figure 1.6).

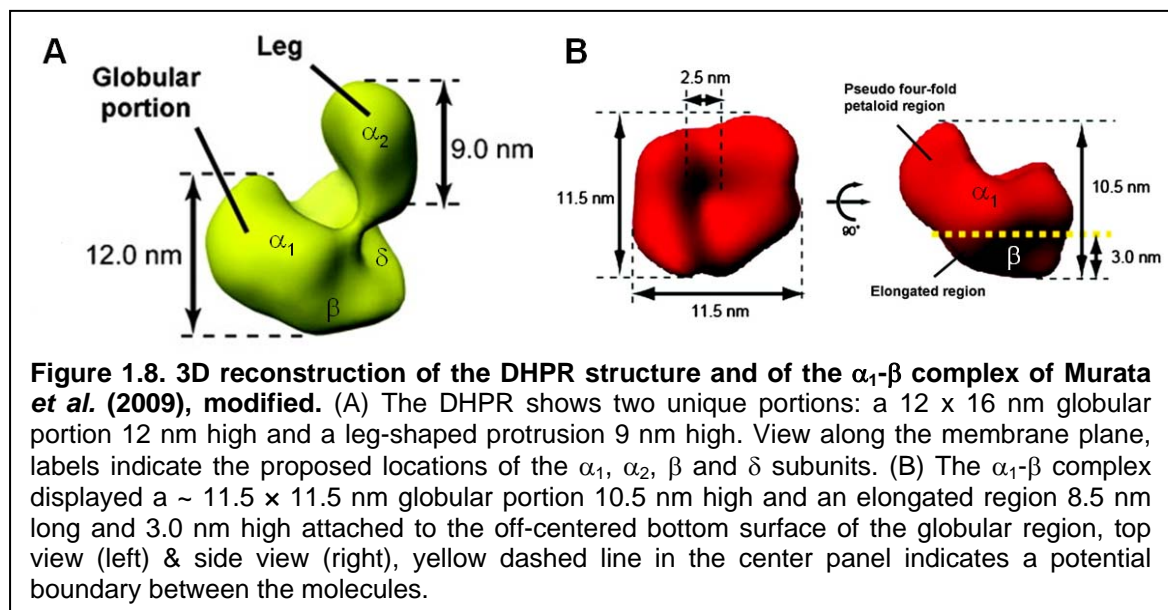


Using the same technique, Wolf *et al.* (2003) presented a 3D structure of the DHPR from skeletal muscle, which allowed them to identify the approximate locations of four of the

five subunits of the channel (Figure 1.7). The proposed arrangement of the subunits is in agreement with functional and biochemical data available for this channel.



Recently, (Murata *et al.* 2009) proposed a single-particle electron microscopy 3D model of the α_1 - β complex alone or in conjunction with the $\alpha_2\delta$ subunit, within the DHPR (Figure 1.8). Their 3D reconstruction of the DHPR shows two portions; a globular portion and a leg-shaped protrusion.



While these three proposed structures display considerable deviations from each other, they nevertheless present the DHPR as a mass with two discrete components, a large and small region. As stated above, none of these 3D models shows sufficient detail to reveal the exact location or orientation of individual DHPR subunits. As a consequence the quaternary structure of the DHPR subunits (including the exact arrangement of the intracellular domains of pore forming α_{1S} subunit) remains unknown. Furthermore, these techniques are generally limited to use *in vitro*, precluding dynamic measurements within living cells. Thus, these approaches are not capable of providing a more detailed picture of the arrangement of the intracellular α_{1S} loops as the important structures for interactions with the RyR1.

1.5 Aims of the present work and description of the experimental approach

The key molecular event in the signal transmission of skeletal muscle EC coupling appears to take place at the interface between the cytoplasmic domains of the DHPR and regions of the RyR1 'foot' yet to be identified. Techniques that are suited to gather information about the interactions and the molecular events of this process in living muscle cells are of crucial importance for the advancement of our understanding in this field. A first basic insight into the identity and the relative spatial arrangement of individual cytoplasmic α_{1S} domains would already be an important step, in that it would enable to ask more specific questions concerning the dynamics of intermolecular interactions in the course of signal transmission from the DHPR to the RyR1. The introduction of the FRET technique has proved a valuable experimental tool to provide answers for this type of questions, not only in the field of EC coupling. In the latter, however, FRET measurements were already used to investigate the tetradic organization of DHPRs, in particular the arrangement of the β_{1a} subunit within tetrads in living muscle cells (Leuranguer *et al.* 2006). Also, studies were carried out to identify potential sites of DHPR-RyR1 proximity (Papadopoulos *et al.* 2004; Lorenzon *et al.* 2004). Basically the same approach is used in the present work to gain a more detailed insight into the spatial arrangement of cytoplasmic α_{1S} domains and of their involvement in RyR1 interactions.

The great importance and suitability of the FRET technique for these investigations derives from the favourable circumstance that the highest sensitivity of FRET to spatial changes is restricted to a narrow, low nm range ($\sim 1-10$ nm), which exactly matches the size of many important proteins and molecular distances. Thus, FRET in principle can answer questions specifically dealing with interactions or dynamic processes in the nm range, like degrees of molecular proximity or orientation, or of their process-dependent, dynamic changes.

A few words to the physical background of the FRET process. FRET is a phenomenon of quantum mechanics (Förster 1948), whose application in bioscience became a powerful tool for the detection of changes in distance and orientation of fluorophore pairs (Tsien 1998). In this process, the donor (CyPet in this study, see Table 1.2), when being in the excited state, transfers the relaxation energy to a neighbouring acceptor (here, YPet) by nonradioactive dipole-dipole interaction. For this transfer to happen, the emission spectrum of the donor must overlap with the excitation spectrum of the acceptor (i.e., there has to be a substantial overlap integral, see Figure 1.9).

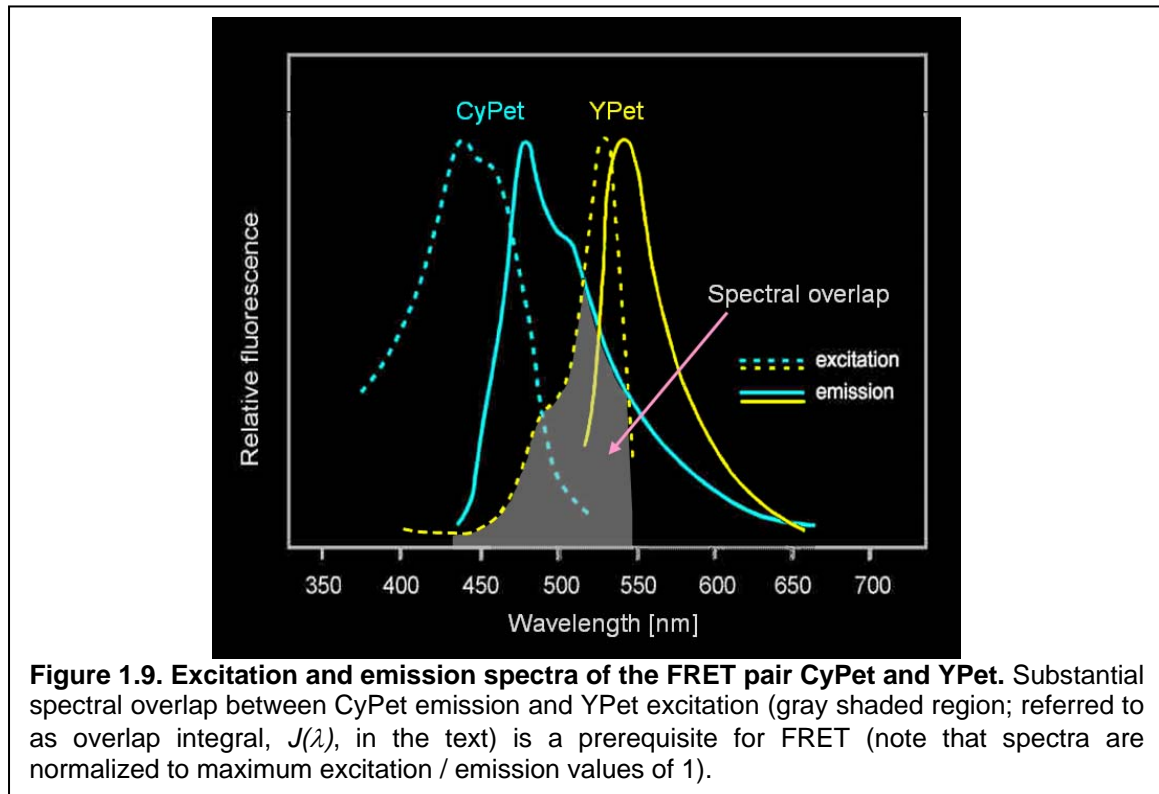
Table 1.2 FRET pair properties. Presented is a compilation of properties displayed by fluorescent protein variants CyPet and YPet (Cyan / Yellow protein for energy transfer, respectively). Along with the common name, the peak absorption and emission wavelengths (given in nanometers), molar extinction coefficient, quantum yield, relative brightness, and *in vivo* structural associations are listed. The computed brightness values were derived from the product of the molar extinction coefficient and quantum yield, divided by the value for enhanced green fluorescent protein (EGFP).¹ The naturally occurring weak dimerization of some FPs, however, can be used to increase the FRET signal in a biosensor (Piston & Kremers 2007).

Protein	Excitation Maximum (nm)	Emission Maximum (nm)	Molar Extinction Coefficient	Quantum Yield (ϕ_D)	<i>in vivo</i> Structure	Relative Brightness (% of EGFP)
CyPet	435	477	35,000	0.51	weak dimer ¹	53
YPet	517	530	104,000	0.77	weak dimer ¹	238

The overlap integral can be calculated according to the equation,

$$J(\lambda) = \frac{\int_0^{\infty} F_D(\lambda) \varepsilon(\lambda) \lambda^4 d\lambda}{\int_0^{\infty} F_D(\lambda) d\lambda} \quad (\text{Eq. 1})$$

where ($\varepsilon(\lambda)$) denotes the extinction coefficient, λ the wavelength in nanometers, and F_D the normalized fluorescence intensity of the donor as a function of wavelength.



A characteristic value for defined FRET partners is the Förster distance (R_0) value. R_0 is the distance at which the donor transfers half of its energy to the acceptor. R_0 depends on several parameters, which are the refractive index of the medium (n), the quantum yield of the donor in the absence of the acceptor (ϕ_d), the orientation factor between the two molecules (κ^2), and the overlap integral mentioned above ($J(\lambda)$):

$$R_0 = 9.78 \times 10^3 (n^{-4} * \phi_d * \kappa^2 * J)^{1/6} \text{ \AA} \quad (\text{Eq. 2})$$

It is apparent from the above equations that for donors having a high quantum yield (ϕ_d) and for acceptors with large extinction coefficients, the spectral overlap integral (J) will be greater, leading to more efficient energy transfer and relatively high R_0 value. In addition, the efficiency of the dipole-dipole interaction between the donor and acceptor depends on the alignment of the two dipoles. The orientation factor (κ), which describes this relative alignment, ranges from 0 (both dipoles perpendicular) to 4 (dipoles parallel). In general, the dipoles can be assumed to be rapidly moving on timescales similar to the donor excited-state lifetime such as the orientations can be described as random, with an average orientation factor of 0.67. However, Förster (1948) demonstrated that the

efficiency of FRET (E) depends on the inverse sixth-distance between donor and acceptor (r),

$$E = R_0^6 / (R_0^6 + r^6), \quad (\text{Eq. 3})$$

making the distance the most critical parameter in this process. It is, thus, not surprising that there is virtually no detectable energy transfer when the fluorophore separation exceeds 10 nm (see Figure 2.10). In most experiments employing FRET, it is actually not known whether the distance (r) between fluorophores, which can be derived from applying Equation 3 to measurements of the FRET intensity, actually represents the real distance. This is due to the merely vague knowledge about the actual value for the orientation factor κ^2 . Also, because of the sixth power dependence of FRET efficiency on fluorophore separation distance, even small errors in the accuracy of FRET measurements can have large effects on both the absolute separation distances estimated from such experiments and on the relative changes. However, these factors which - due to their sensitiveness - make calculations of absolute distances or of their absolute changes problematic, at the same time are very powerful reporters of spatial molecular rearrangements in the low nanometer scale. This is utilized in the present study, in which the focus is more on the qualitative detection of relative spatial changes introduced by the presence of the RyR1, then on the measurement of absolute distances between cytoplasmic DHPR domains. Nevertheless, the data obtained are used in a model to describe for the first time possible RyR1 dependent rearrangements of cytoplasmic DHPR domains.

Genetically encoded FRET biosensors consisting of a donor and an acceptor fluorescence protein can be conveniently introduced into cells and targeted to subcellular compartments. The main limitation of genetically encoded FRET biosensors based on fluorescent proteins is their poor sensitivity (Piston & Kremers 2007). Hence, these biosensors have been widely developed and applied for the detection of various molecular activities in live cells with high spatiotemporal resolution (Wang *et al.* 2008). Enhanced CFP (ECFP) and enhanced YFP (EYFP) have become a very popular FRET pair. Recently, the high-efficiency FRET pair, CyPet and YPet, has been developed and was found to have a greatly extended range of FRET-related fluorescence intensity changes, as

compared to the CFP-YFP pair (Nguyen & Daugherty 2005). CyPet and YPet were derived through a quantitative mutagenesis scanning for fluorescent protein variants with improved FRET properties. A total of seven mutations of EGFP (T¹⁰G, V¹²I, D²⁰E, A⁸⁸V, I¹⁶⁸A, E¹⁷³T, L¹⁹⁵I) resulted in the production of the CyPet protein, which features absorption and emission maxima positioned at 435 and 477 nm, respectively (Table 1.2). When paired with its optimized partner, YPet (see below), this cyan variant exhibits a dynamic range that is more than six times higher than that of CFP-YFP, allowing for a far more sensitive detection of changes in FRET (Nguyen & Daugherty 2005). CyPet's narrow fluorescence emission peak greatly increased its utility in multicolour imaging, and is the most photostable cyan fluorescent protein of the weakly dimeric and monomeric versions currently available. YPet is the brightest yellow fluorescent protein variant yet developed and exhibits very good photostability. However, although the FRET-optimized CyPet-YPet combination appears to be a well-suited tool to study molecular interactions and dynamic spatial reorientations, this fluorophore pair has not yet been tested in studies similar to the present work.

In previous studies, by using CFP and YFP, Papadopoulos and co-workers (2004) could identify potential interaction sites between the DHPR and RyR1 within their natural environment. The authors devised a molecular FRET sensor by generating the CFP-YFP tandem and by incorporating it into defined DHPR domains. Also, recent accessibility studies emphasize the role of defined cytoplasmic domains for interaction and signalling between DHPR and RyR1 (Lorenzon & Beam 2007). These studies demonstrated that FRET is a powerful tool for analyzing the process of EC coupling within living muscle cells by monitoring conformational changes of the cytoplasmic DHPR interface by the presence of RyR1. The work and the results presented in this thesis constitute a continuation of these approaches. However, a novel FRET approach has been undertaken here to investigate the spatial relationship of all cytoplasmic domains of the principal DHPR subunit, α_{1S} . The primary aim was to gain further insight into the possible involvement of individual cytoplasmic α_{1S} domains in interactions with RyR1. The present study constitutes a systematic approach, in which α_{1S} cDNAs were engineered with the CyPet and YPet sequence introduced into positions corresponding to cytoplasmic domains of the α_{1S} subunit. Upon expression in intact muscle cells, the degree of FRET is determined for every combination of the CyPet-YPet double-tag using the technique of sensitized emission. The latter designation refers to the fact that a higher degree of YPet-

related emission is to be expected when the excited donor resides in close proximity to the acceptor. The details of the calculation of the degree of FRET using sensitized emission can be found in the following section (Material & Methods). The rationale for this approach is that one could expect RyR1 dependent changes in the intensity of FRET between two spatially close and potentially movable domains, if the tagged regions represent cytoplasmic α_{1S} domains interacting with RyR1. In first instance, this approach allows to determine whether FRET differs among the different combinations of doubly labelled constructs, providing information about the relative arrangement of the loops in the absence of RyR1. Comparison of FRET efficiencies after expression in dyspedic (RyR1 null) and dysgenic (α_{1S} null) myotubes then allows to determine whether the presence of RyR1 alters the environment of the tagged α_{1S} domains. Unlike the study by Papadopoulos *et al.* (2004), this work does not employ measurements of FRET using a CFP-YFP-tandem as a conformational FRET sensor; rather, the FRET signal depends on the relative position of two different loops.

Upon expression of the α_{1S} constructs in myotubes, sensitive confocal laser scanning microscopy is employed to:

- (1) Assess whether the doubly tagged α_{1S} constructs display correct targeting to the SR / t-tubular junctions.
- (2) Check for the ability of the tagged α_{1S} to restore EC coupling in dysgenic myotubes.
- (3) Determine the degree of FRET between tagged intracellular α_{1S} domains for the different constructs and for the conditions α_{1S} + RyR1 and α_{1S} no RyR1.

The above experiments are expected to provide answers to the following questions:

- (A) Are the loop regions used to insert the fluorescent protein tag critical for channel trafficking to the junctions?
- (B) If the answer to A is no, are the same regions critical for EC coupling, i.e., are the constructs capable of restoring EC coupling upon expression in dysgenic myotubes?
- (C) Which cytoplasmic α_{1S} domains are influenced by the absence / presence of the RyR1 and thus might represent potential interaction sites?

2 Materials and Methods

2.1 Materials and chemicals

All chemicals and reagents used were ‘American Chemical Society’ grade or higher and were purchased from either of the following, Sigma-Aldrich (Muenchen, Germany), Merck (Darmstadt, Germany) GE Healthcare (Freiburg, Germany), Carl Roth (Karslsruhe, Germany), Applichem (Darmstadt, Germany), unless otherwise indicated. Restriction enzymes were obtained from New England Biolabs (Frankfurt am Main, Germany). Cell culture material was ordered from PAA (Cölbe, Germany), MatTek (Ashland, USA), BD Biosciences (Heidelberg, Germany), Biochrom (Berlin, Germany) and Invitrogen (Karslsruhe, Germany). All solutions and lab ware for bacterial cell culture and molecular biology were autoclaved or sterile filtered prior to use. In experiments where water was used, the term water refers to autoclaved tap water from the Institute’s deionized water supply. All cloning end products were subjected to sequencing to ensure no errors were introduced into the cDNA during amplification reactions.

2.1.1 Consumables and kits

Alkaline Phosphatase, Calf Intestinal (CIP)	New England Biolabs
Centrifugal Filter Devices, Durapore PVDF 0,22 µ	Millipore
Crimson <i>Taq</i> Polymerase	New England Biolabs
DNA O’GeneRuler 1 kb DNA Ladder	MBI Fermentas
dNTP Mix, 10 mM each	Fermentas
GeneJuice Transfection Reagent	Merck
NucleoSpin Extract II	Macherey-Nagel
Oligonucleotides	MWG Operon
peqGold Plasmid Miniprep Kit	Peqlab
<i>Pfu</i> DNA polymerase	Stratgene
PRECISOR High-Fidelity DNA Polymerase	Biocat
QuikChange Mutagenesis Kit	Stratagene
Quick Ligation Kit	New England Biolabs
Restriction endonucleases	New England Biolabs
T4 DNA Ligase	New England Biolabs
<i>Taq</i> DNA Polymerase	New England Biolabs

2.1.2 Restriction enzymes

Table 2.1. Restriction endonucleases (RE) used in this work. Position of cleavage indicated by /, BSA = bovine serum albumin.

Enzyme name	DNA target	Buffer NEB	Incubation temperature (°C)
<i>AclI</i>	AA/CGTT	4+BSA	37
<i>AflIII</i>	C/TTAAG	4+BSA	37
<i>AgeI</i>	A/CCGGT	1	37
<i>AgeI</i> -HF	A/CCGGT	4+BSA	37
<i>AscI</i>	GG/CGCGCC	4	37
<i>BamHI</i>	G/GATCC	3+BSA	37
<i>BglII</i>	A/GATCT	3	37
<i>BlpI</i>	GC/TNAGC	4	37
<i>BssHIII</i>	G/CGCGC	3	50
<i>BtsI</i>	GCAGTG(2/0)	4 + BSA	55
<i>DpnI</i>	GA/TC	4	37
<i>EarI</i>	CTCTTC(1/4)	4	37
<i>EcoRI</i>	G/AATTC	EcoRI Buffer	37
<i>EcoRI</i> -HF	G/AATTC	4	37
<i>EcoRV</i>	GAT/ATC	3+BSA	37
<i>HindIII</i>	A/AGCTT	2	37
<i>KpnI</i>	GGTAC/C	1+BSA	37
<i>KpnI</i> -HF	GGTAC/C	4	37
<i>MfeI</i>	C/AATTG	4	37
<i>MfeI</i> -HF	C/AATTG	4	37
<i>NdeI</i>	CA/TATG	4	37
<i>NheI</i>	G/CTAGC	4	37
<i>NheI</i> -HF	G/CTAGC	4+BSA	37
<i>NotI</i>	GC/GGCCGC	3+BSA	37
<i>PflMI</i>	CCANNNN/NTGG	3+BSA	37
<i>PmeI</i>	GTTT/AAAC	4+BSA	37
<i>PmlI</i>	CAC/GTG	1+BSA	37
<i>RsrII</i>	CG/WCCG	4	37
<i>SacI</i>	GAGCT/C	4 + BSA	37
<i>SacI</i> -HF	GAGCT/C	4 + BSA	37
<i>SacII</i>	CCGC/GG	4	37
<i>Sall</i>	G/TCGAC	3+BSA	37
<i>Sall</i> -HF	G/TCGAC	4	37
<i>SgrAI</i>	CR/CCGGYG	4	37
<i>SpeI</i>	A/CTAGT	4 + BSA	37
<i>XcmI</i>	CCANNNNN/NNNNTGG	2	37
<i>XhoI</i>	C/TCGAG	4+BSA	37

2.1.3 Oligonucleotides

Table 2.2 gives an overview of the sequences of oligonucleotides used in this work. All residue numbers refer to the amino sequence of rabbit α_{1S} (GenBank/EMBL/DBJ accession no. X05921).

Table 2.2. Primer-oligonucleotides used in this work. Sequences are given in 5' to 3' direction.

Primer name	Sequence
Fw. CyPet/YPet Age I	CTGCAGTCGACGGTACC
Rev. CyPet Bgl II	CGAGATCTTTTGTACAGTTCGTCCATGC
Rev. YPet Bgl II	CGAGATCTTTTATAGAGCTCGTTCATGC
Rev. CyPet NotI	GTGCGGCCGCTTATTTGTACAGTTCGTCCATGC
Rev. YPet NotI	GTGCGGCCGCTTACTTATAGAGCTCGTTCATGC
FWQC AgeI pos.1636 α_{1S}	GCTGAGATAGAAATGGAACCGGTTGAGTCGCCTG
RVQC AgeI pos.1636 α_{1S}	CAGGCGACTCAACCGGTTCCATTTCTATCTCAGC
FWQC KpnI pos.1666 α_{1S}	CCAATGCCAAGGTACCTATGGCAACAGCAACC
RVQC KpnI pos.1666 α_{1S}	GGTTGCTGTTGCCATAGGTACCTTGGCATTGG
FW Dom.II-III AgeI	GCACCGGTTATGGTCTTCTACTGGCTGGTCATCCTG
Rev Dom.II-III KpnI	CCTGGGTACCCTAGATGACAAAGCCACAAAGATGTTC
Norm Tail dysp Fw.	GGACTGGCAAGAGGACCGGAGC
Norm Tail dysp Rev.	GGAAGCCAGGGCTGCAGGTGAGC
DyspTail Fw.	GGACTGGCAAGAGGACCGGAGC
DyspTail Rev.	CCTGAAGAACGAGATCAGCAGCCTCTGTCCC
Dysg. Skmouse Fw.	GGCATGCAGATGTTTCGGGAAGATC
Dysg. mdg II Rev.	GCAGCTTCCACTCAGGAGGGATCCAGTGT
QCFw-AclI-1/2 pos.350	CAAGTCCAGGGGAACGTTCCAGAAGCTGC
QCRev-AclI-1/2 pos.350	GCAGCTTCTGGAACGTTCCCCTGGACTTG
QCFw-AscI-3/4 pos.1096	GTATGCCCTGAAGGCGCGCCCACTTCGGTG
QCRev-AscI-3/4 pos.1096	GCACCGAAGTGGGCGCGCCTTCAGGGCATAAC
QCFw-PmeI-1/2 pos.406	CGAAATCGAGGGTTTAAACAAAATCATCC
QCRev-PmeI-1/2 pos.406	GGATGATTTTGTTTAAACCCTCGATTTTCG
FW N-term AgeI	GAACCGGTCATGGAGCCATCCTCACCCAG
Fw-sm-SpeI-pos.728	CGATGAGTTCGAAACTAGTGTCAACGAGG
Rev-sm-SpeI-pos.728	CCTCGTTGACACTAGTTTCGAACTCATCG
Fw-SpeI-Y	CTGAACTAGTCCGATGGTGAGCAAAGGCCAAGAGC
Rev-SpeI-Y	GTCTACTAGTCGACTTATAGAGCTCGTTCATGCCCTCG
Fw-SpeI-Cy	CTGAACTAGTCCGATGGTGAGCAAAGGGAGAGGAAC
Rev-SpeI-Cy	GTCTACTAGTCGATTTGTACAGTTCGTCCATGCCGTGG
Fw-AclI-Cy	CTGAAACGTTTCATGGTGAGCAAAGGGAGAGGAAC
Rev-AclI-Cy	GTCTAACGTTTCGTTTGTACAGTTCGTCCATGCCGTGG
Fw-AclI-Y	CTGAAACGTTTCATGGTGAGCAAAGGCCAAGAGC
Rev-AclI-Y	GTCTAACGTTTCGTTTATAGAGCTCGTTCATGCCCTCG
Fw-AscI-Cy	CAGGCGCGCCTGATGGTGAGCAAAGGGAGAGGAAC
Rev-AscI-Cy	GAGGCGCGCCGATTTGTACAGTTCGTCCATGCCGTGG
Fw-AscI-Y	CAGGCGCGCCTGATGGTGAGCAAAGGCCAAGAGC
Rev-AscI-Y	GAGGCGCGCCGACTTATAGAGCTCGTTCATGCCCTCG
Fw-PmeI-Y	CTGAGTTTAAACATGGTGAGCAAAGGCCAAGAGC
Rev-PmeI-Y	CTGGTGTTTAAACGCTTATAGAGCTCGTTCATGCCCTCG

2.1.4 Bacterial strain and plasmids

Bacterial strain

Throughout this work *Escherichia coli* (*E. coli*) strain DH5 α (Genotype F-1-*supE44D(argF-lac) U169 j80dlacZ Δ M15 hsdR17 recA1 endA1 gyrA96 thi-1relA1*) was used for standard plasmid growth and maintenance (Sambrook *et al.*, 1989).

Plasmids used for cloning and expression

The mammalian expression vectors encoding the fluorescent proteins CyPet and YPet (pCyPet and pYPet, kindly provided by Dr. Patrick S. Daugherty, University of California, Santa Barbara) and the vectors pECFP-C1, and pECFP-N1 (Clontech, Palo Alto, CA) served as templates for cloning.

2.2 Molecular biological techniques

2.2.1 PCR

PCR conditions were optimized with respect to annealing temperature for the primers while the magnesium concentration was kept constant for all PCRs. Examples of typical reaction mixes and of the PCR protocols applied are given below. PCR products obtained by amplification using either *Taq* DNA polymerase or PRECISOR High-Fidelity DNA Polymerase were either ligated directly into vectors; However, prior purification of the PCR product from the PCR reaction mix by gel separation or by the use of direct DNA clean-up systems considerably increased the percentage of colonies containing the correct insert. The gel electrophoresis step also served as control to check for the correct size of the PCR product. Electrophoresis was performed using 1-2 % agarose gels stained with ethidium bromide. The appropriate DNA bands – as judged by their size – were cut out and the DNA was extracted from the gel using the NucleoSpin Extract II-kit (Macherey-Nagel, see section 2.2.6) following the manufacturer's protocol.

PCR mixture protocol

40.3µl ddH₂O
 5µl 10 × Thermo Pol buffer + 15 mM MgCl₂
 1.2µl dNTP mix
 1µl template DNA (50 µM)
 1µl Primer fw (25 µM)
 1µl Primer rev (25 µM)
 1µl *Taq* DNA polymerase

Standard PCR protocol

Initial denaturation	94 °C for 2:00	
Denaturation	94 °C for 0:30	} 27 ×
Annealing	59 °C for 0:45	
Elongation	72 °C for 0:50	
Final elongation	72 °C for 7:00	
Cooling	4 °C for ∞	

PRECISOR PCR mixture protocol

34µl ddH₂O
 10µl 5 × High Fidelity buffer
 2µl dNTP mix
 1µl template DNA (50 µM)
 1µl Primer fw (25 µM)
 1µl Primer rev (25 µM)
 1µl PRECISOR High-Fidelity DNA polymerase

PRECISOR PCR protocol to multiply the full-length α_{1S} sequence

Initial denaturation	98 °C for 2:00	
Denaturation	98 °C for 0:30	} 30 ×
Annealing	60 °C for 0:45	
Elongation	72 °C for 3:00	
Final elongation	72 °C for 7:00	
Cooling	4 °C for ∞	

2.2.2 Site-directed mutagenesis

To obtain unique restriction sites within sequence regions corresponding to intracellular domains of the skeletal muscle α₁ subunit, site-directed mutagenesis was performed according to the manufacturer's protocol (Stratagene QuikChange site-directed mutagenesis kit). An example of the reaction mix and the used QuikChange (QC) PCR protocol are listed below.

QuikChange PCR mixture protocol

39µl ddH₂O
 5µl 10 × Reaction buffer
 2µl dNTP mix
 1µl template DNA (50 µM)
 1µl Primer fw (25 µM)
 1µl Primer rev (25 µM)
 1µl *PfuTurbo* DNA polymerase (2.5 U)

QuikChange PCR protocol

Initial denaturation	95 °C for 0:30	} 18 ×
Denaturation	95 °C for 0:30	
Annealing	53 °C for 1:00	
Elongation	68 °C for 13:00	
Final elongation	68 °C for 7:00	
Cooling	4 °C for ∞	

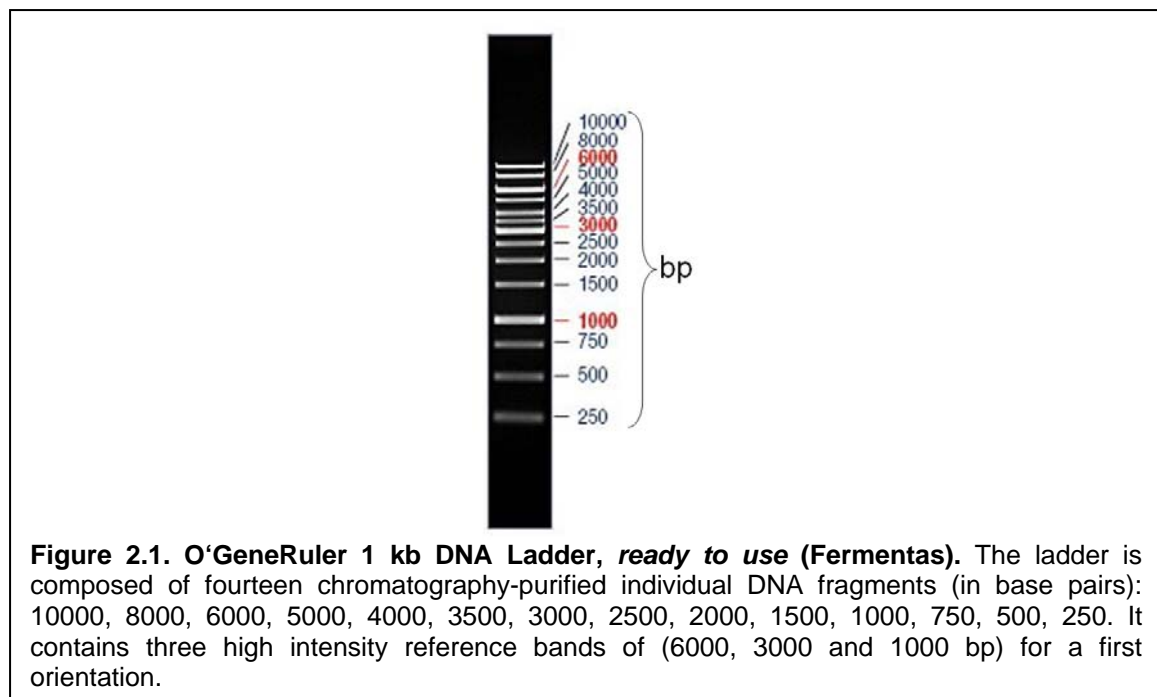
2.2.3 Restriction digest

Digestion of plasmid DNA or PCR-fragments with the appropriate restriction enzymes (Table 2.1) was performed in a final volume of 60 µl for 1-2 h at 37 °C, unless otherwise indicated. In most of the cases, two restriction enzymes were required to remove the sequence of an insert from the donor plasmid. Where possible, a reaction buffer was chosen which allowed for simultaneous usage of both enzymes at the same time (double digest). Shown below is such an example.

1. In a 0.5 ml microcentrifuge tube, add:
 - 3 µg cDNA
 - 6 µl 10 × buffer (NEB)
 - 2 µl Enzyme 1
 - 2 µl Enzyme 2 (if necessary)
 - add sterile water to final total volume of 60 µl
 - Mix well and centrifuge briefly.
2. Incubate at the recommended temperature (usually 37 °C) for 1-2 h.

In the rare cases where either the enzyme buffers or the incubation temperature for the two restriction enzymes were incompatible, sequential digests were run. Table 2.1 gives an overview of restriction enzymes used in the present work.

Subsequent to restriction, agarose gel electrophoresis was used to separate the DNA-fragments (details, see section 2.2.5). The DNA-fragment size standard used in all electrophoretic runs was the “O’GeneRuler 1 kb DNA Ladder from Fermentas (Figure 2.1). After electrophoretic separation, the DNA bands of interest were extracted from the gel as described in section 2.2.6.



2.2.4 Dephosphorylation of DNA

In order to prevent recyclisation of linearized vector DNA, Calf Intestinal Alkaline Phosphatase (CIP) was applied, catalyzing the release of 5’- and 3’-phosphate groups of DNA. The protocol for dephosphorylation was as according to manufacturer's recommendation.

2.2.5 Agarose gel electrophoresis

Agarose gel electrophoresis of DNA was performed to separate and to identify DNA fragments. Agarose gels were run in TAE buffer and were prepared by dissolving 1.0-2.0 % agarose (w/v) and 0.005 % ethidium bromide (v/v) in 1 × TAE buffer (Roth). Samples containing an appropriate amount of DNA were mixed with 6 × DNA Loading Dye (Fermentas) prior to sample application. Gels were run at 60 V - 120 V for a time period sufficiently long to allow for complete separation of DNA fragments. DNA bands were visualized by their fluorescence under excitation of the bound Ethidium bromide with UV light (312 nm).

2.2.6 Purification of DNA fragments

For the purification of DNA fragments after PCR amplification or after digestion with restriction endonucleases, the NucleoSpin Extract II-kit (Macherey and Nagel) was used, according to the manufacturer's manual.

2.2.7 Ligation of DNA fragments

Linearized vector DNA and PCR-derived DNA fragments were prepared as described above and were ligated using the Quick Ligation Kit (NEB). In accordance with the manufacturer's protocol, 50 ng of vector DNA were used in each ligation reaction, whereby the molar ratio of vector-to-insert was set to 1:3. The volume was adjusted to 10 µl with ddH₂O. Afterwards, 10 µl of 2X Quick Ligation Buffer and 1 µl of Quick T4 DNA Ligase were added. Subsequent to incubation of the reaction mixture for 10-15 min at room temperature, 10 µl of the ligation reaction were used to transform chemically competent *E. coli* DH5α cells (section 2.2.10). After transfection, the entire medium volume containing the bacteria was plated on agar plates containing the appropriate antibiotic.

2.2.8 Culture growth

E. coli-cultures were cultivated over night in Luria Bertani (LB) medium at 37 °C and under vigorous shaking at 200 rpm. Here too, antibiotics provided appropriate selection conditions. The following final concentrations of antibiotics were used: Ampicillin, 100 µg/ml; Kanamycin, 50 µg/ml.

LB Medium

Casein peptone (tryptic) 1.0 % (w/v)
Yeast extract 0.5 % (w/v) and
NaCl 1.0 % (w/v)
Agar plates additionally contained 1.5 % (w/v) Agar-Agar (Roth).

2.2.9 Preparation of chemically competent *E. coli*

To prepare chemically competent *E. coli*, a small amount of the required *E. coli* strain was incubated over night in 2.5 ml SOB media at 37 °C under vigorous shaking. The overnight culture was then transferred to 250 ml SOB media, resulting in a 1:100 dilution, and the flask was incubated on a platform shaker at 200 rpm at 37 °C until the bacterial culture reached an OD₆₀₀ between 0.4 and 0.6. Cells were then pelleted in sterile centrifuge tubes by centrifugation at 2,500 x g for 10 min at 4 °C, the supernatant was decanted and the cell pellet was gently resuspended in 20 ml of ice-cold standard transformation buffer (TFB). After subsequent incubation of the resuspended cells on ice for 10 min a second centrifugation step followed at 2,500 x g for 10 minutes at 4 °C. The resultant cell pellet again was gently resuspended in 20 ml of ice-cold TFB. After addition of 1.4 ml of DMSO cells were further incubated on ice for 10 min and 200 µl aliquots were prepared and stored at -80 °C.

SOB medium

Casein peptone (tryptic) 2 % (w/v)
Yeast extract 0.5 % (w/v)
KCl 2.5 mM
NaCl 10 mM
MgSO₄ 10 mM
MgCl₂ 10 mM

TFB buffer

Hepes	10 mM
CaCl ₂	15 mM
KCl	30 mM
MnCl ₂	55 mM

(pH 6.7 titrated with acetic acid)

2.2.10 Transformation of chemically competent *E. coli*

For the transfer of DNA plasmids into chemically competent *E. coli*, the bacteria were thawed by incubating them on ice for ~14 min. In all cases where DNA from plasmid preparations was to be transferred, 200 µl of thawed *E. coli* cells were mixed with 100 ng of plasmid DNA which was prepared as described in section 2.2.7. When DNA from ligation reactions was used for transfection, 12 µl of the ligation reaction mixture were combined with 200 µl of thawed, chemically competent *E. coli*. The bacteria were then incubated on ice for 30 min. In order to provide the heat shock required for transfection, the microcentrifuge tube containing the bacteria was submerged into 42 °C warm water for 45 sec. and was afterwards placed on ice for 2 min. After the addition of 500 µl SOC medium, the cells were incubated for 60 min at 37 °C and 200 rpm. Then, a volume of 200 µl to 500 µl of the SOC medium containing the bacteria was plated per agar plate (containing the appropriate antibiotic) and the plates were incubated overnight at 37 °C.

SOC medium

Casein peptone (tryptic)	2 % (w/v)
Yeast extract	0.5 % (w/v)
KCl	2.5 mM
NaCl	10 mM
MgSO ₄	10 mM
MgCl ₂	10 mM
Glucose	20 mM

SOC medium was prepared without addition of Glucose and autoclaved at 121 °C for 20 min. Immediately before use, a volume of 20 ml/l of a 1 M glucose-solution was added to achieve a final glucose concentration of 20 mM. pH adjustment was not necessary, since in repeated measurements and the pH ranged between 6.8 to 7.0.

2.2.11 Preparation of plasmid DNA

After transformation and overnight growth of the bacteria streaked on agar plates, single colonies were picked and were grown in LB medium containing the appropriate antibiotic for 8~12 hours at 37 °C. Plasmid DNA was isolated from these cultures using the peqGOLD Plasmid Miniprep Kit I (Peqlab), which is based on the commonly used alkaline lysis method (Sambrook and Russell, 2001).

2.2.12 Restriction digests

All newly created constructs were subjected to restriction analysis to verify presence and correct orientation of the cloned insert. The protocol shown below gives a representative example of a diagnostic restriction digest.

1. In a 0.5 ml microcentrifuge tube, add:
 - 3 μ l DNA (eluate)
 - 2 μ l 10 \times buffer
 - 0.5 μ l Enzyme 1
 - 0.5 μ l Enzyme 2
 - add sterile water to final total volume of 20 μ l
 - Mix well and centrifuge briefly.
2. Incubate at the recommended temperature (depending on the enzyme used, usually 37 °C) for 10-20 min.

Upon digestion, the DNA fragments in the reaction mixture were fractionated electrophoretically using 1-2 % agarose gels. The DNA band pattern was recorded by taking digital images. The DNA was visualized via fluorescence excitation by illumination with UV light (312 nm). The “O’GeneRuler™ 1 kb DNA Ladder, ready to use” was applied as a size standard (Figure 2.1).

In addition to restriction analysis, a further control for all new constructs containing a fluorescent protein sequence was to express them in tsA-201 cells and to check for presence of fluorescence (see section 2.4.1). In doubly labelled α_{1S} constructs, co-localization of CyPet and YPet fluorescence, as well as the exclusive association with an intracellular network (α_{1S} expressed in tsA-201 is associated with the ER) confirmed the integrity of the protein. In these controls, tsA-201 cells were examined 24 h after transfection using the FV1000 confocal laser-scanning microscope (Olympus)

2.2.13 Determination of DNA concentration in aqueous solution

DNA concentrations were determined spectrophotometrically by measuring the absorption at 260 nm ($A_{260} = 1.0$ corresponds to 50 $\mu\text{g/ml}$ ds DNA) and by correcting for the dilution factor (usually 1:50 in ddH₂O). The purity of the preparation was evaluated by the absorption ratio of A_{260}/A_{280} (Sambrook *et al.* 1989). Only DNA preparations with absorption ratios >1.8 were used for the experiments.

2.3 Generation of cDNA constructs for cellular expression

Figure 2.2 shows cartoons of the doubly tagged α_{1S} constructs used in this study. The constructs contain the FRET partners CyPet and YPet at defined sites within the protein sequence.

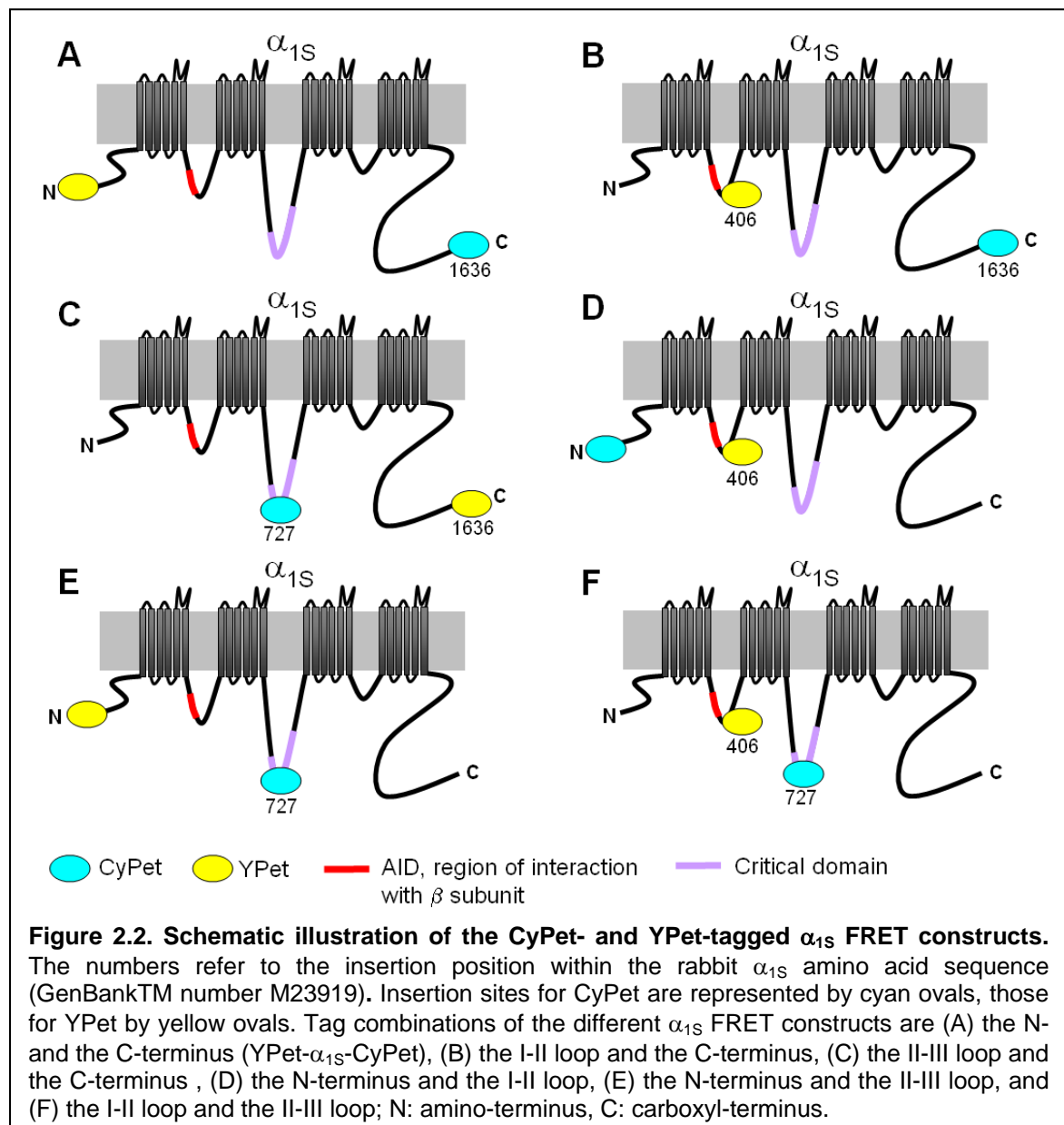
2.3.1 Generation of fluorescent protein vectors

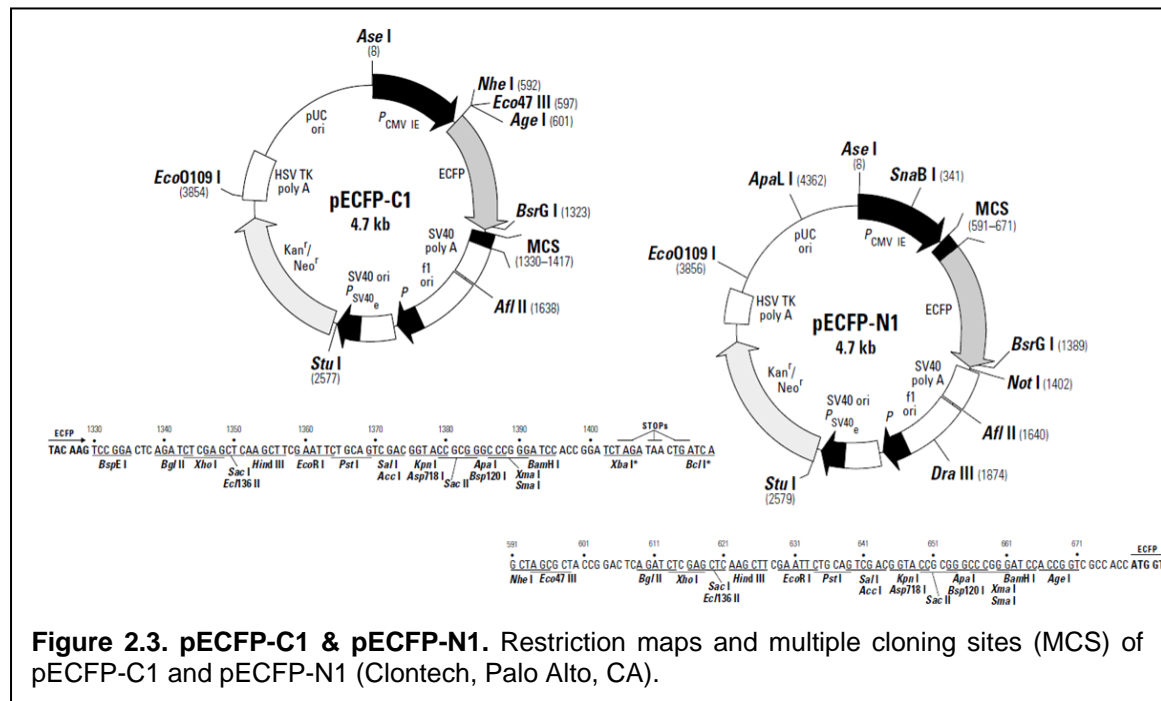
pCyPet-C1, pYPet-C1, pCyPet-N1, pYPet-N1 Mammalian expression plasmids encoding the ‘Cyan / Yellow fluorescent Protein for energy transfer’ (CyPet & YPet, respectively) (Nguyen & Daugherty 2005) served as templates and were kindly provided by Dr. Patrick S. Daugherty, University of California, Santa Barbara.

First, flanking recognition sites for *AgeI* (5') and *BglII* (3') were added to the coding sequences of CyPet and YPet by standard PCR using the following primers. For both, CyPet and YPet the same forward primer was used, (fw) 5'-CTG CAG TCG ACG GTA CC-3'. The reverse primer (rev) for CyPet was 5'-CGA GAT CTT TTG TAC AGT TCG TCC ATG C-3' and rev for YPet was 5'-CGA GAT CTC TTA TAG AGC TCG TTC ATG C-3'. The *AgeI-BglII* fragment was ligated into *BglII* treated pECFP-C1 (Clontech, Palo Alto, CA; Figure 2.3) to create the vectors pCyPet-C1 and pYPet-C1.

To receive pCyPet-N1 and pYPet-N1, both having a TAA stop codon right behind the triplet encoding the terminal residue K²³⁹, flanking recognition sites for *AgeI* (5') and *NotI* (3') were added to the coding sequences of CyPet and YPet using PCR with the following primers. The same forward primer was used for both CyPet and YPet, (fw) 5'-CTG CAG TCG ACG GTA CC-3'. For CyPet, (rev) was 5'-GTG CGG CCG CTT ATT TGT ACA GTT CGT CCA TGC-3' and for YPet (rev) was 5'-GTG CGG CCG CTT ACT TAT

AGA GCT CGT TCA TGC -3'. Upon digest of the PCR products with *AgeI* and *NotI* to produce overhangs, the fragments were ligated into *AgeI* / *NotI* digested pECFP-N1 (Clontech, Palo Alto, CA) to create the vectors pCyPet-N1 and pYPet-N1.





2.3.2 Generation of fluorescently tagged rabbit skeletal muscle α_{1S}

2.3.2.1 N-terminal labelled α_{1S}

CyPet- / YPet- α_{1S} (XPet- α_{1S})

The coding sequence for rabbit skeletal muscle α_{1S} (GenBankTM number M23919) was excised from its original vector (Grabner *et al.* 1998) using a *SalI* site immediately before the ATG start codon and a *SalI* site at nucleotide 5581 (immediately after amino acid Q¹⁸⁶⁰ of α_{1S} , where 1,873 is full-length), and was inserted into the multiple cloning site of the *SalI*-digested pEYFP-C1 (or pEYFPN1) to create the N-terminally labelled fusion protein YFP- α_{1S} (Papadopoulos *et al.* 2004). To transfer the α_{1S} sequence into the CyPet and YPet expressions plasmids, the *SalI-SalI* fragment was excised from YFP- α_{1S} and the α_{1S} encoding sequence was inserted into the multiple cloning site of *SalI*-digested pCyPet-C1 (or pYPet-C1). The constructs manufactured this way were the N-terminally labelled fusion proteins CyPet- α_{1S} and YPet- α_{1S} .

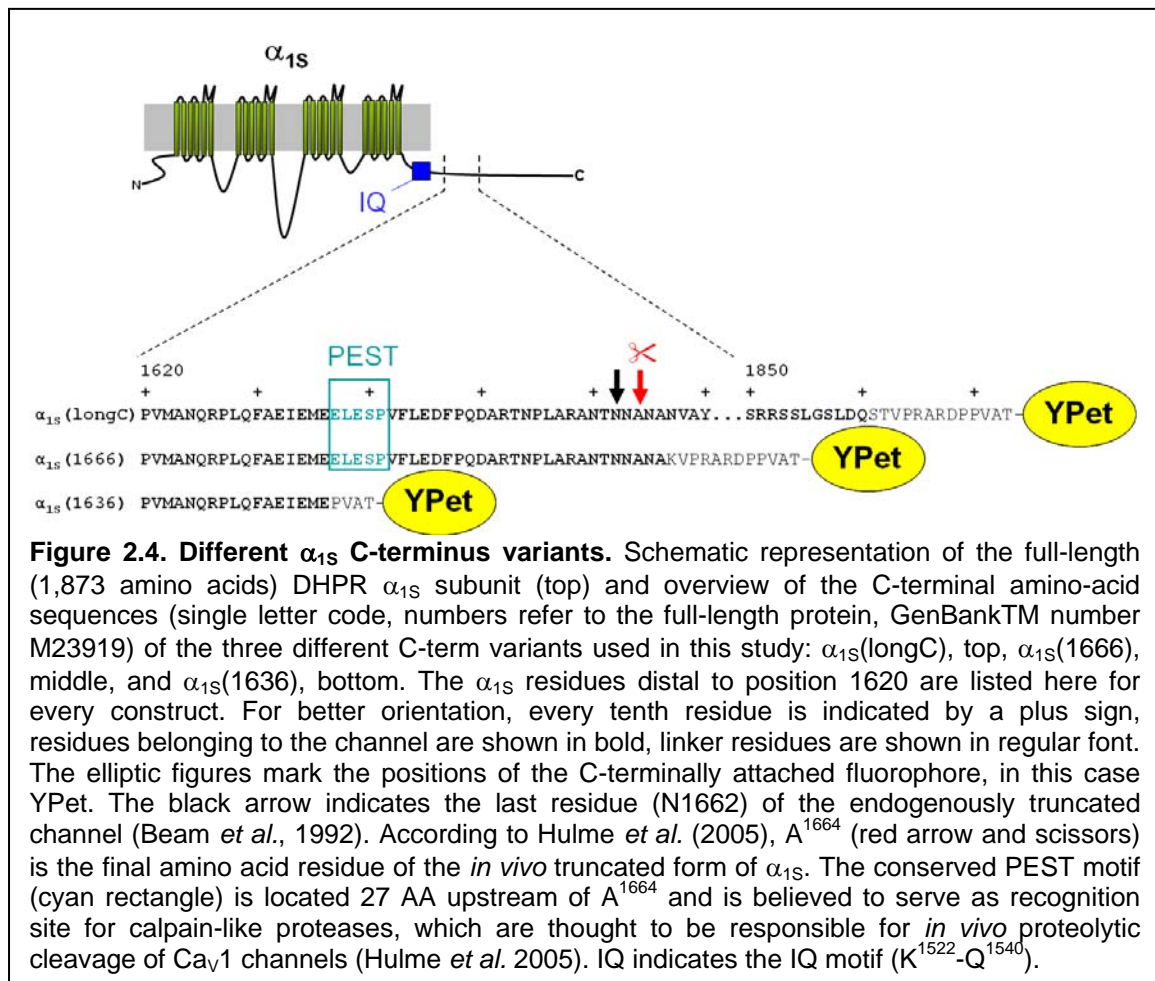
2.3.2.2 C-terminally labelled α_{1S}

Figure 2.4 gives a schematic overview of the three different, C-terminally labelled α_{1S} constructs used in this study. Three cDNA sequences, encoding α_{1S} subunits differing in

length with respect to the number of carboxyl-terminal residues (i.e. ending at residue Q¹⁸⁶⁰ / A¹⁶⁶⁶ / E¹⁶³⁶, respectively) were ligated to the N-terminal site of the CyPet / YPet sequence as follows.

α_{1S} (longC)-CyPet and α_{1S} (longC)-YPet

To yield α_{1S} (longC)-CyPet /-YPet, the *SalI*-*SalI* fragment of YPet- α_{1S} containing the α_{1S} coding sequence was inserted into the multiple cloning site of the *SalI*-digested pCyPet-N1 (or pYPet-N1), resulting in the creation of the C-terminally labelled fusion proteins α_{1S} (longC)-CyPet and α_{1S} (longC)-YPet. The introduced C-terminal *SalI* site erased the TGA stop codon of α_{1S} wild-type sequence while allowing in-frame ligation into the pCyPet-N1 or pYPet-N1 expression plasmid. At the protein level, a 12 residue linker (STVPRARDPPVAT), resulting from translation of the mcs region, separated the two proteins.



$\alpha_{1S}(1666)$ - CyPet and $\alpha_{1S}(1666)$ -YPet

To obtain a plasmid for expression of fluorescently labelled α_{1S} with moderate C-terminal truncation, $\alpha_{1S}(1666)$, a second *KpnI* site was introduced into sequence of α_{1S} (long C)-YFP by site directed mutagenesis, altering the wild-type α_{1S} sequence from ⁴⁹⁹⁹AATGTTGCC to ⁴⁹⁹⁹AAGGTACC. Digestion with *KpnI* then removed the cDNA encoding the α_{1S} residues distal to residue 1666. Upon this excision, the plasmid was religated, yielding the expression plasmid (α_{1S} (shortC)-YFP) (Papadopoulos *et al.* 2004). The YFP sequence was then replaced by the CyPet / YPet sequence by cutting the plasmids $\alpha_{1S}(1666)$ -YFP and CyPet-N1 (or YPet-N1) with *AgeI* and *MfeI*, and ligating the fragment containing $\alpha_{1S}(1-1666)$ to the one carrying the CyPet-N1 (YPet-N1) sequence, giving $\alpha_{1S}(1666)$ -CyPet / -YPet. In the corresponding proteins, α_{1S} was attached to the dyes via a 12-residue linker (amino acid sequence KVPRARDPPVAT).

 $\alpha_{1S}(1636)$ -CyPet and $\alpha_{1S}(1636)$ -YPet

To label the C-terminus of α_{1S} right behind glutamic acid 1636, an *AgeI* site was introduced at the corresponding region, changing the wild-type α_{1S} sequence ⁴⁹⁰⁵GGAAGAGCTT to ⁴⁹⁰⁵GGAACCGGTT. The primers used for this maneuver were *AgeI* (fw) 5'-GCT GAG ATA GAA ATG GAA CCG GTT GAG TCG CCT G-3' and *AgeI* (rev) 5'-CAG GCG ACT CAA CCG GTT CCA TTT CTA TCT CAG C-3'. After digestion with *AgeI* and *MfeI* to remove the sequence encoding the α_{1S} part distal to 1636, the plasmid was ligated to the 0.8 kb *AgeI*-*MfeI* fragment of pCyPet-N1 (or pYPet-N1), creating the α_{1S} -(1636)-CyPet /-YPet expression vector.

YPet- $\alpha_{1S}(1636)$ -CyPet / CyPet- $\alpha_{1S}(1636)$ -YPet

To generate doubly labelled α_{1S} , the constructs described above, α_{1S} -(1636)-CyPet (or α_{1S} -(1636)-YPet), were opened with *NdeI* and *SacII* immediately 5' to the α_{1S} cDNA and were ligated with the 1.2 kb *NdeI*-*SacII* fragment excised from YPet- α_{1S} (or CyPet- α_{1S} ; see section 2.3.2.1).

2.3.2.3 Insertion of CyPet or YPet into cytoplasmic α_{1S} loops

Intercalative incorporation of the CyPet and YPet sequence at defined α_{1S} positions was performed after generation of appropriate restriction sites using silent site directed mutagenesis. In addition, two expression plasmids were used here, which had been generated in a previous study (Papadopoulos *et al.* 2004). These were, α_{1S} (domainI–II)-CFP-YFP and α_{1S} (domainIII-IV), which encode α_{1S} repeats I & II, and III & IV, respectively. A third expression plasmid was generated, which encoded domains II and III (α_{1S} (domainII-III)), by first introducing into the α_{1S} sequence flanking recognition sites for *AgeI* (including an ATG codon, 5') immediately before the sequence encoding Domain II, and for *KpnI* (including a TAG stop codon, 3') at nucleotide 3195 (immediately after I¹⁰⁶⁵ of α_{1S}). In this procedure, a PRECISOR PCR protocol was used, with the primers being (fw) 5'-GCA CCG GTT ATG GTC TTC TAC TGG CTG GTC ATC CTG-3' and (rev) 5'-CCT GGG TAC CCT AGA TGA CAA AGC CCA CAA AGA TGT TC-3'. The *AgeI-KpnI* fragment, containing the coding sequence for domains II and III of α_{1S} , was ligated to the CyPet-C1 vector that had been opened with the same restriction enzymes. In doing so, the CyPet sequence was replaced by the PCR fragment. Figure 2.5 illustrates the cloning procedure for the introduction of CyPet or YPet into defined cytoplasmic α_{1S} loops. The three two-domain expression plasmids (i.e., α_{1S} (domainI–II)-CFP-YFP, α_{1S} (domainII-III), and α_{1S} (domainIII-IV), Figure 2.5 A-C top left) served as a starting point for the additional insertion of CyPet and / or YPet into cytoplasmic loops. First, single recognition sites were introduced into the two domain α_{1S} constructs mentioned above, at sequence regions corresponding to cytoplasmic α_{1S} domains (*PmeI* or *AcII* for the I-II-loop, *SpeI* for the II-III-loop and *AscI* for the III-IV-loop; Figure 2.5 A-C top right). Corresponding recognition sites were then also added to the ends of CyPet and / or YPet cDNA by standard PCR, and after digestion to generate sticky ends the fragments were placed into the introduced restriction sites within the α_{1S} sequence (Figure 2.5 A-C middle left). The α_{1S} sequence of the recipient vector encompassing the inserted dye sequence was then excised via cut at two flanking recognition sites (*XcmI* for the I-II-loop, *BlpI* for the II-III-loop, and *PmlI* for the III-IV-loop, Figure 2.5 A-C middle right), and these fragments were ligated into the corresponding recipient α_{1S} expression vectors which had been opened either

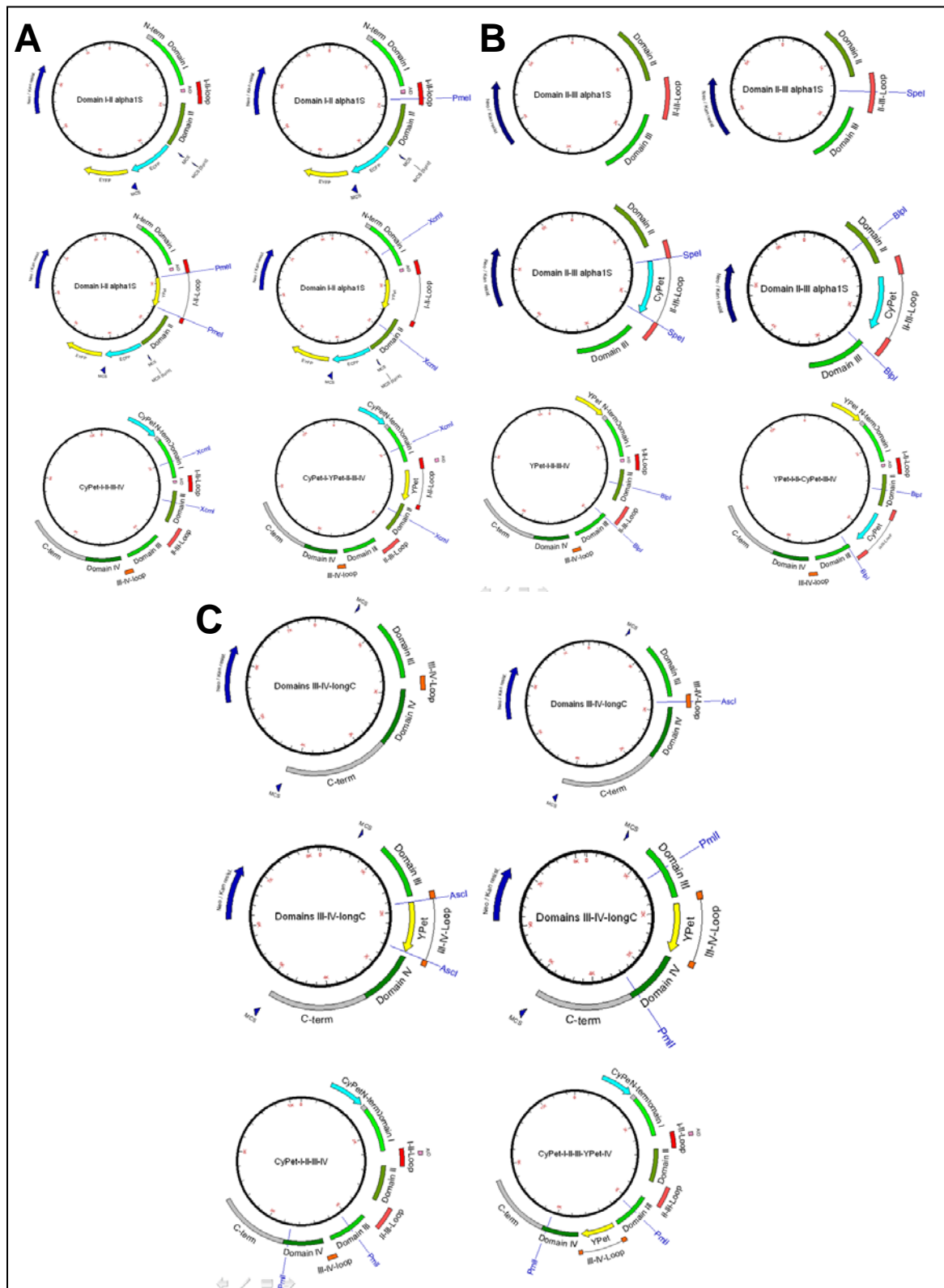
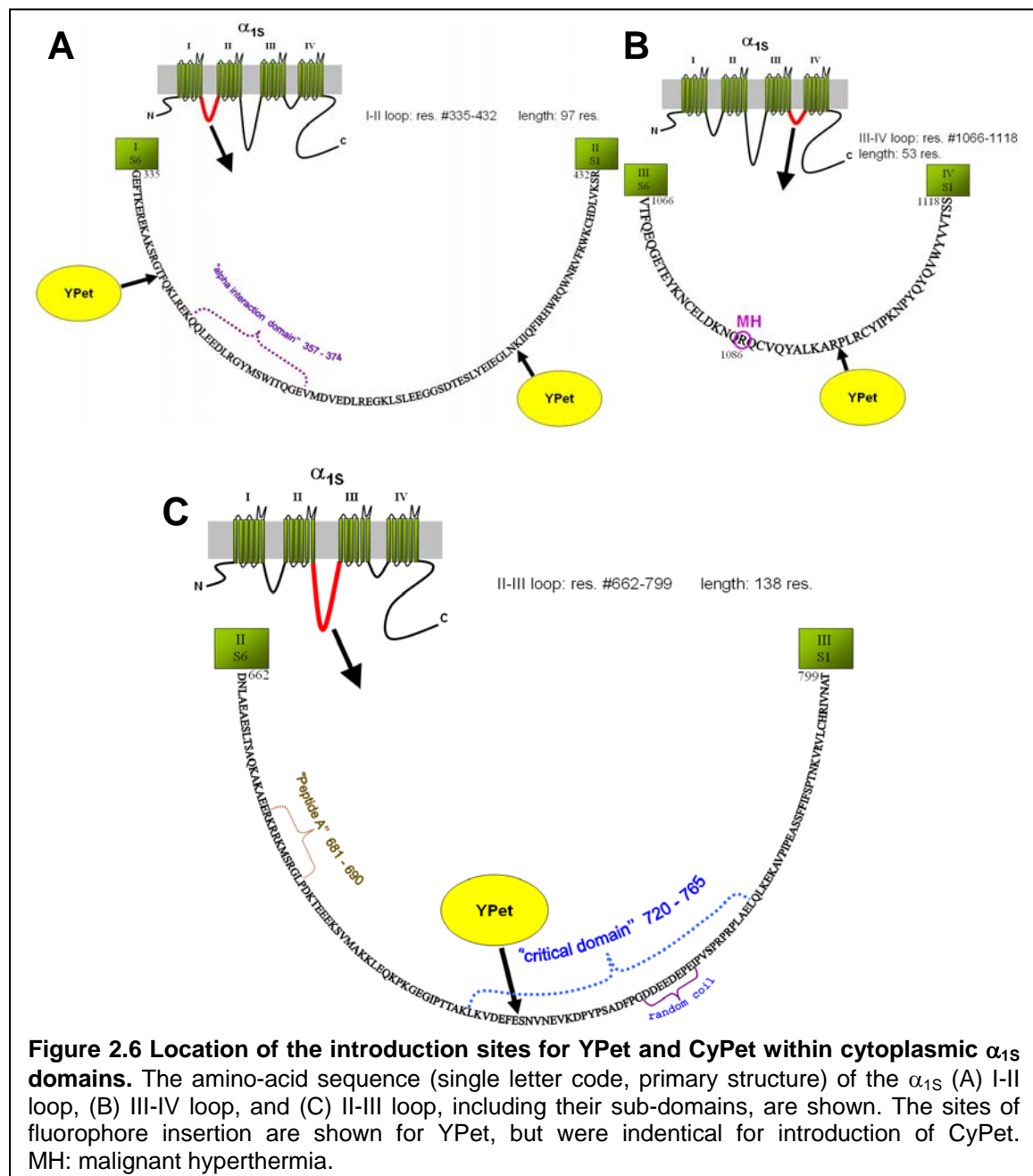


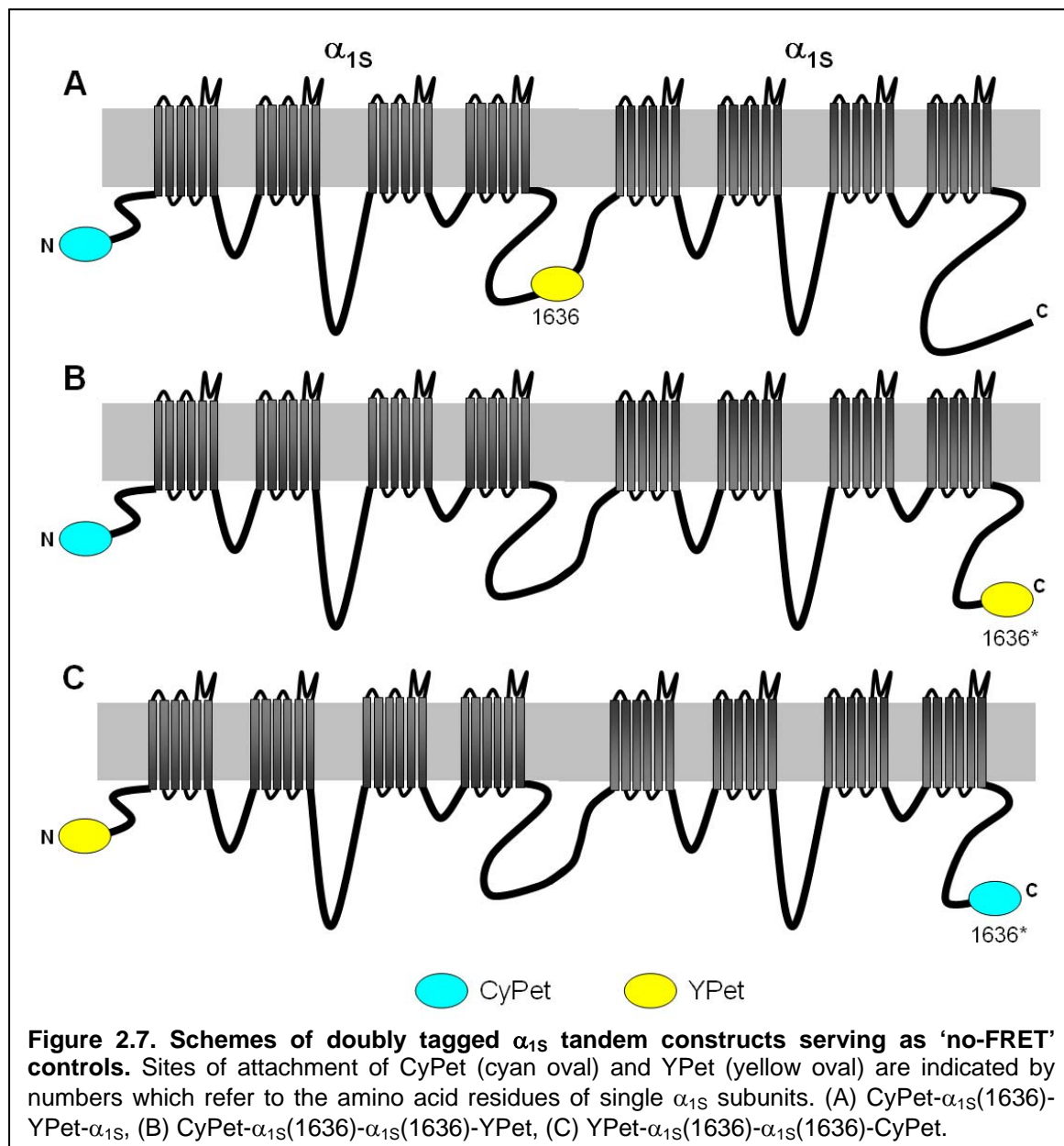
Figure 2.5. Introducing YPet or CyPet into the α_{1S} I-II loop (A), II-III loop (B) and III-IV loop (C). Schematic overview of the output vectors for the construction of α_{1S} constructs with FRET partners located at defined cytoplasmic domains, see text for details.

with *XcmI*, *BlnI*, or *PmlI*. In cases in which these recipient vectors already contained the sequence of the FRET partner at a different position, this procedure resulted in generation of the complete construct for FRET measurements (Figure 2.5 A-C bottom). Using this modular way of cloning, fluorophores were introduced into following α_{1S} positions: within I-II loop, at residue 350 or 406; within II-III loop, at residue 727; within III-IV loop, at residue 1096 (Figure 2.6).



2.3.2.4 Generation of ‘no-FRET’ control constructs

Three different CyPet- & YPet-tagged tandem- α_{1S} constructs (Figure 2.7) served as ‘no-FRET’ control constructs. In these, the fluorescent tags were far enough from each other to exclude the occurrence of significant energy transfer.



CyPet- α_{1S} (1636)-YPet- α_{1S} -long-C-term

Both, YPet- α_{1S} and CyPet- α_{1S} , contain a unique *AgeI* restriction site N-terminally to the dye sequence. After introduction of an additional *AgeI* site into CyPet- α_{1S} at nucleotide 4907 (immediately behind E¹⁶³⁶ of α_{1S} , see section 2.3.2.2), and after digest with the product with *AgeI*, the fragment containing the CyPet- α_{1S} (1636) sequence was ligated 5' to the YPet sequence of the YPet- α_{1S} -vector after the latter had been opened with *AgeI*.

CyPet- α_{1S} (1636)- α_{1S} (1636)-YPet / YPet- α_{1S} (1636)- α_{1S} (1636)-CyPet

First, two recognition sites for *AgeI* (5' and 3'), one immediately in front of the ATG start codon, the second at nucleotide 4907 (immediately behind E¹⁶³⁶ of α_{1S} , see section 2.3.2.2), were added to the coding sequences of α_{1S} by PRECISOR PCR using the primers (fw) 5'-GAA CCG GTC ATG GAG CCA TCC TCA CCC CAG-3' and (rev) 5'-CAG GCG ACT CAA CCG GTT CCA TTT CTA TCT CAG C-3'. After restriction with *AgeI*, the C-terminally shortened α_{1S} sequence was ligated into the α_{1S} (1636)-YPet vector that had been opened with *AgeI* 5' to the α_{1S} sequence to create the C-terminally labelled tandem α_{1S} (1636)- α_{1S} (1636)-YPet. After digesting this tandem with *SacII* (an inherent, unique recognition site for this enzyme is present within every α_{1S}), the fragment - comprising two incomplete α_{1S} sequences - was ligated to CyPet α_{1S} (1636)-YPet (or YPet- α_{1S} (1636)-CyPet, see section 2.3.2.2) which had been opened with the same enzyme. The resulting plasmids encoded the N- and C-terminally labelled tandems CyPet- α_{1S} (1636)- α_{1S} (1636)-YPet and YPet- α_{1S} (1636)- α_{1S} (1636)-CyPet.

2.4 Cell culture & plasmid-DNA injection

2.4.1 tsA-201 cell culture and transfection procedure

Modified HEK-293 cells (tsA-201; ECACC, Salisbury, UK) were maintained in high glucose (4.5 g/l) Dulbecco's modified Eagle's medium (DMEM) with 10 % fetal bovine serum in a humidified incubator with 5 % CO₂ at 37 °C. One day before transfection, cells were seeded at a density of 2×10^5 cells in 35-mm glass bottom dishes (MatTek) and transiently transfected by GeneJuice Transfection Reagent at ~ 80 % confluency according to the manufacturer's protocol. Twenty-four hours following transfection,

positively transfected cells were identified by blue or yellow fluorescence and documented using an Olympus FV1000 confocal laser-scanning microscope.

tsA-201 cell maintaining medium (560 ml)

500 ml DMEM high glucose
50 ml Fetal Bovine Serum (FBS)
5 ml 100 × Pen/Strep
5 ml 200 mM L-Glutamine

2.4.2 Primary skeletal muscle cell culture

2.4.2.1 Mouse models

Muscular dysgenesis (*mdg*) mice and dyspedic (*dys*) mice lack functional DHPR α_{1S} subunit or RyR1, respectively (Tanabe *et al.* 1988; Takeshima *et al.* 1994b). Cultured muscle cells from homozygote newborns (see section 2.4.2.3) were used as expression systems for different cDNAs to allow for analysis of the DHPR - RyR1 interaction. Dysgenic mice are homozygous for a single nucleotide deletion (1297^{del}) in the gene encoding Ca_v1.1 (skeletal muscle DHPR), resulting in an unstable mRNA and, thus, in minute amounts of a truncated, non-functional channel fragment (Chaudhari 1992). Dyspedic mice were generated via a targeted disruption of the gene encoding RyR1 (Takeshima *et al.* 1994b; Buck *et al.* 1997). In skeletal muscle fibers and in cultured myotubes from both models there is a loss of EC coupling resulting in complete paralysis, as well as a substantial (in the case of dyspedics) or complete (in dysgenics) loss of L-type Ca²⁺ current, as compared to myotubes of normal or heterozygous animals (Takeshima *et al.* 1994a; Takeshima *et al.* 1995; Avila & Dirksen 2000). Every time when a myotube culture was set up, it was checked whether the animals used for preparation were homozygous for either mutation (described in the following section).

2.4.2.2 Genotyping

Genotyping was conducted as follows: Short tail biopsies (~ 2 mm) were incubated in 100µl alkaline lysis buffer (25 mM NaOH, 0.2 mM disodium EDTA, pH 12.0) for 30 min at 95 °C in a thermal block. Subsequently, samples were cooled on ice and 100µl of neutralizing buffer (40 mM Tris-HCl, pH 5.0) were added. 5 µl of this solution, containing DNA extracted from the tissue, were used for the PCR reactions described below (Truett *et al.* 2000).

PCR to check for presence of the dysgenic genotype

Genotyping by PCR (amplification product 271 bp) using (fw): 5'-GGC ATG CAG ATG TTC GGG AAG ATC-3'; and (rev): 5'-GCA GCT TTC CAC TCA GGA GGG ATC CAG TGT-3' was followed by digestion with *EarI* and electrophoresis on an agarose gel (2 %). A PCR fragment amplified from wild-type genomic DNA has an *EarI* site (result 171 and 100 bp) whereas the mutated allele does not have a *EarI* recognition sequence.

PCR to check for presence of the dyspedic genotype

Specific pairs of primers enabling the distinction between wild type, heterozygous, and homozygous mice were used in the same reaction set. Primer pair norm tail ((fw) 5'-GGA CTG GCA AGA GGA CCG GAG C-3'; (rev) 5'-GGA AGC CAG GGC TGC AGG TGA GC-3') amplifying 400 bp, indicative of the wild type allele, and primer pair dyspedic tail ((fw) 5'-GGA CTG GCA AGA GGA CCG GAG C-3'; (rev) 5'-CCT GAA GAA CGA GAT CAG CAG CCT CTG TCC C-3'), amplifying a 300 bp fragment of the mutant allele. Heterozygous DNA produces both sizes of fragments.

Mice tailing PCR mixture protocol (dysgenics & dyspedics)

31.75 µl ddH₂O
 5 µl template DNA
 10 µl Crimson *Taq* Reaction Buffer (5 ×)
 1 µl dNTP mix
 1 µl Primer skmouse_fw (25 µM)
 1 µl Primer mdgII_rev (25 µM)
 0.25 µl Crimson *Taq* DNA polymerase

PCR protocol dysgenics

Initial denaturation	95 °C for 2:00	
Denaturation	95 °C for 0:30	} 35 ×
Annealing	60 °C for 0:45	
Elongation	72 °C for 0:50	
Final elongation	72 °C for 7:00	
Cooling	4 °C for ∞	

PCR protocol dyspedics

Initial denaturation	94 °C for 5:00	
Denaturation	94 °C for 0:40	} 29 ×
Annealing	60 °C for 0:30	
Elongation	72 °C for 0:30	
Final elongation	72 °C for 5:00	
Cooling	4 °C for ∞	

2.4.2.3 Preparation of primary skeletal muscle cultures

Primary cultures of dysgenic (no α_{1S} ; mice kindly provided by Dr. Flucher, University of Innsbruck, Austria), dyspedic (no RyR1; mice kindly provided by Dr. Sorrentino, University of Siena, Italy) or wildtype (wt) skeletal muscle were prepared either from late-term foetal mice or from newborn mice (Beam & Franzini-Armstrong 1997). Muscle material was excised from the shoulders and the fore- and hindlimbs and was minced in Ca^{2+} / Mg^{2+} -free (CMF) Ringer's solution. After replacing the CMF Ringer by warmed (37 °C) CMF Ringer containing trypsin and DNase the muscles were incubated at 37 °C with gentle agitation (80 rpm, 30 minutes for dysgenics / wt and 20 minutes for dyspedics). To reduce the trypsin concentration, primary muscle plating medium was added to the cell trypsin mixture. The tissue was dispersed by trituration and was centrifuged (1,000 g) for 7 min. The supernatant was gently removed while the digested tissue remained at the bottom of the tube. The tissue was then redispersed by trituration and was filtered through nylon cell strainers (70 μm and 40 μm , consecutively). The singularized cells in the flow through were plated onto a 10 cm sterile plastic petri dish and incubated for 2 h at 37 °C. This preplating step led to considerable enrichment in the fraction of muscle cells because it allowed the fibroblasts to adhere to the dish while the muscle cells developed considerably less adherence during this time. After attachment of the fibroblasts, the dish was swirled gently, the solution was transferred to a new dish and the preplating step was repeated. The supernatant was then centrifuged (1,000 g for 7 min) and the cell pellet was resuspended in plating medium. The cells were seeded at a density of 2×10^4 cells, initially by placing a drop of 300 μl plating medium in the center of an entactin-collagen IV-laminin (ECL) cell attachment matrix coated, 35-mm glass bottom dish (MatTek) in a humidified incubator at 37 °C and 5 % CO_2 . After 4-5 h, an additional amount of 2 ml plating medium was added and the myoblasts were allowed to proliferate for a period of 5-7 days during which fresh medium was added daily. Then, the plating medium was replaced by differentiation medium, which resulted in the initiation of cell fusion and in formation of myotubes.

Primary Muscle Plating Medium (250 ml)

186.25 ml DMEM high glucose
6.25 ml 1M HEPES
25 ml Fetal Bovine Serum (FBS)
25 ml Horse Serum (HS)
2.5 ml 100 × Pen/Strep
5 ml 200 mM L-Glutamine

Differentiation Medium (250 ml)

231.25 ml DMEM high glucose
6.25 ml 1M HEPES
5 ml Horse Serum
2.5 ml 100 × Pen/Strep
5 ml 200 mM L-Glutamine

CMF Ringer's solution

NaCl 156 mM
KCl 5 mM
HEPES 10 mM
Glucose 11 mM
pH was adjusted to 7.4 with NaOH

Entactin-Collagen IV-laminin (ECL) Cell attachment Matrix

55 ml DMEM high glucose
5 ml ECL (Millipore)

CMF Ringer's solution (0.3 % Trypsin / 0.01 % DNase)

100 ml 1X CMF Ringer's solution
300 mg Trypsin
10 mg DNase

2.4.3 Transfection of myotubes via intranuclear plasmid-DNA microinjection

Upon formation of myotubes, the multinucleated cells were transfected by intranuclear pressure-microinjection of solutions containing the expression plasmid(s) for FRET measurements. The DNA concentration of the injection solution was 80 to 100 ng/ μ l water. Fluorescent myotubes were examined 24-48 h after cDNA microinjection using a Fluo View 1000 confocal laser-scanning microscope (Olympus).

2.5 Electrophysiology

2.5.1 Electrically evoked contractions

To test for the occurrence of contractions, the differentiation medium was replaced by a solution with defined Ca^{2+} concentration (HEPES buffered Rodent Ringer, composition listed below). Contractions were elicited by stimuli of 30 ms duration at 80 V, applied via an extracellular pipette filled with 150 mM NaCl and placed near the myotube of interest (Tanabe *et al.* 1988). A standard silver chloride (AgCl) agar bridge (3 M KCl) served as reference electrode. Contractions were assayed by the movement of an identifiable portion of a myotube across the visual field.

Rodent Ringer's solution

NaCl 146 mM
KCl 5 mM
CaCl₂ 2 mM
MgCl₂ 1 mM
HEPES 10 mM
Glucose 11 mM
pH was adjusted to 7.4 with NaOH

2.5.2 Measurement of L-type Ca^{2+} currents

These experiments were carried out in cooperation with Prof. Dr. Kurt G. Beam & Dr. Joshua D. Ohrtman, University of Colorado Health Sciences Center. Whole-cell voltage clamp (Hamill *et al.* 1981) was used to record macroscopic Ca^{2+} currents. Borosilicate glass pipettes (WPI) were polished to a final resistance of approximately 2.0-3.0 M Ω and filled with internal solution (listed below). Replacement of the external solution happened by perfusing the recording chamber with 20 ml of the new solution at a rate of 6 ml min⁻¹. Test currents were elicited by rectangular test potentials applied from a -80 mV holding potential. Whole-cell voltage clamp traces were recorded from dysgenic myotubes expressing different α_{1S} constructs.

Internal solution

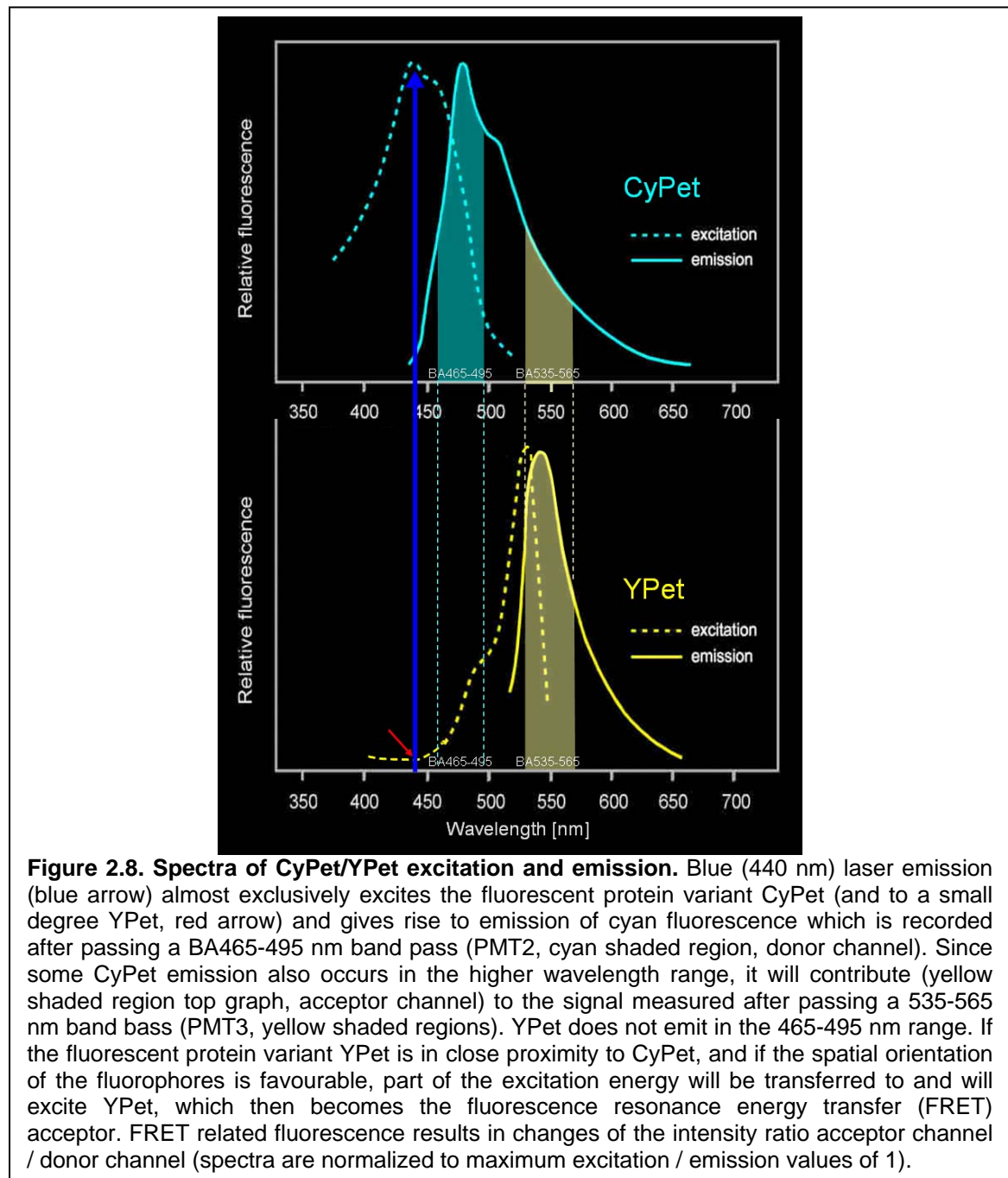
CsAsp 140 mM
MgCl₂ 5 mM
Cs₂EGTA 10 mM
HEPES 10 mM
pH 7.4 with CsOH

External solution

CaCl₂ 10 mM or
BaCl₂ 10 mM
TEACl 145 mM
HEPES 10 mM
pH 7.4 with TEAOH

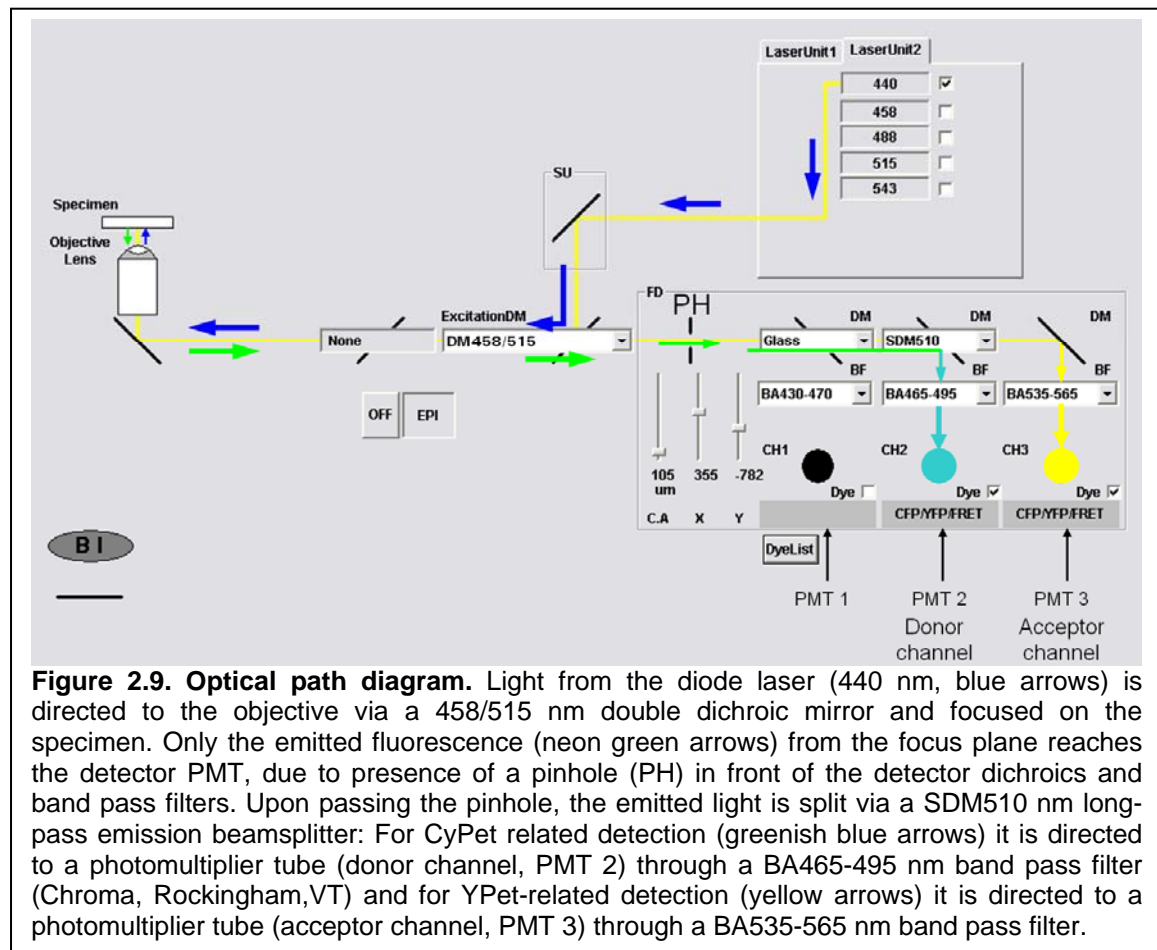
2.6 Confocal laser-scanning microscopy

24-48 hrs after microinjection, culture dishes were mounted on the stage of an inverted microscope which is part of a confocal system (Olympus FluoView 1000). The myotubes were checked for expression of fluorescence, for proper targeting of the tagged channel protein, and for the presence and the intensity of FRET (as detailed in section 2.7) under oil immersion at 60 ×, NA = 1.35. The confocal system was operated via the Olympus ‘FV10-ASW 1.7’ software package. The confocal approach, by making use of an axially located pinhole in the image plane in front of the detector, allowed for elimination of out-of-focus light and for the exclusive observation of DHPR-associated fluorescent foci, at or very close to the surface of the myotubes. The latter localization documented proper targeting of the expressed construct(s) to the junctional SR / t-tubule connections (Figure 2.1, Results), whereas diffuse or exclusively intracellular fluorescence indicated deficiency in this process. In a typical laser scan for image acquisition, the fluorescence emitted from a defined spot of the myotube surface was detected by the two photomultiplier tubes (i.e. donor and acceptor channel, respectively) and was recorded under the same excitation and emission settings (laser intensity, photomultiplier gain, pinhole, averaging) for every myotube. CyPet and YPet (Table 2.3) were excited using a 440 nm diode laser (Figure 2.8) and 515 nm argon laser line, respectively, directed to the cell via a 458/515 nm dichroic mirror. The optical path diagram through the dichroic mirrors, excitation and emission filters for FRET are shown in Figure 2.9. The emitted fluorescence was split via a SDM510 nm long-pass emission beamsplitter and directed to separate photomultipliers (PMT). The bulk of CyPet related fluorescence reached the PMT after passing a 465-495 nm bandpass filter (PMT2 - donor channel, I_{CY}) while most of the YPet fluorescence intensity reached the photomultiplier after passing a 535-565 nm bandpass filter (PMT3 - acceptor channel, I_Y). Since some CyPet emission also occurs in

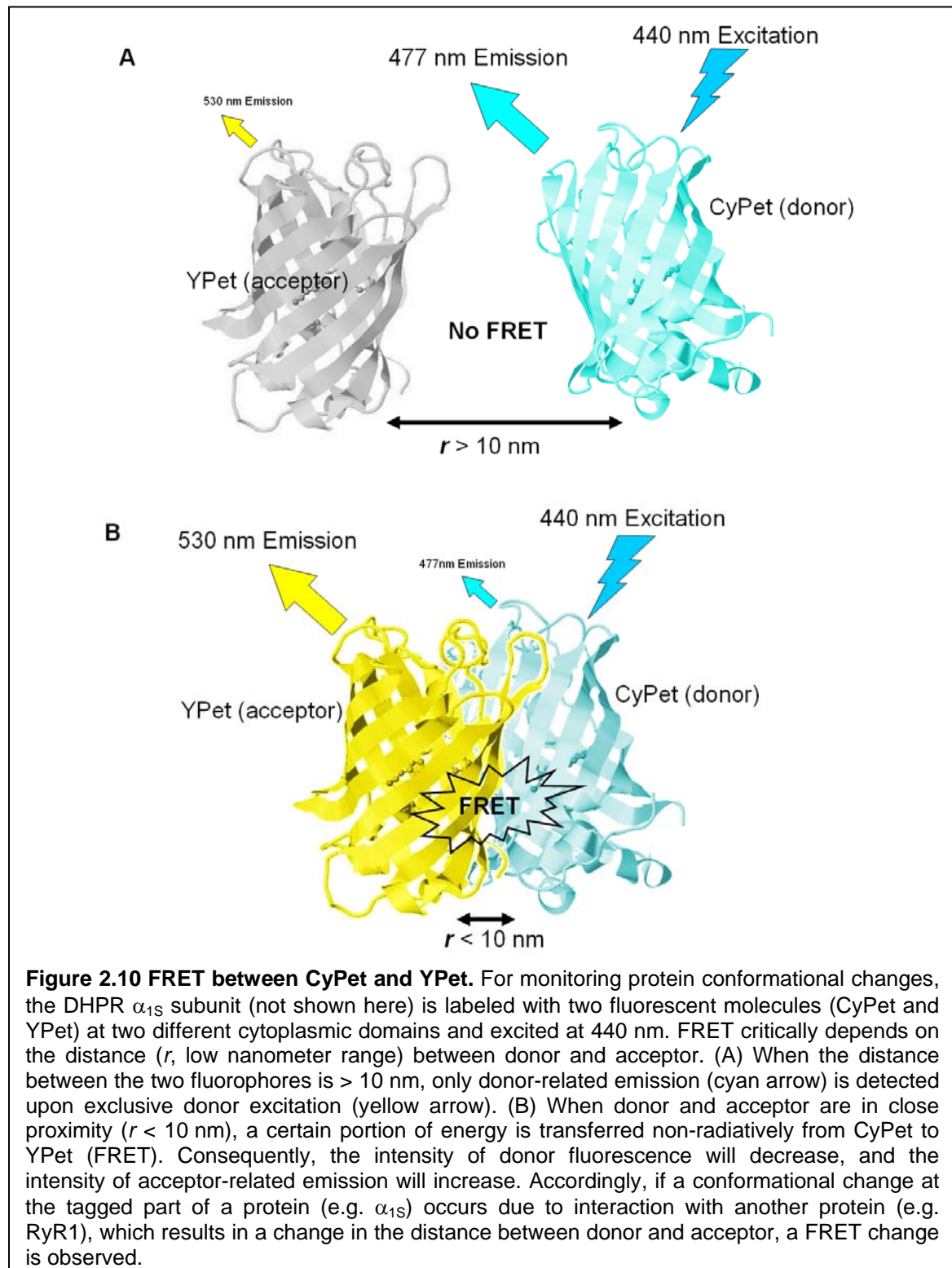


the higher wavelength range, it contributed to the signal measured for YPet. Accordingly, the PMT3 signal was corrected for this contribution by CyPet ($I_{Y,CY}$). $I_{Y,CY}$ was determined upon expression of constructs tagged solely with CyPet (e.g., CyPet- α_{1S}) and was found to amount to 28 % of I_{CY} ($I_{Y,CY} / I_{CY} = 0.28 \pm 0.02$, $n=25$). The signal of PM3 was corrected by applying $I_Y - I_{Y,CY}$. As a relative measure for the degree of energy transfer the ratio $(I_Y - I_{Y,CY}) / I_{CY}$ (or, briefly, I_{FRET}) was used, being aware that every increase in “yellow” intensity (BA 535-565 nm signal) due to energy transfer leads to a decrease of

I_{CY} , resulting in a disproportionate increase of the calculated I_{FRET} with increasing energy transfer (Figure 2.10).



Upon collection of the FRET data using excitation with the 440 nm line of the blue diode laser, an additional scan was run under exclusive excitation of YPet, to verify colocalization of CyPet and YPet fluorescence. This was of special importance when one of the tags involved the C terminus, where any occurrence of proteolytic cleavage would have led to fluorophore separation (discussed below). In the second scan, YPet was excited by the 515 nm argon laser, using the same, 458 / 515 nm, dichroic mirror. The emitted YPet fluorescence was directed to PMT3, after passing a 535-565 nm bandpass filter. This second scan at the same time served as an estimate for the degree of autofluorescence, which was sometimes observable under excitation with the 440 nm diode but which had to be removed from the overall signal in order to obtain the net CyPet emission. Autofluorescent myotube regions identified by this second scan were excluded from FRET calculations (see section 2.7.6).



2.7 Measurements of Fluorescence / Förster Resonance Energy Transfer (FRET) ratio

As is the case with normal myotubes bathed in physiological saline, spontaneous contractions occurred in a large fraction of dysgenic myotubes expressing fluorescently labelled α_{1S} constructs. Because the movements associated with such contractions would interfere with analysis of FRET, the contractile activity was eliminated by bathing the cells in CMF Ringer's solution.

2.7.1 Donor to acceptor stoichiometry

FRET proved a suitable tool for studying protein-protein interactions in living cells. However, an unknown stoichiometry between donor and acceptor molecules within a molecular complex will be an issue, regarding the calculation of FRET efficiency. This is because FRET efficiency is a function of how close acceptor and donor are, but also how many acceptors are near the donor (Lakowicz *et al.* 1999). Thus, the correct interpretation of FRET signals requires knowledge about the stoichiometry of the different fluorophores within the examined protein complexes. However, in the present study **intramolecular** (or, single-molecule) FRET analysis is conducted, with a molar CyPet:YPet ratio of 1, avoiding uncertainties due to unknown stoichiometry (assuming that FRET between the tagged DHPR's, **intermolecular** FRET, is negligible). Therefore, the FRET changes recorded here can be attributed to structural changes within one α_{1S} subunit. This approach is therefore suitable to find out whether the tagged regions undergo conformational changes and are therefore putative parts of the DHPR-RyR1 interaction interface.

2.7.2 Measurement of sensitized emission for the calculation of the degree of FRET

A defined area of the myotube surface was selected from the field of view, which included the part of the myotube to be analyzed and also an adjacent, non-cellular region for measurement of background fluorescence. To measure FRET by sensitized emission, an almost exclusive excitation of the donor, CyPet, was conducted via the 440 nm diode laser line, operated at constantly 30 % laser intensity. Confocal fluorescence intensity data from the donor PMT channel (I_{CY}) and the acceptor PMT channel (I_Y) were recorded as

tenfold average per pixel and digitized 12-bit. Further parameters as pinhole diameter, photomultiplier gain and offset were kept constant in the course of an experiment after they had been adjusted to keep maximum pixel intensities no more than 80 % saturated. The problem of donor bleaching was minimized by using very weak intensity at 440 nm excitation for adjusting the focus plane at or very close to the surface membrane. This way, even the repeated (up to 4 times) excitation of cells containing tagged proteins caused less than 1 % decline in fluorescence intensity. Figure 3.5 (see section Results) shows a typical example for recorded I_{CY} and I_Y from a myotube expressing an α_{1S} construct.

2.7.3 Background correction

For background correction, a region of interest (ROI) outside the myotube was chosen. The background correction toolbar of the Olympus software was then used to subtract a constant background intensity value from all pixel intensities in the image (Figure 2.11). The background correction was applied independently to both channels, because of different levels of autofluorescence in each channel. After correcting for the background, the Olympus software (*Edit Experiment* tool) was used to create intensity images of I_{CY} and I_Y , as well as a third intensity distribution which was recorded by PMT3 while scanning with 515 nm excitation and 1-3 % laser intensity, to detect and to exclude from the ROI intracellular regions of co-localization between CyPet / YPet and cellular autofluorescence (as described in 2.7.4).

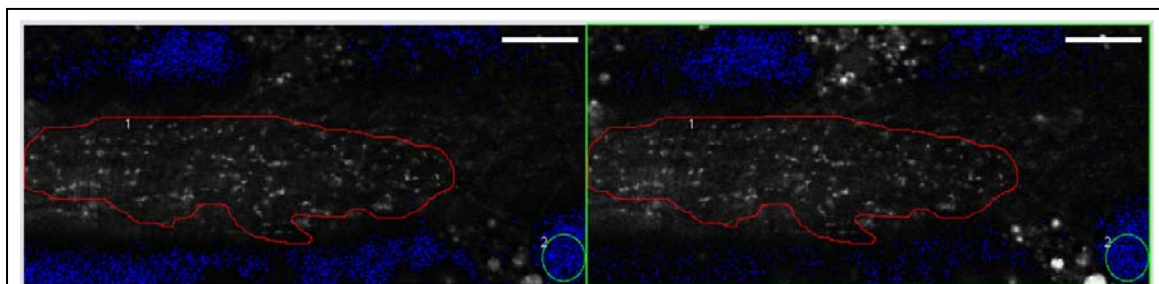


Figure 2.11. Background correction and ROI definition. The background intensity is determined for every channel (PMT2, left and PMT3, right) by calculating of the average intensity within a region outside the myotube (e.g., within the green circle). The respective value is then subtracted from every pixel of the scan. For some pixels, this subtraction produces negative intensity values (blue pixels). The intensity for those pixels is set to zero. The red free hand form represents the region of interest for this example, containing the fluorescent foci used for calculating the degree of FRET. Bars represent 5 μm .

2.7.4 Detection of cellular autofluorescence

Relatively short wavelengths like the 440 nm blue diode laser line used for CyPet excitation provoke significant amounts of cellular and extracellular autofluorescence. Longer wavelengths like the yellow 515 nm laser channel is far less prone to produce autofluorescence artefacts, and this fact was used to identify and exclude from the calculations signals emerging from unspecific excitation. To restrict the FRET calculation to fluorescent puncta representing junctionally targeted constructs, after conduction of the 440 nm scan an additional scan at the same focus plane was conducted but this time under 515 nm excitation. Fluorescent spots or regions which were present under 440 nm excitation but which were absent (or much weaker in intensity) under 515 nm excitation, most likely represented autofluorescence and were omitted from the regions used to calculate FRET. Figure 2.12 shows an example of application of the procedure to identify autofluorescence. In the figure, dots of cellular autofluorescence are marked by arrows, and are easily identified by observing the image captured using the 515 nm laser (in which they are not present). In essence, the fluorescence intensity ratio is calculated only for dots which are excited by both the 440 nm diode laser and the 515 nm argon laser.

2.7.5 Calculation of the degree of FRET within fluorescent foci

Correctly targeted constructs tagged with CyPet and YPet were visible as numerous, discrete foci localized at the cell surface. Therefore, the I_{FRET} ratio had to be calculated only for pixels contained in these foci. For this purpose, the software package 'F10-ASW 1.7' (Olympus) was used in combination with Excel 2003 (Microsoft). First, a 'binary mask' was defined for the two scans obtained under excitation with 440 nm. The masque assigned the pixels exceeding a defined intensity value - a threshold set by the user - the value of 1, whereas the other pixels were assigned zero (blue in Figure 2.13). In the next step, the pixels which had been assigned the value of 1 were transferred as two-dimensional intensity matrix into an Excel spreadsheet (Figure 2.14). A self-made macro was then started, which calculated the ratio I_Y/I_{CY} for every pixel assigned with the value of unity. More precisely, first, the macro summed up the intensities of the foci within the ROI, separately for the cyan and the yellow channel (I_{CY} and I_Y , respectively). It then generated the average ratio I_Y/I_{CY} for a given intensity cut-off, before increasing

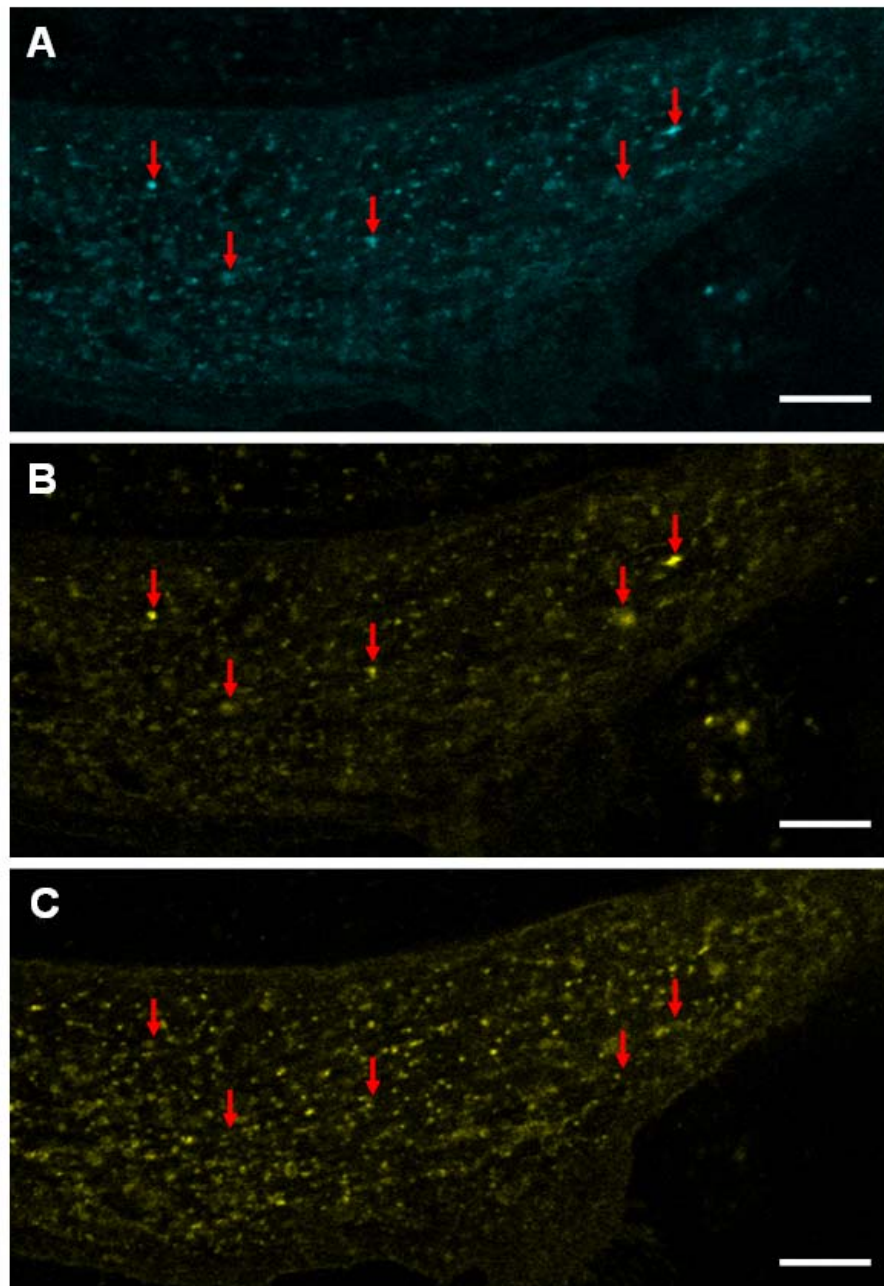
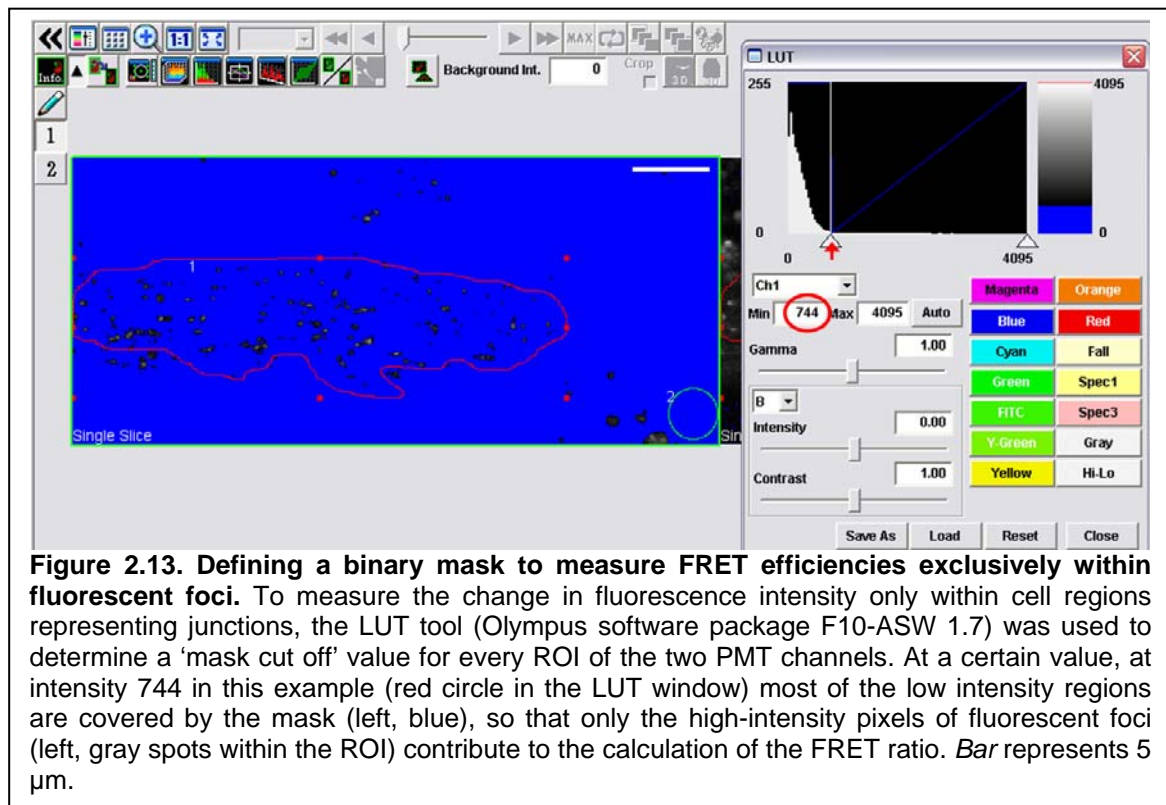


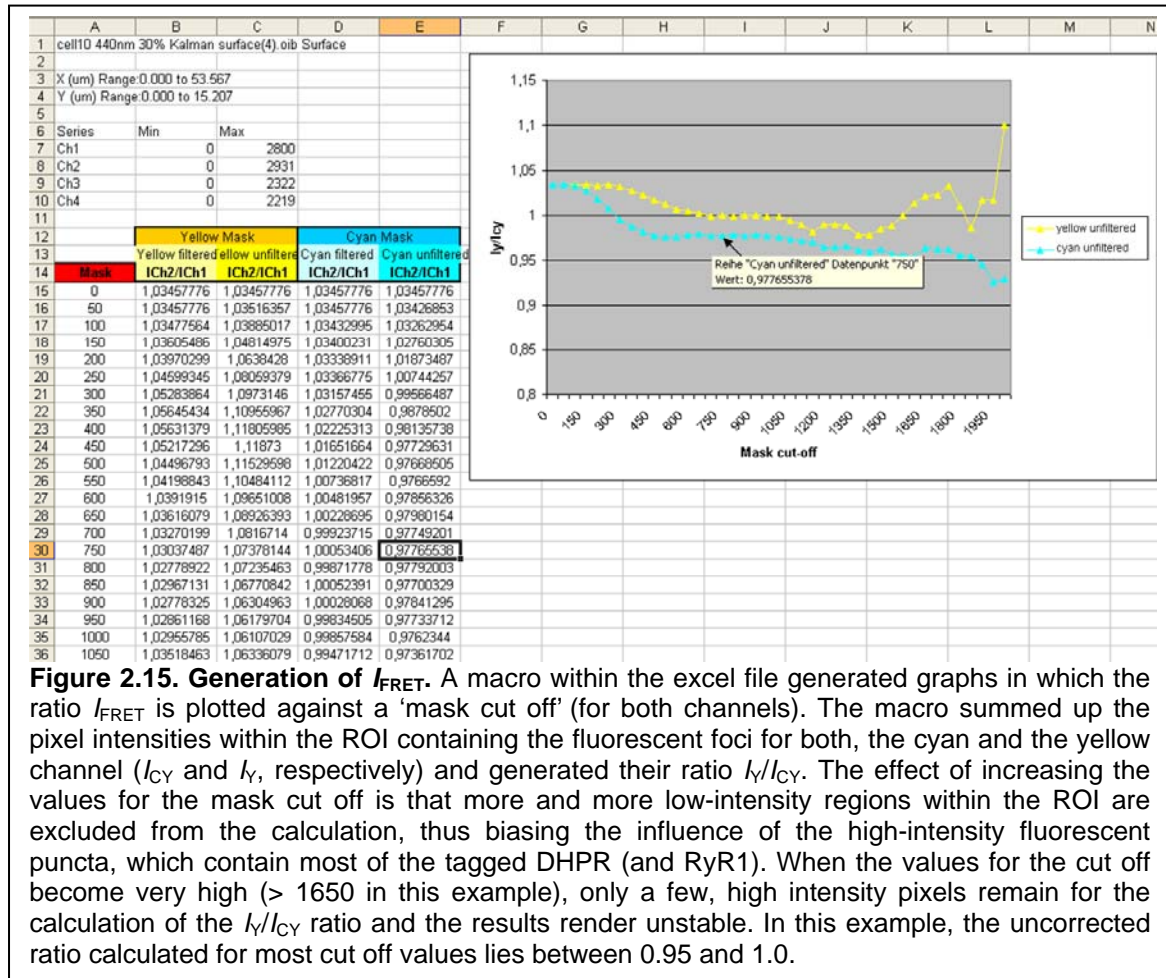
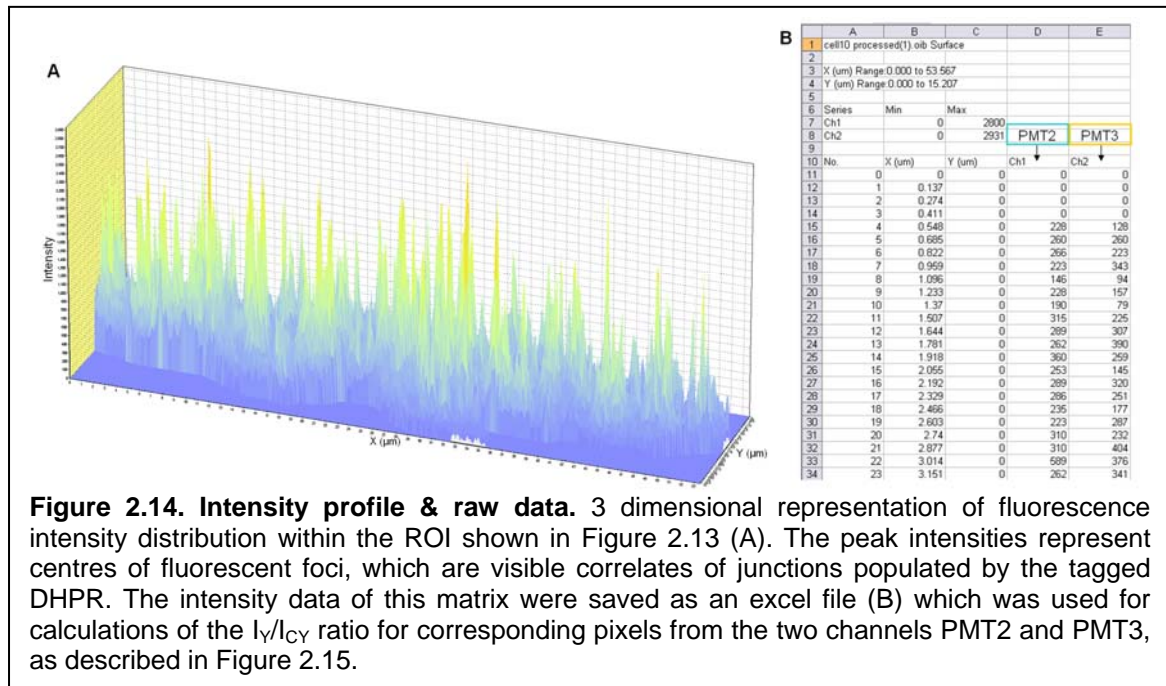
Figure 2.12. Detection of cellular autofluorescence. Fluorescent dots (indicated by red arrows) which were present in both channels PMT2 (A) and PMT3 (B) recorded under 440 nm excitation but were absent when the same myotube was excited by the 515 nm argon laser (C). Bars represent 5 μm

the cut-off value and proceeding to the next round of calculation. This procedure led to the successive omittance of more and more pixels with intensities below the new threshold for cut-off. For each calculation round, the ratio I_Y/I_{CY} was generated by dividing the sum of pixel intensities in the acceptor channel by the sum of pixel intensities in the donor channel. It is important to note that the increments in the value for cut-off only led to a reduction in the number of pixels to be analysed, but did not change the

intensities of the pixels within the remaining foci (ROI pixels with values below the threshold for cut-off were assigned the value 0 in the mask and just dropped out of calculations, while the remaining pixels kept their initial values). In the process of increasing the cut-off, i.e., at a certain threshold, the mask did only contain pixels exclusively from fluorescent foci (Figure 2.13). This user-specified ‘threshold’ for the ‘mask cut off’ value was determined separately for each myotube to be analysed (Figure 2.15). Finally, the macro generated a graphical representation of I_{FRET} plotted against increments of the applied intensity cut-off threshold (Figure 2.15). The reference channel chosen for creating the mask by increasing the cut-off threshold was the donor channel (I_{CY}). This channel was chosen because the intensity distribution within fluorescent foci was more homogeneous than in the acceptor channel. Accordingly, the FRET ratio values produced using increasing ‘mask cut off’ values were more consistent with the donor channel as reference than with the acceptor channel.



The I_Y/I_{CY} ratios calculated in the macro procedure had to be corrected for the contribution of CyPet emission to the signal measured in the YPet channel (I_Y). This correction was straightforward because the degree of contamination of the YPet channel by CyPet emission was known from experiments where CyPet was expressed in the absence of YPet (see section 2.6).



2.8 Statistical analysis

To check for significant differences between the FRET ratios calculated for the condition \pm RyR1 for a particular construct, the unpaired t test function of the Sigma Plot software package, version 8.0, was used. A significant difference was regarded a p value < 0.001 .

3. Results

3.1 Tagged α_{1S} constructs restore EC coupling

Because the central goal of the present work was to use sensitive FRET for probing the proximity of cytoplasmic α_{1S} regions within the junctional membranes in the absence vs. in the presence of the RyR1 (which in the latter case means, within the functional EC coupling apparatus), it was important that the sites of tag incorporation met certain requirements. Specifically, it was important for at least some of these sites to be close to regions which might be involved in signaling interactions with RyR1, whereas others had to be placed into regions not expected to be involved in critical EC-coupling tasks and, thus, serve as controls. Furthermore, it was important that incorporation of the fluorophores did not interfere with the ability of α_{1S} to target to the junctional membranes and to function as a voltage sensor for EC coupling. When N-terminally fluorescent protein-tagged DHPR α_{1S} subunits (e.g., YPet- α_{1S}) are expressed in cultured dysgenic myotubes, punctate foci are observed on the myotube surface (see Figure 3.1) (Grabner *et al.* 1998; Kasielke *et al.* 2003; Papadopoulos *et al.* 2004; Lorenzon *et al.* 2004; Kugler *et al.* 2004a; Kugler *et al.* 2004b; Bannister & Beam 2005). This distinct staining pattern in myotubes is believed to represent clusters of DHPRs within individual junctions because other known triadic proteins (e.g., RyR1, triadin) also are observed as punctuate foci that colocalize with the DHPR (Flucher *et al.* 1993; Protasi *et al.* 1998). Labelling of the **N-terminus** with a single fluorescent protein does not interfere with α_{1S} targeting or EC-coupling function (Grabner *et al.* 1998). Control experiments carried out in the present study upon expression of YPet- α_{1S} in myotubes are in agreement with these previous findings, since the construct exhibited normal targeting efficiency (Figure 3.1) and electrophysiological function (Table 3.1). In addition to the N-terminus of α_{1S} fluorophores were fused or inserted to other cytoplasmic positions, including the C-terminus right behind A¹⁶⁶⁶ or right behind E¹⁶³⁶, within the I-II loop up- or downstream the AID, within the critical domain of the II-III loop, and within the short III-IV loop (see Figure 2.2 and Table 3.1). However, not all single tagged constructs were able to correctly target to junctions (Figure 3.2) and, thus, could not restore EC coupling (Table 3.1).

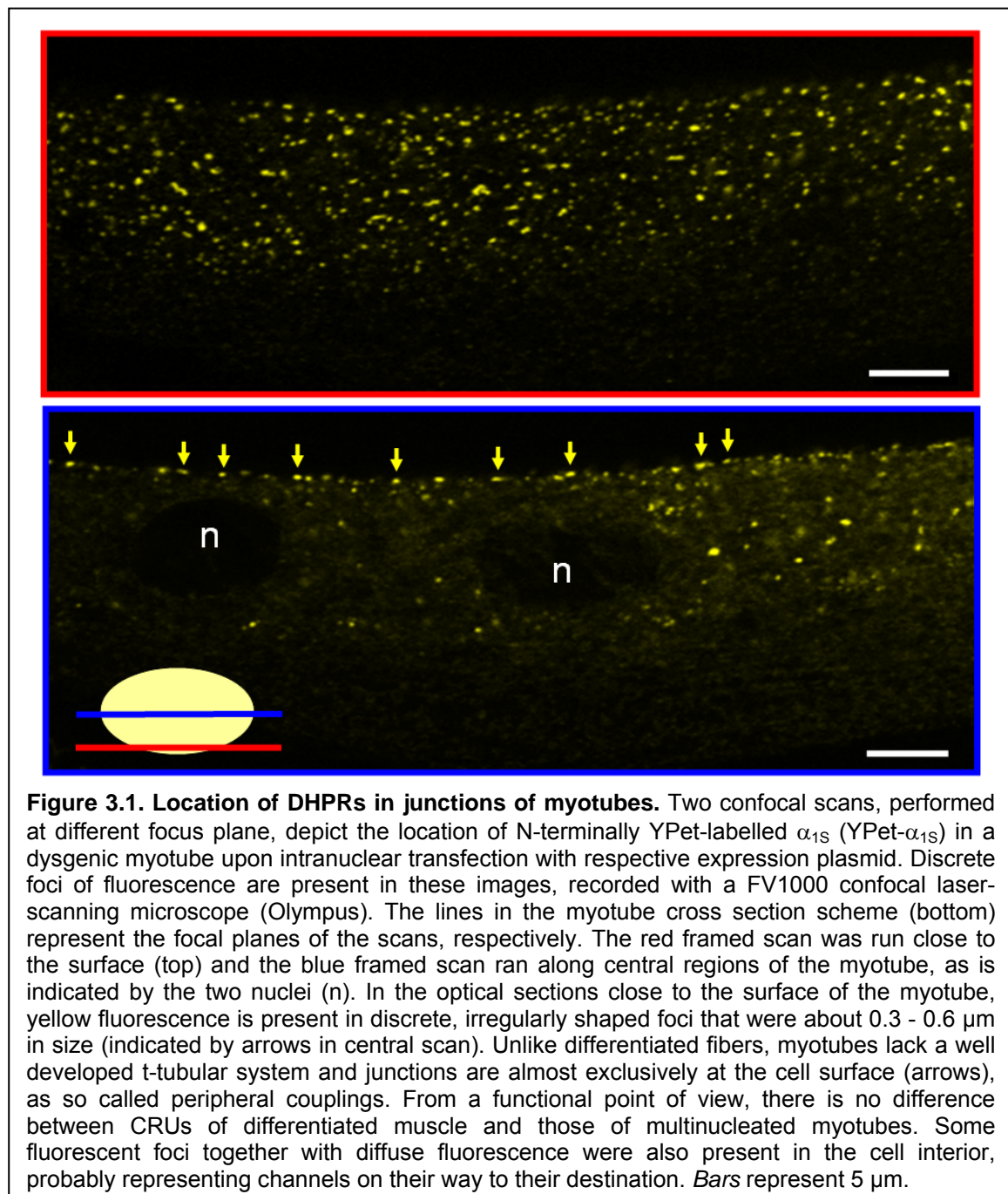
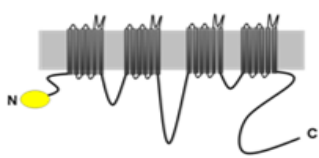
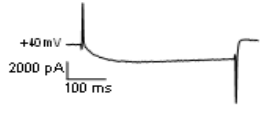
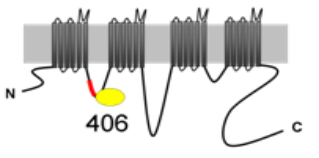
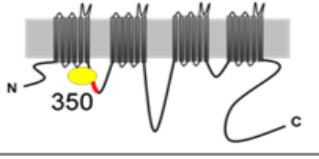
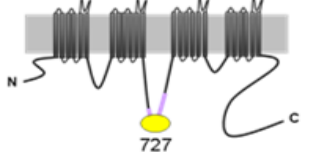
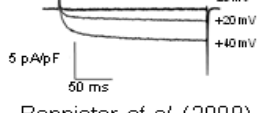
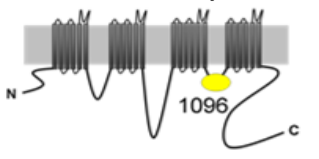
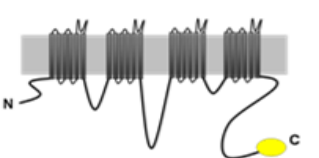
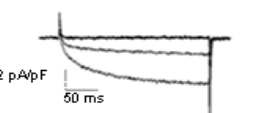
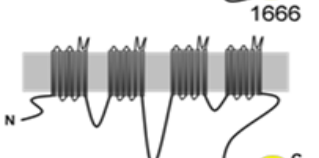


Table 3.1 and Figure 3.2 summarize the targeting and electrophysiological properties of constructs, carrying a single fluorophore tag at different relevant positions. Reference currents for the designated constructs expressed in dysgenic myotubes are shown from the recent literature. Most of the constructs displayed electrically evoked contractions.

Table 3.1. Schematic illustration of single tagged α_{1S} constructs including their targeting and electrophysiological properties. Numbers refer to amino acid residues of α_{1S} position of fluorophore insertion (see section 2.3, Materials and methods for construction details). The AID and critical domain of α_{1S} are only indicated for constructs tagged within the corresponding loop. Contractions were evoked after cDNA expression in dysgenic myotubes by local, electrical stimulation (see section 2.5.1, Material and Methods). Reference currents for the designated constructs expressed in dysgenic myotubes from the current literature are shown. * in injected dysgenic myotubes, ¹ construct should show L-type Ca^{2+} currents, not measured/quantified yet; ² injected dysgenic myotubes did not contract after stimulation; ³ no L-type currents expected due to targeting deficiency.

α_{1S} construct / tagged domain	Targeting in		Spontaneous contractions*	Evoked contractions / currents*	Current trace / source / construct name
	dyspedic myotubes	dysgenic myotubes			
N-terminus 	+	+	+	+	 This study, YPet- α_{1S}
I-II loop 	+	+	+	+ ¹	
	+/-	+	-	- ²	-
II-III loop 	+	+	+	+	 Bannister <i>et al.</i> (2009), α_{1S} (726-YFP-727)
III-IV loop 	-	-	-	- ³	-
C-terminus 	+	+	+	+	 Bannister & Beam (2005), α_{1S} -YFP
	+	+	+	+ ¹	

 YPet OR CyPet
  AID, region of interaction with β -subunit
  Critical domain

In multiple attempts to generate a functional construct carrying a fluorescent tag within the α_{1S} **I-II loop** two different fluorophore insertion positions were tested. These positions are located either upstream (between residues 350 and 351) or downstream (between residues 406 and 407) of the AID of α_{1S} (Q³⁵⁷-E³⁷⁴, see Figure 2.6A). The AID is essential for β_{1A} subunit interaction (Pragnell *et al.* 1994) and junctional targeting of α_1 subunits (Neuhuber *et al.* 1998b; Papadopoulos *et al.* 2004; Leuranguer *et al.* 2006). Typical examples for targeting ability of these α_{1S} constructs, tagged solely with YPet at different positions within the I-II loop, are shown in Figure 3.2 and Figure 3.3. Constructs with a single fluorophore inserted downstream the AID regularly produced a typical pattern of fluorescent foci on the myotube surface when expressed in dysgenic or dyspedic myotubes (Figure 3.3). The construct containing the fluorophore upstream the AID produced a similar pattern of fluorescence in dysgenic myotubes, but in dyspedic myotubes the fluorescence pattern was much more reticular (Figure 3.3). Insertion of the dye upstream the AID left a considerable part of α_{1S} stuck within central regions of

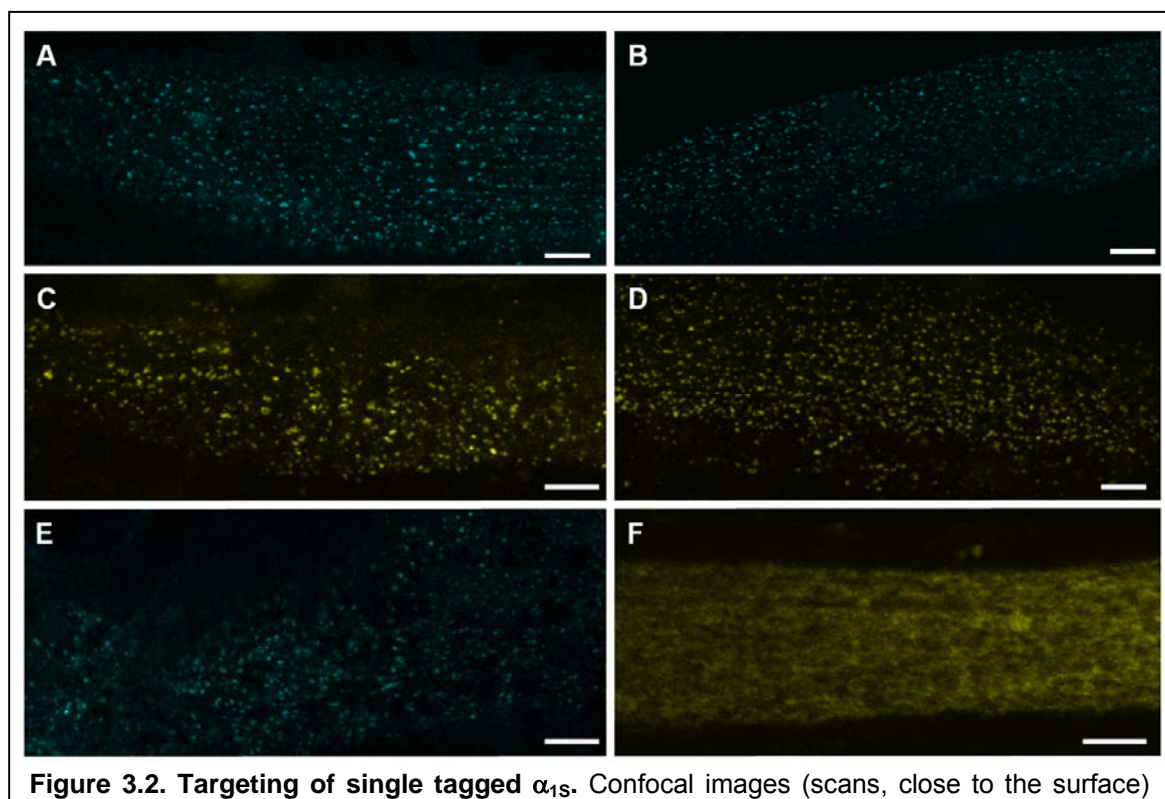
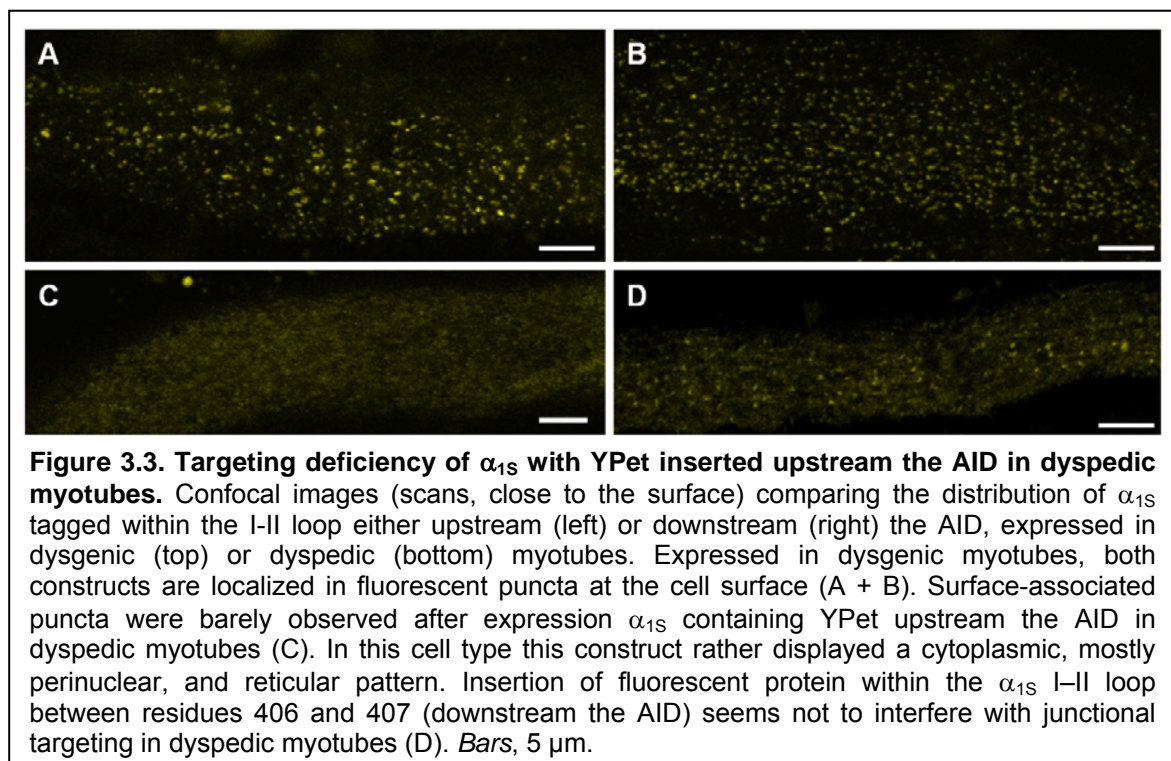


Figure 3.2. Targeting of single tagged α_{1S} . Confocal images (scans, close to the surface) showing the distribution of single tagged α_{1S} constructs upon their expression in dysgenic myotubes, respectively. Tag positions of the different α_{1S} constructs are (A) the N-terminus, (B) the C-terminus at pos. 1636, (C) the I-II loop at pos. 350, (D) the I-II loop at pos. 406, (E) the II-III loop at pos. 727, and (F) the III-IV loop at pos. 1096. Except for construct tagged within the III-IV loop (F) every singularly tagged α_{1S} construct was concentrated at the cell surface, as is indicated by the localization of fluorescent puncta. Insertion of a fluorophore into the III-IV loop at pos. 1096 however, completely eliminated the targeting ability of α_{1S} . Bars represent 5 μ m.

dyspedic myotubes, probably at the sarcoplasmic reticulum. In contrast, insertion of XPet into the α_{1S} I-II loop downstream the AID at pos. 406 did not significantly affect junctional targeting, β_{1A} interaction with α_{1S} in both myotube types, and EC coupling (no attempts were made to record currents for this single tagged construct in dysgenic myotubes, Table 3.1). Due to these observations the FRET experiments were performed with α_{1S} constructs containing CyPet or YPet downstream the AID. In summary, insertion of CyPet or YPet into the α_{1S} I-II loop may affect junctional targeting by interfering with $\alpha_{1S}:\beta_{1A}$ interaction at the AID. However, this can be overcome by labelling the I-II loop at the AID downstream position 406.



There is general agreement that the **II-III loop** of the α_{1S} subunit plays a key role in transmitting the EC coupling signal to RyR1. The importance of the DHPR α_{1S} II-III loop in EC coupling has been demonstrated by a number of groups (Tanabe *et al.* 1990; Nakai *et al.* 1998; Grabner *et al.* 1999; Carbonneau *et al.* 2005). Bannister and co-workers (2009) gave a detailed report of the effects on EC coupling when one or two fluorescent proteins are inserted into various positions of the α_{1S} II-III loop. On the basis of numerous previous studies, this loop appears to be a strong functional determinant for bidirectional coupling with RyR1. Thus, this loop is a desirable site for fluorescent labelling and FRET measurements. To create constructs labelled within the II-III loop, XPet was placed

between α_{1S} residues 726 and 727 (Figure 2.6C), which is within the N-terminal portion of the "critical domain" (residues 720-765). This part of the II-III-loop was found to be indeed critical for bidirectional signaling with the RyR1 (Nakai *et al.* 1998; Grabner *et al.* 1999). Constructs with a single inserted fluorophore at position 727, expressed in dysgenic or dyspedic myotubes, produced a typical pattern of fluorescent foci on the myotube surface (see Figure 3.2E). The functional consequences of fluorescent protein insertion between α_{1S} residues 726 and 727 have been investigated extensively by Bannister *et al.* (2009, see trace in Table 3.1). Bidirectional coupling was partially ablated when a single YFP was inserted at this position. Here, spontaneous and evoked contractions were observed frequently in dysgenic myotubes expressing this construct (Table 3.1). In summary, insertion of a fluorescent protein within the α_{1S} II–III loop between α_{1S} residues 726 and 727 does not interfere with junctional targeting or channel function.

The **III-IV loop** of α_{1S} is relatively short, consisting of only 53 amino acids (Figure 2.6B). Consequently, XPet (239 amino acid long) was inserted into the center of this loop, to ensure the highest possible level of flexibility for the fluorophore. However, insertion of the fluorophore at a central position, right behind the 31st residue of the 53 amino acid long III-IV loop (see Figure 2.6B) completely abolished the targeting ability of α_{1S} . A typical example of reticular fluorescence indicative of stuck α_{1S} construct tagged with XPet within the III-IV loop is illustrated in Figure 3.2F. This observation applied to all constructs labelled in the III-IV loop in both dysgenic and dyspedic myotubes (Table 3.1 and Table 3.2). The insertion of a dye within III-IV loop left α_{1S} trapped in the biosynthetic pathway, most likely within the SR. Thus, inserting of XPet into α_{1S} III-IV loop affects junctional targeting, probably by compromising its interaction with other α_{1S} loops and/or other proteins of the cellular channel trafficking machinery.

Functionality and targeting ability of α_{1S} fluorescently labelled at the **C-terminus** was already demonstrated (Papadopoulos *et al.* 2004; Bannister & Beam 2005, see trace in Table 3.1). In the present study labelling of the C-terminus was carried out with some modifications. A fluorophore was attached to the C-terminus of α_{1S} (1666) to generate the construct α_{1S} (1666)-XPet (see Figure 2.4), in analogy to the construct α_{1S} short-CFP-YFP described in Papadopoulos *et al.* (2004). This variant terminates at α_{1S} residue A¹⁶⁶⁶ (the native coding sequence terminates at residue 1873) to avoid loss of the fluorescent tag due

to proteolytic cleavage within the α_{1S} C-terminus. Papadopoulos *et al.* (2004) showed that truncation of the C-terminal to residue 1667 and adding two fluorophores did not alter the function of α_{1S} as a Ca^{2+} channel or its targeting ability, thus, labelling at position 1666 should not pose a problem regarding FRET studies. However, when expressed in dyspedic myotubes the α_{1S} constructs carrying CyPet or YPet at position 1666 tended to lose the dye at the C-terminus (Figure 3.4). There, puncta of the C-terminal dye were largely absent from the periphery of the myotube and a diffuse to reticular cellular distribution of the fluorophore was present. This observation is in agreement with Hulme and co-workers (2005) who predicted that the carboxyl-terminus of α_{1S} is subject to proteolytic cleavage at residue A¹⁶⁶⁴ (see Figure 2.4). Considering this possibility an even shorter version of α_{1S} was cloned which terminated at residue E¹⁶³⁶. This variant did not contain A¹⁶⁶⁴ or the PEST motif required for recognition of the cleavage site (Figure 2.4).

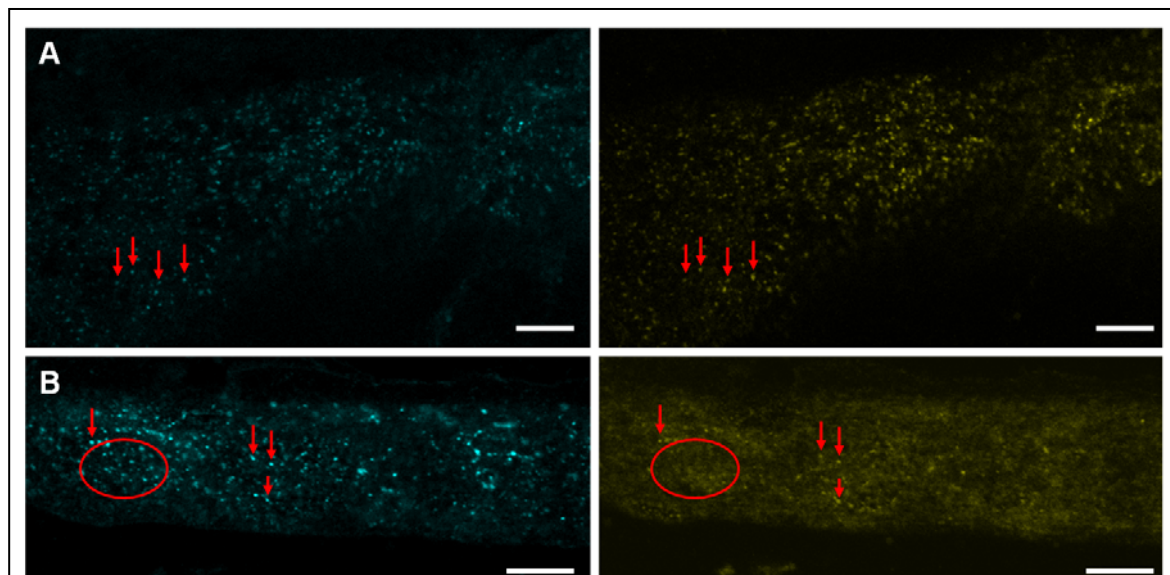
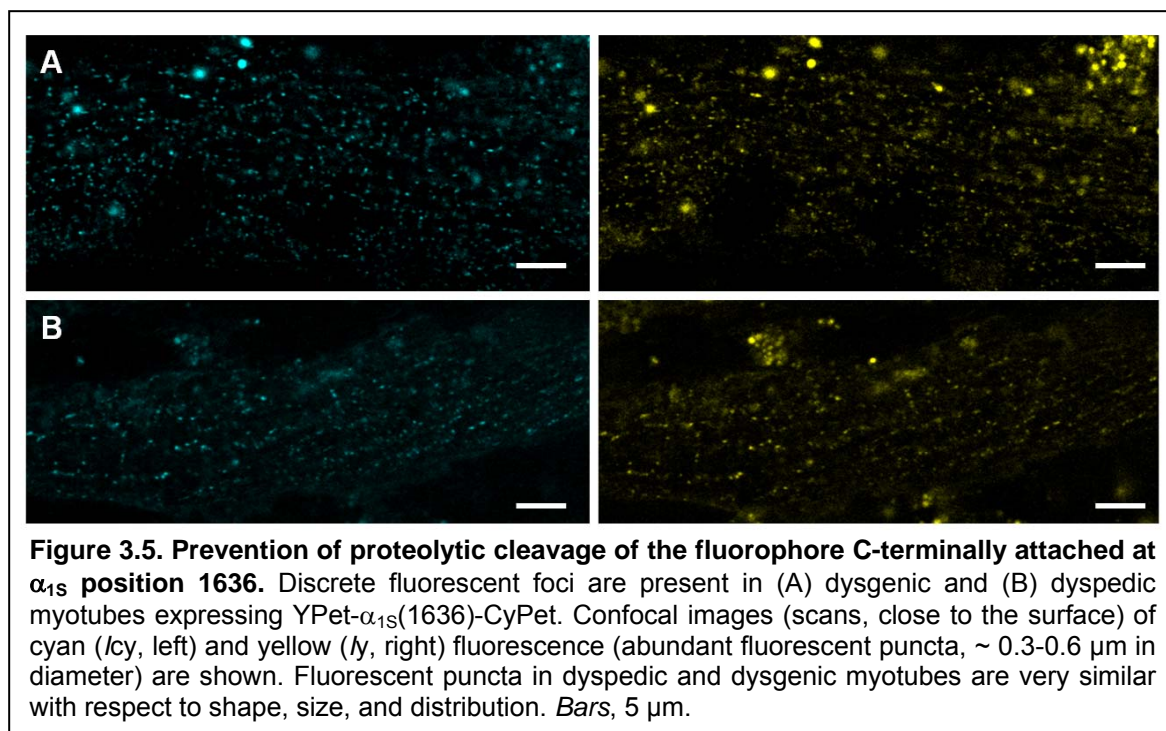


Figure 3.4. Proteolytic cleavage of $\alpha_{1S}(1666)$ -XPet in dyspedic myotubes. Confocal images (scans, close to the surface) comparing the distribution of an α_{1S} construct carrying CyPet N-terminally and YPet at the C-terminus at pos. 1666 expressed in (A) dysgenic and (B) dyspedic myotubes under specific excitation of each fluorophore (440 nm for CyPet, left; 515 nm for YPet, right). Expressed in dysgenic myotubes this construct localized in fluorescent puncta, which were concentrated at the cell surface. Fluorescent puncta of the C-terminally attached dye in dysgenic myotubes perfectly overlap with those of the second fluorophore, attached to the N-terminus (arrows in A). In dyspedic myotubes, the N-terminal fluorescent protein displayed the typical pattern of fluorescent foci on the myotube surface. In contrast, in these myotube type surface-associated puncta were barely observed under excitation of the fluorophore attached to the C-terminal (at pos. 1666; arrows in B), but the fluorescence showed a reticular intracellular pattern (red oval). Bars, 5 μm .

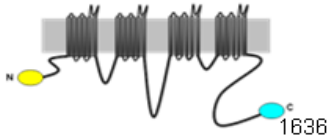
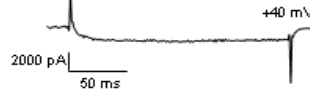
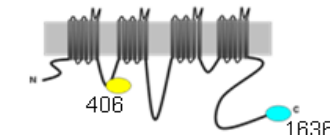
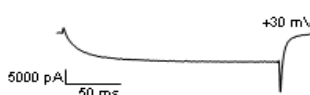
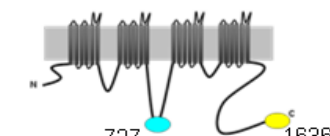

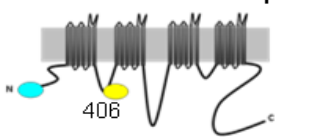

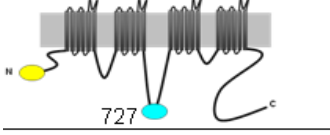
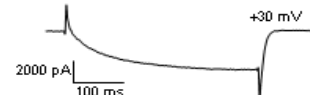
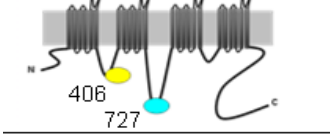

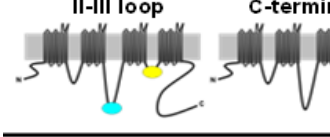
This way, proteolytic cleavage of the C-terminally attached dye at position 1636 (construct $\alpha_{1S}(1636)$ -XPet) could be averted in dysgenic and dyspedic myotubes (Figure 3.2B & Figure 3.5). This further shortening, most importantly, did not alter the function of α_{1S} as a Ca^{2+} channel or as voltage sensor for EC coupling since spontaneous and electrically evoked contractions could be observed regularly for dysgenic myotubes expressing this shortest C-terminal variant (see Table 3.1). Figure 3.5 illustrates a dysgenic and a dyspedic myotube that were injected with cDNA encoding the construct YPet- $\alpha_{1S}(1636)$ -CyPet. In optical sections close to the surface of the myotubes, both the cyan and yellow fluorescence were present in discrete foci that were of typical size and distribution. Thus, the fluorescent foci observed for constructs labelled at position 1636 very likely represent clusters of DHPRs at their normal location in both myotube types. The presence of such fluorescent foci in a dyspedic myotube is consistent with previous results which demonstrated that junctions are formed between the plasma membrane and the SR membrane in the absence of RyR1, and that DHPRs target to those junctions, proving that RyR1 is not absolutely required for α_{1S} trafficking (Takekura & Franzini-Armstrong 1999). To summarize this point, the present data show for the first time that truncation just upstream the PEST motif of the α_{1S} C-terminus does not interfere with targeting and function of the DHPR. This raises questions concerning the physiological function of the α_{1S} residues downstream E¹⁶³⁶.





Once the functionality of single-tag channels was established, the insertion of the respective FRET partner into α_{1S} was carried out. These FRET constructs were also checked for targeting ability and influence on the functionality during the process of EC coupling. Only then, it could be tested whether the presence of RyR1 gave rise to conformational rearrangement of the cytoplasmic domains which could be detected as changes in FRET signals between CyPet and YPet. The targeting and electrophysiological properties of α_{1S} constructs tagged with both, CyPet and YPet at different cytoplasmic domains, including the energy transfer ratios measured for the various constructs examined, are summarized in Table 3.2. Like for the single tagged constructs, α_{1S} constructs tagged with CyPet- and YPet form functional Ca^{2+} channels, except for those which are tagged within the III-IV loop. Spontaneous as well as electrically evoked contractions were frequently observed in dysgenic myotubes expressing the α_{1S} constructs generated for FRET measurements. This indicates that most of the tagged α_{1S} subunits (1) were capable of successfully targeting to the junctions and (2) were functional in terms of EC-coupling. The α_{1S} constructs used for FRET experiments in this study were tested for electrophysiological properties. Hereby, L-type Ca^{2+} currents were recorded with the whole-cell, voltage clamp mode of the patch-clamp technique after cDNA expression of the α_{1S} constructs in dysgenic myotubes (Table 3.2). These traces show that the constructs used for FRET measurements in this study represent functional α_{1S} subunits. The electrophysiological measurements do not include the shortest C-terminal constructs labelled at pos. 1636 since these constructs had not yet been cloned when this collaboration project was carried out. However, since the constructs tagged at pos. 1636 show spontaneous contractions and contractions in response to electrical stimulation (see Table 3.2) it is highly likely that they were also fully functional in terms of skeletal type EC-coupling. The electrophysiological characterization was carried out in a cooperational exchange programme by Dr. Joshua D. Ohrtman (Department of Physiology & Biophysics, University of Colorado, Denver, CO).

In summary, all the tagged α_{1S} constructs with the ability to target to junctions were also able to restore EC coupling (Table 3.2). The presence of two fluorescent proteins within different cytoplasmic domains did not appear to grossly interfere with either the targeting or function of α_{1S} in dysgenic cells, with the exception for constructs carrying a fluorophore within the III-IV loop.

Table 3.2. Schematic display of all CyPet- AND YPet-tagged α_{1S} constructs used for FRET analysis in this study including their targeting and electrophysiological properties. Numbers refer to amino acid residues of α_{1S} position of fluorophore insertion (see section 2.3, Materials and methods for a detailed overview and construction details). Contractions were evoked after cDNA expression in dysgenic myotubes by local, electrical stimulation (see section 2.5.1, Material and Methods) and L-type Ca^{2+} currents were recorded under the whole-cell, voltage clamp mode after cDNA expression in dysgenic myotubes (see section 2.5.2 Material and Methods). * in injected dysgenic muscle, ¹ showed L-type currents but the recorded traces were unusable.

α_{1S} construct / tagged domains	Targeting in				Current trace
	dyspedic myotubes	dysgenic myotubes	Spontaneous contractions*	Evoked contractions / currents*	
N-terminus / C-terminus 	+	+	+	+	
I-II loop / C-terminus 	+/-	+	+	+	
II-III loop / C-terminus 	+	+	+	+	
N-terminus / I-II loop 	+/-	+	+	+	
N-terminus / II-III loop 	+	+	+	+	
I-II loop / II-III loop 	+/-	+	+	+ ¹	
III-IV loop (pos. 1096) / ...  	-	-	-	-	-

 CyPet  YPet

3.2 Quantification of FRET in fluorescent spots

Only for correctly targeted and functional constructs can it be assumed that a correct spatial arrangement of the DHPR subunits (including their intracellular domains) took place within the junctional environment. After inserting the fluorescent proteins into suitable positions of the cytoplasmic domains of α_{1S} it was examined whether the presence of and the potential bidirectional interactions with the RyR1 affected their relative arrangement. Therefore the constructs containing all possible combinations of FRET partners at the different cytoplasmic positions were expressed in dyspedic and dysgenic myotubes, respectively. Comparison of the energy transfer ratios (I_{FRET}) after expression of a particular construct in dyspedic and dysgenic myotubes allowed a determination of whether the spatial arrangement of tagged cytoplasmic sites was affected by the functional coupling to the RyR1. A special technique was used to selectively monitor the I_{FRET} signal from the plasma membrane. Since the correctly targeted CyPet- and YPet-tagged constructs were localized in junctional membranes, FRET analysis required exclusive measurement of pixel intensities within fluorescent foci, rather than from entire myotubes. In the latter case proper analysis would be compromised by the fluorescence intensities in the large areas between the foci, unrelated to the junctional environment. This was an important point to consider, since there can be a substantial fraction of ‘free’ fluorescence within the cytoplasm or at the SR. The determination of energy transfer presented here relied on the 1:1 stoichiometry of FRET partners tagged to the α_{1S} subunits. The sensitized acceptor emission variant was employed to determine the degree of energy transfer. Because the fluorescent foci have an irregular shape, the approach employed was to use the unfiltered donor channel intensity image (I_{CY}) to create a binary mask. The latter had the value of unity for all cyan pixels above an adjustable threshold intensity (= cut-off intensity) and a value of zero below the threshold (see Figure 2.13). The threshold was adjusted so that all low intensity pixels outside the fluorescent puncta vanished, leaving a binary mask that was congruent with the majority of the fluorescent foci of cyan fluorescence. The cyan and yellow fluorescence intensity values (I_{CY} and I_{Y} , respectively) were used for calculations only for those pixels with assigned value of unity within the binary mask (additional details are provided in section 2.7). Assuming there is FRET, as a consequence of resonance energy transfer to YPet the CyPet fluorescence should be lower than would be expected from the quantum yield, and thus would appear quenched (see Figure 2.10). In order to quantify the changes in FRET

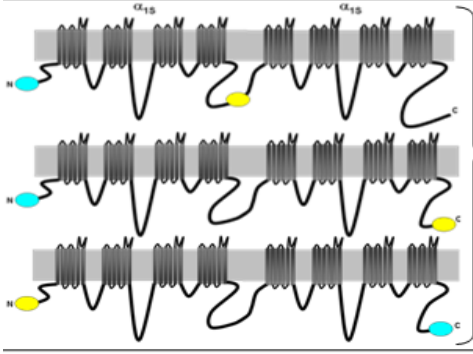
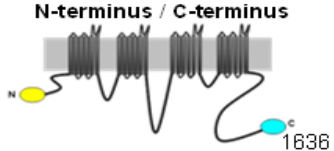
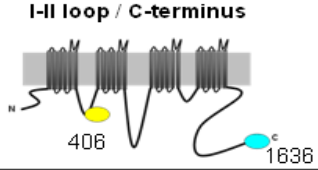
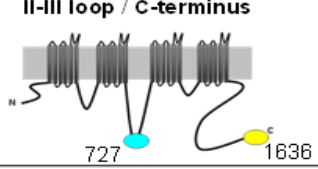
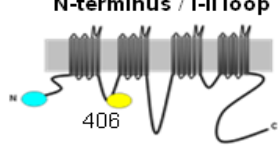
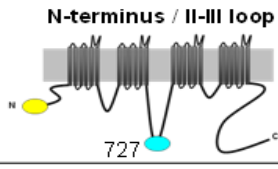
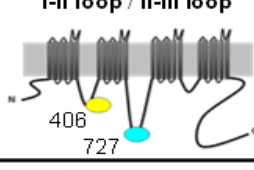
due to absence / presence of RyR1, the ratio I_Y/I_{CY} , corrected for "bleed through" of CyPet emission into the PMT3 channel ($I_{Y,CY}$), was used (see section 2.6 for details).


3.2.1 Significant FRET occurs between the intracellular loops of the DHPR α_{1S}

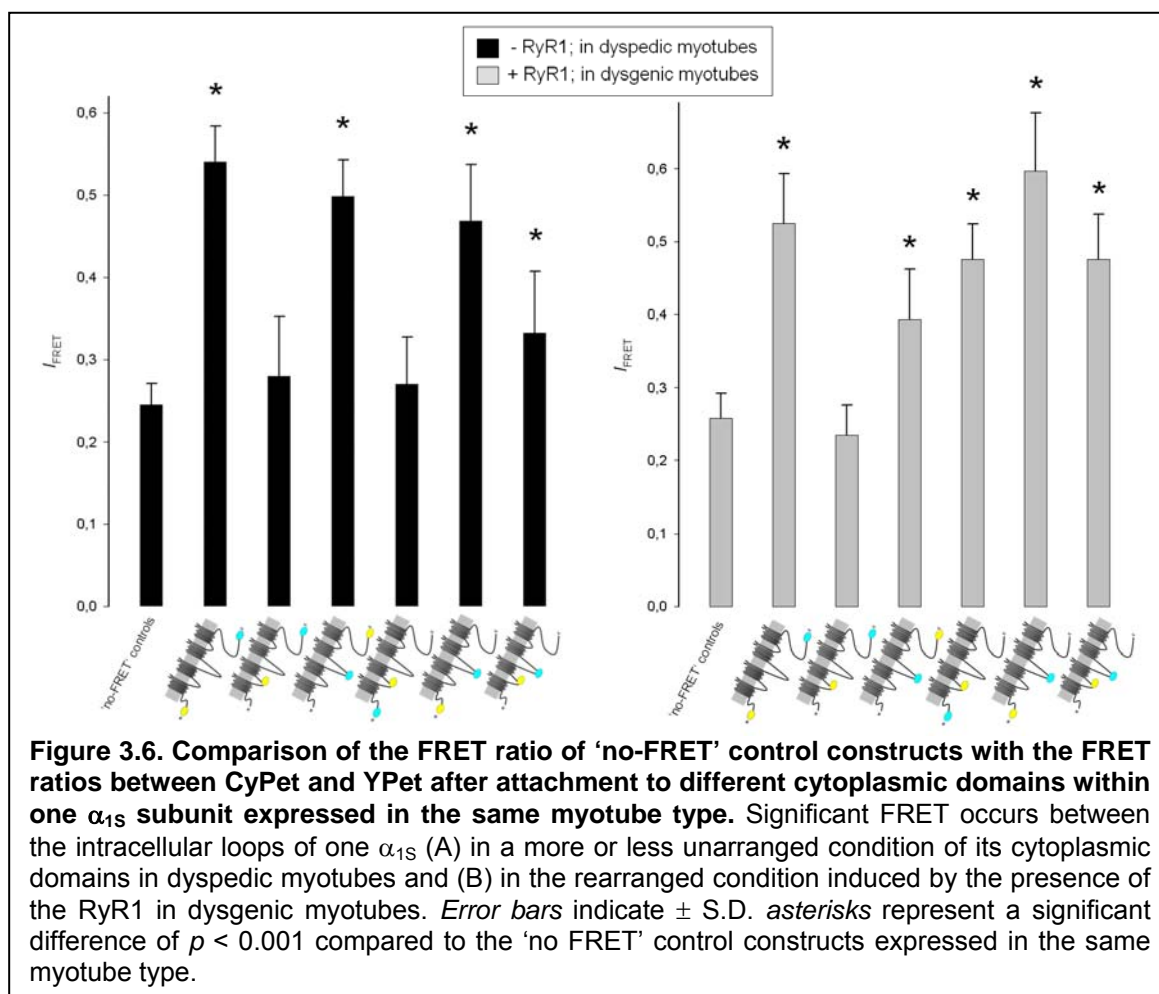
Table 3.3, Figure 3.6 and Figure 3.7 summarize the energy transfer results of this study for CyPet and YPet attached to different cytoplasmic sites of α_{1S} , as well as the effects of the presence of RyR1 on energy transfer ratios I_{FRET} . As 'no-FRET' controls, three discrete tandem α_{1S} constructs were used. In these constructs, the fluorescent tags were far enough apart to exclude the appearance of any significant FRET (Figure 2.7). Every one of **these** control constructs displayed the same relatively low FRET ratio after expression in dyspedic ($I_{FRET} = 0.24 \pm 0.03$) or in dysgenic ($I_{FRET} = 0.26 \pm 0.03$) myotubes. The similar I_{FRET} values found for the different 'no FRET' control constructs in dyspedic and dysgenic myotubes suggest that the energy transfer ratios determined for the single α_{1S} constructs reflect energy transfer process within one α_{1S} subunit (= intramolecular FRET), rather than between fluorophores of adjacent α_{1S} subunits (= intermolecular FRET).

Only a few double tagged α_{1S} constructs generated equally low I_{FRET} values as the 'no-FRET' controls, in the corresponding myotube type (Figure 3.6). In absence of the RyR1 the I_{FRET} values of the 'no-FRET' control constructs and the construct tagged at its I-II loop / N-terminus and of the construct tagged at its I-II loop / C-terminus were similar. Moreover the latter construct produced in presence of the RyR1 an I_{FRET} value that was also similar to the I_{FRET} values generated by the 'no-FRET' control constructs in dysgenic myotubes (Figure 3.6). However, a significant ($p < 0.001$) increase of energy transfer was found for every other functionally expressed FRET construct compared to the 'no FRET' controls expressed in the same myotube type (Figure 3.6). This suggests that the FRET moieties of most combinations within different cytoplasmic domains of one α_{1S} are separated by less than 10 nm in the absence and in the presence of RyR1.

Table 3.3. Schematic display of all CyPet- AND YPet-tagged α_{1S} constructs used for FRET analysis in this study including the I_{FRET} ratios and RyR1 induced changes of the FRET partners attached to different cytoplasmic sites of the DHPR α_{1S} . I_{FRET} values were calculated as described in section 2.6 for the designated constructs expressed and junctional targeted in dyspedic or dysgenic myotubes, as indicated. Data are given as mean \pm S.D., with the numbers of cells indicated in parentheses. Also the (significant) changes from the I_{FRET} ratio of the 'no FRET' control (tandem α_{1S}) constructs (see section 2.3.2.4) to the I_{FRET} ratios between CyPet and YPet after attachment to different cytoplasmic domains within one α_{1S} subunit for the respective myotube type and the I_{FRET} changes induced by the presence of RyR1 for the designated constructs are shown.

α_{1S} construct / tagged domains	I_{FRET}		I_{FRET} change (\pm %)		
	dyspedic myotubes (n)	dysgenic myotubes (n)	control to dyspedics	control to dysgenics	dyspedics to dysgenics
	0.24 \pm 0.03 (35)	0.26 \pm 0.03 (40)	-	-	+8.3
N-terminus / C-terminus 	0.54 \pm 0.04 (23)	0.52 \pm 0.06 (32)	+125.0	+100.0	-3.7
I-II loop / C-terminus 	0.28 \pm 0.07 (36)	0.23 \pm 0.04 (52)	+16.7	-11.5	-17.9
II-III loop / C-terminus 	0.50 \pm 0.04 (44)	0.39 \pm 0.06 (48)	+108.3	+50.0	-22.0
N-terminus / I-II loop 	0.27 \pm 0.06 (12)	0.48 \pm 0.05 (41)	+12.5	+84.6	+77.8
N-terminus / II-III loop 	0.47 \pm 0.07 (38)	0.60 \pm 0.08 (69)	+95.8	+130.7	+27.7
I-II loop / II-III loop 	0.33 \pm 0.08 (14)	0.48 \pm 0.06 (42)	+37.5	+84.6	+45.5

 CyPet  YPet

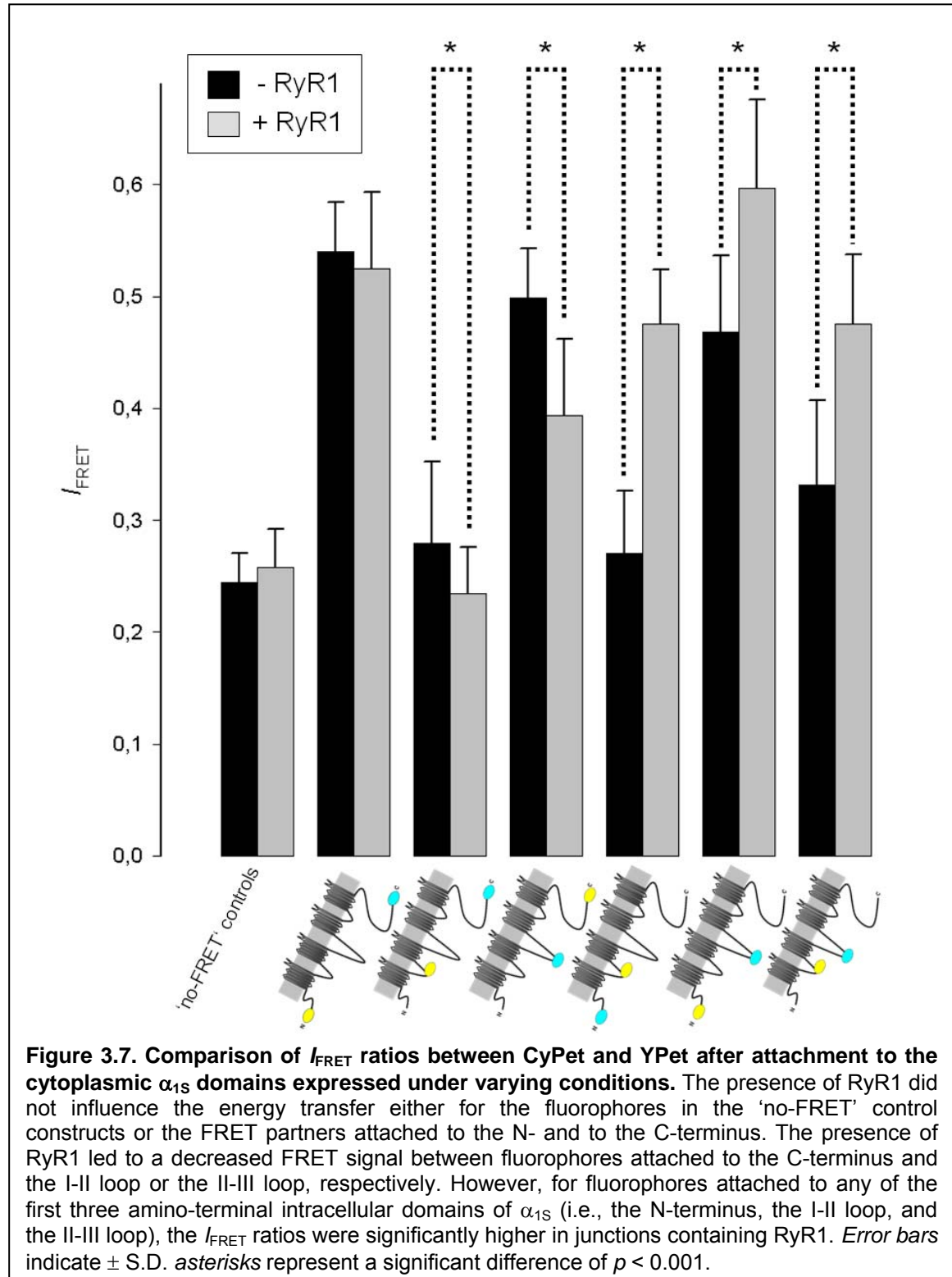


In the absence of RyR1 the relatively long α_{1S} II-III-loop exhibits strong FRET to both the N-terminus and the C-terminus of α_{1S} , indicating close proximity of these regions when mechanical coupling is lacking (Figure 3.6). In contrast, relatively low FRET intensities were found for constructs tagged within the I-II loop and one of the aforementioned three cytoplasmic domains as second tag site in dyspedic myotubes. The respective relatively high I_{FRET} values for the α_{1S} II-III-loop and the two termini range from 0.47 ± 0.07 (N-terminus / II-III loop) over 0.50 ± 0.04 (C-terminus / II-III-loop) to 0.54 ± 0.04 (N-terminus / C-term), whereas the (significantly lower) I_{FRET} values for the energy transfer between the α_{1S} I-II loop and these three cytoplasmic domains range from 0.27 ± 0.05 (N-terminus / I-II loop) over 0.28 ± 0.07 (C-terminus / I-II loop) to 0.33 ± 0.07 (II-III loop / I-II loop) (see Table 3.3). This changed significantly ($p < 0.001$) when the FRET constructs were expressed in dysgenic myotubes, in which the cytoplasmic loops of α_{1S} are believed to undergo direct functional interaction with the RyR1 (Table 3.3 and Figure 3.7).

3.2.2 Quantifying differences in FRET ratio associated with absence or presence of RyR1

The presence of RyR1 altered significantly the intramolecular energy transfer signal for every double tagged construct with the exception of the N- and C-terminally tagged α_{1S} (Figure 3.7). Thus, for α_{1S} subunits that are (1) functionally expressed in dysgenic myotubes and (2) able of targeting in dyspedic myotubes, RyR1 presence induces considerable spatial rearrangements within the cytoplasmic interface of α_{1S} . For the N- and C-terminally tagged α_{1S} , YPet- $\alpha_{1S}(1636)$ -CyPet, the relatively strong I_{FRET} values did not change significantly upon expression in dyspedic ($0,54 \pm 0.04$) and dysgenic myotubes ($0,52 \pm 0.06$) (Table 3.3 and Figure 3.7). All other α_{1S} FRET constructs showed significant changes in their FRET signal when their expression in dysgenic myotubes is compared to that in dyspedic myotubes (Figure 3.7). The energy transfer between the C-terminus and the I-II loop and between the C-terminus and the II-III loop decreased significantly from expression in dyspedic to dysgenic myotubes. Quantitatively, the I_{FRET} signal between the C-terminus and the I-II loop decreased by 18 % in presence of RyR1 (from 0.28 ± 0.07 to 0.23 ± 0.04), and the signal between the C-terminus and the II-III loop decreased by 22 % (from 0.50 ± 0.04 to 0.39 ± 0.06) (Table 3.3 and Figure 3.7). At the same time the presence of RyR1 caused a significant increase of energy transfer between the N-terminus and the two aforementioned α_{1S} loops (i.e., the I-II and II-III loop) in dysgenic myotubes. The energy transfer signals for the N-terminus to the I-II loop and to the II-III loop in dysgenic myotubes were significantly higher, by 78 % (0.27 ± 0.06 to 0.48 ± 0.05) and by 28 % (0.47 ± 0.07 to 0.60 ± 0.08), respectively, compared with the same constructs expressed in dyspedic myotubes (Table 3.3 and Figure 3.7). The fluorophores attached to α_{1S} within these two specific loops showed a significantly increased energy transfer of about 45 % (from an I_{FRET} of 0.33 ± 0.08 to 0.48 ± 0.06) in the presence of RyR1. Thus, the presence of RyR1 seems to bring these first three amino-terminal cytoplasmic domains of α_{1S} (i.e., the N-terminus, the I-II loop, and the II-III loop) into closer proximity while it seems to increase the distances between the C-terminus and the two examined α_{1S} loops (i.e., I-II loop and II-III loop). Thus, the fluorophores within the cytoplasmic loops of α_{1S} in dysgenic myotubes (i.e., within the functional skeletal muscle-type EC coupling apparatus) are clearly positioned in a different environment, in terms of inter-fluorophore distance or orientation, as compared

to the arrangement in dyspedic myotubes. This likely occurs due to rearrangements caused by interactions with the RyR1. These observations strongly support the idea of direct protein-protein interactions between the DHPR and RyR1 as the characteristic feature of skeletal muscle-type EC coupling.



4. Discussion

4.1 Significant FRET between cytoplasmic loops of the DHPR α_{1S} subunit

This study demonstrates that FRET measurements using the sensitized emission variant can provide convincing information about conformational rearrangements of biomolecules within living cells. Thus, it could be shown here that the α_{1S} cytoplasmic interface undergoes significant spatial reorganization upon association with the RyR1. FRET signals (I_{FRET}) could be obtained from dyspedic and dysgenic myotubes for all doubly-tagged constructs capable of junctional targeting. In this context, the fluorophore pair CyPet / YPet has proven a very sensitive indicator for FRET and for changes of the latter, when used within the molecular dimensions of a single α_{1S} subunit. But which are the molecular dimensions of α_{1S} or of the entire DHPR? A 3D reconstruction of a α_1 - β complex of the DHPR presented by Murata *et al.* (2009) (see Figure 1.8B) displayed a globular structure with estimated dimensions of 11.5×11.5 nm (10.5 nm high), pretty much within the sensitive range of FRET. The significantly higher FRET signals in nearly every single- α_{1S} construct, as compared to the I_{FRET} values measured for the ‘no-FRET’ tandem- α_{1S} constructs (see Figure 3.6) reflect the constriction to one α_{1S} , imposed by the limited spatial range available for FRET measurements. However, excessive FRET changes were not expected for the cytoplasmic α_{1S} loops upon co-expression with the RyR1: One could expect that in dyspedic myotubes, i.e., in the absence of RyR1, the cytoplasmic α_{1S} domains reach more or less freely from their transmembrane anchors into the cytoplasmic gap of the junctions. However, it is important to note that the N- and C-terminus of α_{1S} have only a single site of attachment to the channel, whereas the α_{1S} loops are anchored to the transmembrane domains at both sites (see Figure 1.5). Thus, the unarranged sites of attachment show differences in length, stabilization properties, and motional freedom. However, the I_{FRET} values recorded from dyspedic myotubes varied within a smaller range (from 0.28 ± 0.07 to 0.54 ± 0.04) than those received from dysgenic myotubes (from 0.23 ± 0.04 to 0.60 ± 0.08). This by 42 % increased range of I_{FRET} values within the dysgenic data set may reflect a powerful interaction with the

RyR1, which forces a rearrangement (approximation / bending apart) of the loops and termini.

As to the potential presence of intermolecular α_{1S} FRET, i.e., between adjacent DHPRs, a number of studies argues against this possibility. Paolini *et al.* (2004) convincingly demonstrated that the average distance between centers of adjacent DHPRs within a tetrad is ~ 17.5 to 19.5 nm. I_{FRET} values generated from dyspedic and dysgenic myotubes expressing ‘no-FRET’ control constructs were not significantly different (0.24 ± 0.03 for dyspedic, 0.26 ± 0.03 for dysgenic myotubes, respectively). If, in contrast to the present observations, the ‘no-FRET’ control constructs exhibited proteolytic cleavage at the C-terminus, it could be reasoned that they would spatially dissociate into individual α_{1S} subunits. Wolf *et al.* (2003) presented a model for the functional interaction between DHPR and RyR1 in which the N- and the C-terminus of α_{1S} subunits were directed towards the center of a tetrad (Figure 4.1). One might assume that this orientation would allow intermolecular FRET to occur between α_{1S} subunits of the same tetrad when tagged at the N- or at the C-terminus. Relatively high, albeit not significantly different, I_{FRET} values (0.54 ± 0.04 in dyspedic and 0.52 ± 0.06 in dysgenic myotubes, respectively) were measured for the construct YPet- $\alpha_{1S}(1636)$ -CyPet (Figure 3.7). Yet, similar I_{FRET} values for this construct in dyspedic and dysgenic myotubes suggest that the FRET signal does not result from intermolecular energy transfer. Specifically, intermolecular FRET might be expected to decrease in dyspedic myotubes where, unlike dysgenic myotubes, the tagged α_{1S} subunits do not organize into tetrads (Takekura *et al.* 1995). As stated above, no such decrease was observed. Thus, the energy transfer ratios presented in this study are truly reflecting energy transfer between CyPet and YPet moieties of the same α_{1S} . Moreover, the relatively high I_{FRET} values between the N- and the C-terminus in dyspedic and dysgenic myotubes are indicative of their close proximity (although it is not possible to extract from this finding any information about the actual molecular orientation of DHPRs within one tetrad). This statement also applies to all other double-tagged α_{1S} constructs, indicating that their significantly higher I_{FRET} values, as compared to the I_{FRET} of the ‘no-FRET’ constructs, exclusively reflect intramolecular FRET.

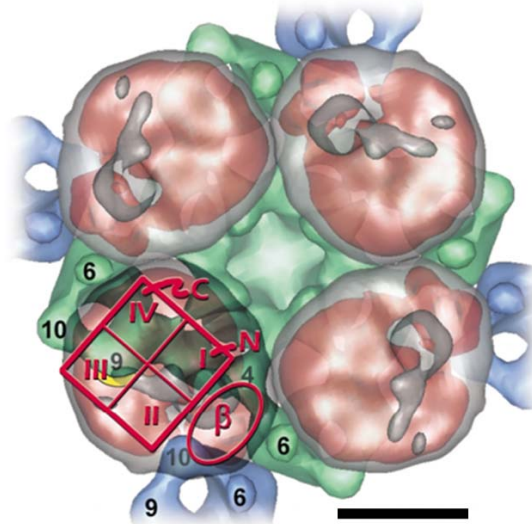
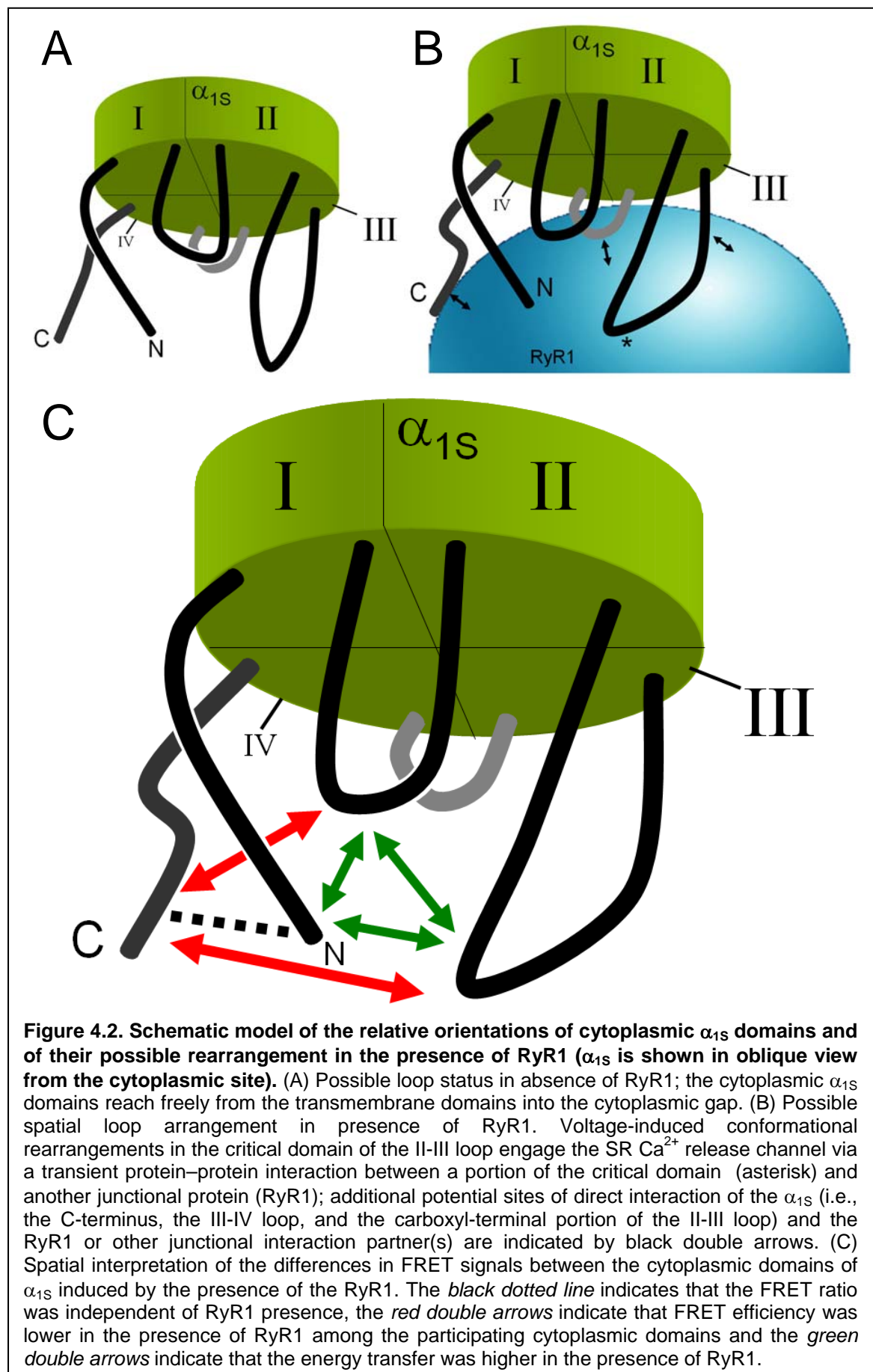


Figure 4.1. Model of the DHP-RyR1 complex by Wolf *et al.* (2003), modified. DHPRs (grey and red) are arranged in tetrads opposing a homotetrameric RyR1 channel (green). View from the t-tubular side, the red square indicates the putative α_1 domain structure. The N-terminus and parts of the C-terminus are shown to point into the center of the tetrad. The molecular edges of neighboring RyR1s are shown in blue. The black numbers designate RyR regions as defined by Wagenknecht & Radermacher (1997). Bar represents 10 nm.

4.2 Rearrangements of cytoplasmic α_{1S} domains in the presence of RyR1

In light of the presented FRET results it appears that most of the cytoplasmic domains of α_{1S} are less than 10 nm apart in dyspedic as well as in dysgenic myotubes. Figure 4.2 illustrate how the effects of RyR1 on the degree of FRET between cytoplasmic α_{1S} sites could be interpreted in terms of spatial rearrangements. It should be noted that the model, although it accounts for the observed FRET changes caused by the presence of RyR (Figure 3.7), does not permit to draw conclusions about the actual location of RyR1 interaction sites. Unlike the study by Papadopoulos *et al.* (2004), this work employed not a singular FRET sensor within α_{1S} to search for potential interaction sites with the RyR1. The focus here lay more on the detection of spatial arrangements within α_{1S} , introduced by the presence of the RyR1 (arrows in Figure 4.2C). However, as the finding of significant differences in energy for a given construct upon expression in the two myotube types shows (Figure 3.7), every cytoplasmic domain of α_{1S} appears to be spatially influenced by the DHP-RyR1 interaction. The energy transfer between the C-terminus and the I-II loop and between the C-terminus and the II-III loop decreased significantly by 18 % and 22 %, respectively, when switching the expression environment from dyspedic



to dysgenic myotubes (red arrows in Figure 4.2C). In contrast, presence of RyR1 caused a significant increase in energy transfer between the N-terminus and the I-II loop (by 78 %), and between the N-terminus and the II-III loop (by 28 %). Furthermore, energy transfer between the fluorophores introduced into these two loops increased by 46 % when RyR1 was present (green arrows in Figure 4.2C). However, presence of RyR1 had no influence on the energy transfer between the N-terminus and the C-terminus (dotted line in Figure 4.2C).

4.3 On the molecular basis of RyR1-caused rearrangement of cytoplasmic α_{1S} domains

Using the CFP-YFP fusion protein tag as a FRET reporter, Papadopoulos *et al.* (2004) found no difference in FRET efficiency between dyspedic and dysgenic myotubes when CFP-YFP was attached to the α_{1S} **N-terminus** (CFP-YFP- α_{1S}). In their study, any observed difference in FRET between dysgenic and dyspedic myotubes, for a particular construct, was regarded as indication that the presence of RyR1 had an impact on the environment of the CFP-YFP attachment site. From the lack of FRET difference for the N-terminal attachment site, Papadopoulos *et al.* (2004) concluded that there may not be close proximity between RyR1 and the N-terminus of α_{1S} . Lorenzon and co-workers (2004) supported this idea in an independent approach employing a streptavidin accessibility strategy, to gauge the distances between sites of the DHPR and the RyR1 or RyR1 associated junctional proteins. In accordance with the important functional role of this α_{1S} region for excitation contraction coupling, both groups presented a model in which the RyR1 may be in close proximity to the α_{1S} **C-terminus** (Figure 4.2B): RyR1-dependent differences in FRET efficiency of the CFP-YFP tandem fused to the α_{1S} C-terminus (α_{1S} short-CFP-YFP) indicated that this region might directly interact with the RyR1 or with structures brought to close proximity to the α_{1S} C-terminus by the presence of the RyR1. Lorenzon *et al.* (2004) demonstrated that the C-terminus of α_{1S} , when tagged with a biotin acceptor domain, is accessible for streptavidin labeling in dyspedic myotubes but not in dysgenic myotubes. Thus, in contrast to the freely moving α_{1S} N-terminus, the C-terminus in dysgenic myotubes is expected to be in a more rigid state. However, of crucial importance for the measurements of the present study was to ensure the integrity of the 1:1 donor to acceptor ratio. This absolute requirement is illustrated by the following

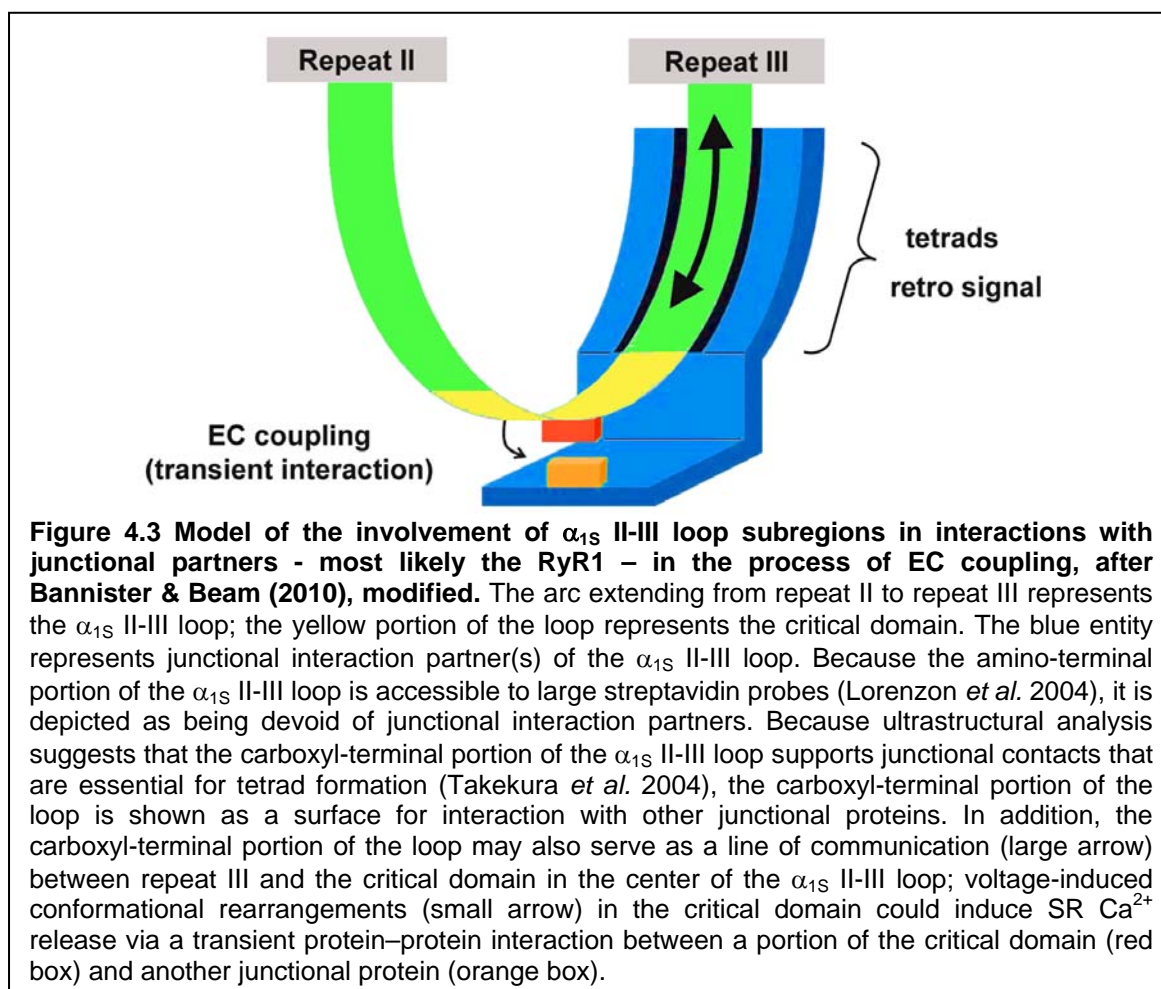
example: Assuming that, for instance, 50 % of the double labeled α_{1S} subunits would lose one of their tags, so that half of the α_{1S} subunits in the junctions would be devoid of the acceptor or of the donor. In the first case, absence of 50 % of the acceptor, the FRET signal calculated would be too low, because (1) the orphaned CyPet molecules would fluoresce brighter and (2) the dissociated YPet molecules would be absent from the junctions and thus would not contribute to the YPet-related fluorescence intensity. In the second instance, absence of 50 % of the donor, the effect of cleavage on the measured FRET degree would depend on whether the donor remains at the junctions or not. If not, the resulting high acceptor-to-donor ratio would lead to overestimation of the FRET degree. If the donor would remain at the junctions, the increased donor-to-acceptor distance would decrease any FRET and would lead to underestimation of the degree of this process. In view of these deleterious effects of cleavage on the reliability of calculated FRET values, the likelihood of such an event had to be minimized. Therefore, the α_{1S} C-terminus was shortened, initially to end at residue 1666. Beam *et al.* (1992) and Papadopoulos *et al.* (2004) had already shown that despite the loss of > 200 residues such a construct was fully functional in terms of targeting and EC-coupling. Furthermore, Papadopoulos *et al.* (2004) did not observe proteolytic release of their C-terminally (position 1666) attached FRET reporter, the CFP-YFP tandem. However, when - in the present study - $\alpha_{1S}(1666)$ -XPet was expressed in dyspedic myotubes, there were indications for proteolytic cleavage upstream the fluorophore sequence. Figure 3.4 illustrates the diffuse to reticular distribution of the proteolytically released fluorophore allegedly attached to α_{1S} position 1666. The reasons for this disagreement with the observations by Papadopoulos *et al.* (2004) are not clear but anyway, it was concluded here that $\alpha_{1S}(1666)$ was not short enough to prevent cleavage and loss of the fluorescent protein. Indeed, by using mass spectrometric analysis, Hulme *et al.* (2005) identified the precise cleavage site on the α_{1S} C-terminus to be at A¹⁶⁶⁴. To ensure persistence of the C-terminal label on α_{1S} , the α_{1S} C-terminus was further shortened, to position E¹⁶³⁶. It was reasoned that, since this shortest construct did not contain A¹⁶⁶⁴ nor the PEST motif (Figure 2.4) (Hulme *et al.* 2005), the proteolytic cleavage of the C-terminus should be prevented in both myotube types. Indeed, this was the case and the FRET measurements with this type of constructs proved reliable, yielding constant energy transfer signals. Yet, there is still no satisfactory explanation for the preferred proteolytic cleavage of the C-terminus of $\alpha_{1S}(1666)$ -XPet constructs in **dyspedic** myotubes. It has been assumed that a

calpain-like protease may be responsible for *in vivo* proteolytic cleavage of α_1 subunits (Hulme *et al.* 2005). It could be speculated that in dyspedic myotubes (which possess endogenous α_{1S}) this protease could be upregulated to meet the requirement for cleavage of the endogenous, full length α_{1S} . The finding of the present study that deletion of an even larger part of the α_{1S} C-terminus (as is the case with $\alpha_{1S}(1636)$ -XPet) is compatible with targeting and EC-coupling (see Table 3.1 and 3.2), is surprising. Based on observations upon expression of different α_1 subunit isoforms in dysgenic myotubes, Flucher *et al.* (2000) concluded that the α_{1S} C-terminus region 1607–1661 is critical for specific targeting of α_{1S} to the junctions. A transfer of this α_{1S} ‘targeting domain’ to the corresponding region of the neuronal α_{1A} subunit enabled junctional targeting of the latter (which wild-type α_{1A} normally does *not*). However, the FRET constructs used in the present study terminate at α_{1S} residue E¹⁶³⁶ (see Figure 2.4) which would mean there is a massive deletion within Flucher's ‘targeting domain’, yet there is no interference with junctional targeting (Figure 3.2 and 3.5). Thus, at least the carboxyl-terminal half of the ‘targeting domain’ (residues 1637-1661) can not be essential for junctional targeting of α_{1S} . In addition to correct targeting, the frequently observed spontaneous and evoked contractions of dysgenic myotubes expressing these constructs (Table 3.2) shows that deletion of the last 237 α_{1S} residues does not interfere with EC-coupling. Thus, the present study reveals that the RyR1 interaction sites of the α_{1S} C-terminus which are relevant for EC-coupling have to be located upstream of α_{1S} residue E¹⁶³⁶.

The relatively strong energy transfer for N/C-terminally labelled α_{1S} suggests that the N-terminus and the shortened C-terminus of α_{1S} are in close proximity. The fact that this high I_{FRET} was not significantly different when comparing expression in dyspedic and dysgenic myotubes, argues against appreciable changes in the relative positions of these domains (Figure 3.7 and 4.2). This could also imply that they are relocating as a set in the presence of the RyR1. Alternatively, the rather flexible N-terminus (for which there are no indications for interactions with the RyR1) could, upon association of the C-terminus with the RyR1, be passively dragged to a position which would not alter the energy transfer between the two fluorophores. Another possibility is that the position of both termini is refractory with respect to RyR1 presence. However, this appears to be very unlikely, since (1) the α_{1S} C-terminus displays significant FRET changes between dysgenic and dyspedic

myotubes when the second tag is not the N-terminus and (2) numerous studies argue towards a direct interaction between C-terminus and the RyR1.

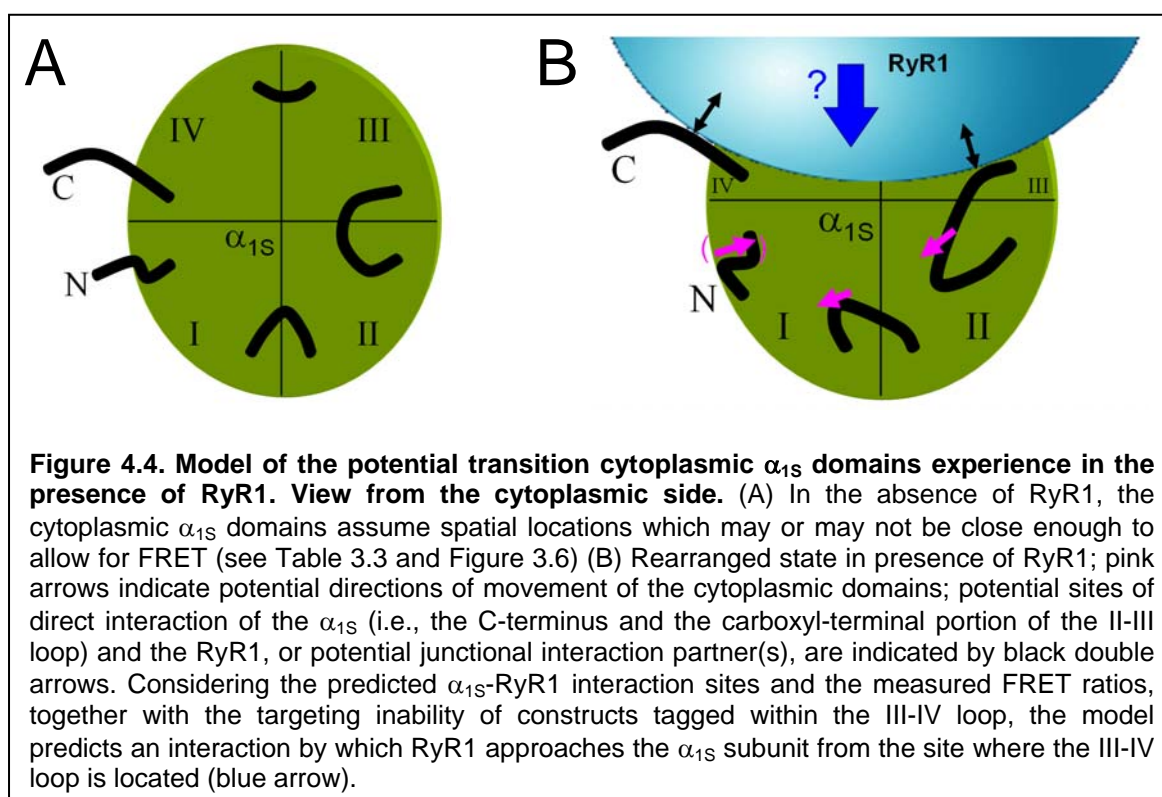
Papadopoulos *et al.* (2004) showed that presence of RyR1 changed the FRET efficiency when the CFP-YFP tandem was inserted into the **II-III loop**, replacing the 'peptide A' region (see Figure 2.6C) upstream the critical domain (construct name: $\alpha_{1S(I-II)}$ -CFP-YFP- $(III-IV)$). EC coupling could be restored in dysgenic myotubes by expression of this construct. Thus, it seems unlikely that the proximal (amino-terminal) segments within the α_{1S} II-III loop directly participate in protein-protein interactions with the RyR1. In support of this idea are the streptavidin-accessibility experiments by (Lorenzon *et al.* 2004; Lorenzon & Beam 2007). In contrast, the 'critical domain' region, a sequence located in the center of the II-III loop, was identified as essential for skeletal muscle-type EC coupling (Nakai *et al.* 1998b). Takekura *et al.* (2004) suggested that additional conserved elements within the II-III loop of α_{1S} , in addition to the critical domain region, would contribute - though weakly - to tetrad formation. Thus, Bannister and co-workers (2009) investigated the relevance of the α_{1S} II-III loop region downstream of the critical domain for EC coupling. This region of the II-III loop is highly conserved among α_1 subunits of L-type Calcium channels (α_{1C} and α_{1M} , for instance (Wilkins *et al.* 2001)), although subunits other than α_{1S} display no indications for mechanical linkage to the RyR1 (for instance, there is no tetrad formation). Yet, this conserved region within the α_{1S} II-III loop may be an important accessory site of for RyR1 interaction (Bannister *et al.* 2009). A model illustrating the roles assigned to the critical domain and the carboxyl-terminal region of the α_{1S} II-III loop in the communication with the RyR1 is presented in Figure 4.3, (Beam & Bannister 2010). In this model, the α_{1S} II-III loop (represented by the green/yellow arc) is juxtaposed to the RyR1, or to one or more other junctional interaction partners (represented collectively by the blue moiety, see also Figure 4.2B). There are portions of the model which are intentionally kept vague because of substantial gaps in the current knowledge about the structural components engaged by the process of EC coupling in skeletal muscle. So far, there is only very sparse information about the identities of junctional proteins other than the RyR1, which could undergo interactions with the DHPR. Several motifs that may facilitate interactions with various signaling and scaffolding proteins, additionally to RyR1, have been localized within the α_{1S} C-terminus but not specifically within its carboxyl-terminal region of the II-III loop (see Figure 1.5).



From the RyR1 point of view, several regions of its tremendous cytoplasmic domain appear to contribute to bidirectional signalling with the DHPR (Protasi *et al.* 2002; Sheridan *et al.* 2006). In these latter studies, chimeric RyRs (e.g., half RyR1, half RyR2) were expressed in dyspedic myotubes and it was attempted to identify the RyR1 regions whose presence within the chimera was essential for tetrad formation and, thus, for skeletal muscle type EC-coupling (Nakai *et al.* 1998; Perez *et al.* 2003). However, given the poorly understood molecular topology of the RyR1, the RyR1 regions identified in the above studies might as well be involved in an indirect way, for instance, by conformational stabilization or interdomain interaction within the RyR1 (Uchinoumi *et al.* 2010). Also, the participation of other proteins associated with the DHPR-RyR1 complex (e.g., Homer, Calmodulin), which could mediate the interaction by exerting a bridge-function, can not be excluded (Hamilton *et al.* 2000; Treves *et al.* 2009). Thus, the blue moiety shown in Figure 4.3 could include components of RyR1, β_{1A} or other yet-to-be identified proteins. Whatever the interaction partner, the significant I_{FRET} changes found in

the present study for constructs tagged at the α_{1S} II-III loop, reflect the critical role of this cytoplasmic domain in EC coupling.

Can the II-III loop be further dissected in terms of subregions with discrete functions in the interaction with RyR1? The regions outside the critical domain could have a modulatory role or could function as molecular hinge for transmission of conformational changes accompanied by the association and/or activation of the two channels to other parts of the macromolecular complex. For instance, the central region of the II-III loop could be **indirectly** affected by the interaction of RyR1 with the carboxyl-terminal II-III loop region. In such a scenario, the moiety (RyR) shown in blue in Figure 4.3 could push the II-III loop regions upstream the interacting segment towards the amino-terminal site of the loop (see also Figure 4.4). This could explain the significant increase in energy transfer between the II-III loop and the two amino-terminally located intracellular domains of α_{1S} (i.e., the N-terminus and the I-II loop) in presence of the RyR1 (Figure 4.2C and Figure 3.7). Such a molecular shoving of the cytoplasmic α_{1S} interface by the presence of RyR1 could also explain the observed increases in energy transfer between the I-II loop and the N-terminus (Table 3.3 and Figure 3.7).



In dyspedic myotubes, the relatively extended II-III-loop (138 residues long) and the two allegedly more mobile termini of α_{1S} appear to be in closer proximity than either of them with the considerably shorter **I-II loop** (97 residues long; see Figure 3.6 and 4.2A). A possible explanation for this observation could be that the β_{1A} subunit, in the course of its interaction with I-II loop, intercalates into the α_{1S} interface where the other loops and the termini reside and pushes that loop apart from these structures. Leuranguer *et al.* (2006), by combining measurements of FRET with fluorescence recovery after photobleaching (FRAP), demonstrated that the β_{1A} subunit is stably associated with the α_{1S} subunit in junctions of living myotubes, independent of the presence of the RyR1. This firm association between α_{1S} and β_{1A} reflects the essential role the β_{1A} subunit plays in α_{1S} targeting (Strube *et al.* 1996; Neuhuber *et al.* 1998; Schredelseker *et al.* 2005). The essential requirement for an α_{1S} - β_{1A} interaction is also documented by the finding that incorporation of a fluorophore into the I-II loop upstream the AID resulted in suppression of junctional targeting of the α_{1S} , though most prominent in dyspedic myotubes (Figure 3.3C). This attempt to insert a fluorophore into the short sequence segment (22 residues; see Figure 2.6A) connecting the end of α_{1S} repeat I with the AID could lead to steric hindrance or even to disruption of the microdomain structure of this region, thus affecting the AID- β_{1A} interaction. However, the effect of fluorophore insertion was not too severe, since the respective constructs exhibited an almost normal targeting behaviour in dysgenic myotubes (Figure 3.3A). One point to consider though arises from the fact that in dyspedic myotubes, considerable amounts of endogenous α_{1S} are present (Takeshima *et al.* 1994; Takekura *et al.* 1995). Thus, the manoeuvre of inserting a fluorophore so close to the AID could lead to preferred interaction of β_{1A} with endogenous α_{1S} subunits instead of the expressed FRET constructs. This possible unequal competition for binding to β_{1A} for being targeted does not exist in dysgenic myotubes, which are defined by the lack of endogenous α_{1S} (Tanabe *et al.* 1988). However, the problem of differential targeting capability vanished when fluorophore insertion into the I-II loop was carried out downstream the AID. This type of constructs did not show any restrictions in junctional targeting in any cell type (see Figure 3.3), indicating that interaction with β_{1A} (or with other proteins relevant for targeting and for EC coupling) remained unaffected. By virtue of its firm interaction with β_{1A} , the orientation of the I-II loop may be stabilized already in dyspedic myotubes, and undergo only minor spatial reorganisation, while the final

functional position of the other cytoplasmic α_{1S} structures will be dictated by the RyR1 interaction, which, as stated above, could lead to spatial separation from or approximation to the I-II loop.

The α_{1S} **III-IV loop** appears to participate indirectly in EC coupling, by influencing DHPR gating transitions important both for EC coupling and activation of L-type conductance (Bannister *et al.* 2008). However, when the mode of α_{1S} -RyR1 interaction is according to the model in Figure 4.4, an intimate proximity between RyR1 and III-IV loop is very probable (Figure 4.2B and Figure 4.4B). Unfortunately, junctional targeting of α_{1S} was disrupted by attempts to tag the III-IV loop (see Figure 3.2), a channel region previously thought to be of only minor importance for effective targeting (Weiss *et al.* 2004; Bannister *et al.* 2008). Though not very likely in view of the robust AID- β_{1A} interaction, it can not be ruled out that the failure of III-IV loop-tagged constructs to target could result from an impairment of the α_{1S} association with the β_{1A} subunit. In such a case, a possible mechanism could be that the α_{1S} - β_{1A} interaction is massively hindered by the presence of the fluorescent protein so close to the regions of membrane insertion of the loops, including that of the I-II loop. Thus, tagging the rather short III-IV loop could have a similar steric effect as the insertion of the fluorescent protein within the I-II upstream the AID.

Interestingly, susceptibility to malignant hyperthermia is not only caused by RyR1 mutations, but has also been mapped to the α_{1S} III-IV loop (R¹⁰⁸⁶H, for instance; (Monnier *et al.* 1997) (Figure 2.6B). Obviously, these mutations are not localized within the membrane domains involved in channel gating, nor to the allegedly essential ‘critical domain’ or to potential phosphorylation sites. Thus, when even a single Arginine-Histidine substitution within the III-IV loop affects the α_{1S} -RyR1 interaction, it is conceivable that introduction of a 27 kDa fluorophore almost at the same position (right behind R¹⁰⁹⁶, see Figure 2.6B) could prevent targeting to the junctions. In summary, the α_{1S} III-IV loop of the α_{1S} seems to be not only important for the communication with RyR1 but also for targeting (Figure 4.2B).

It has been assumed that there is an interaction of β_{1A} with the RyR1 and that this interaction of equal importance to EC coupling as is the α_{1S} -RyR1 interaction (Gregg *et al.* 1996; Leuranguer *et al.* 2006). However, if there is such interaction, it has an affinity

not high enough to cause stable association of fluorescently labelled β_{1A} at junctions equipped only with RyR1 (dysgenic myotubes) (Papadopoulos *et al.* 2004). Yet, in the presence of α_{1S} , the interaction of β_{1A} with the AID might cause a structural reorganization of the accessory subunit which then exposes interaction sites for the RyR1 essential for EC coupling. Indeed, recent experiments by Polster & Papadopoulos (unpublished data) show that when, in dysgenic myotubes, β_{1A} is coexpressed with the I-II loop peptide of α_{1S} instead of the complete subunit, the β_{1A} -loop complex translocates to the myotube surface, where it also co-localizes with fluorescently labelled RyR1. It should be noted that individual expression of either the I-II loop or the β_{1A} (in the absence of α_{1S}) leads to an exclusively diffuse distribution of the proteins within dysgenic myotubes. Because tetrad formation and, thus, skeletal muscle type EC coupling is only then present when both α_{1S} and β_{1A} are together in junctions, β_{1A} 's contribution can be regarded as essential. However, as to what degree the subunit contributes to the dynamic interactions between the DHPR and the RyR1 during EC coupling remains to be elucidated. From the current point of view, it can not even be excluded that β_{1A} is an immediate component of the trigger mechanism for SR Ca^{2+} release. The observations of the present study allow the speculation that the interaction of RyR1 with the distal region of the α_{1S} II-III loop and with the β_{1A} subunit could push the II-III loop and drag the I-II loop towards the N-terminus of α_{1S} . These motions generate a 'meeting point' for the two loops and the N-terminus (Figure 4.2C and 4.4B). This notion is based on the observation that energy transfer significantly increases when the two fluorophores are introduced into any of the first three amino-terminal intracellular domains of α_{1S} (i.e., the N-terminus, the I-II loop, and the II-III loop) in presence of the RyR1 (Table 3.3 and Figure 3.7). Thus, these findings rather support the view of a direct protein-protein interaction between α_{1S} and RyR1. As discussed above, the first three cytoplasmic α_{1S} domains display closer proximity in the presence of the RyR1. However, at the same time the energy transfer between the C-terminus and both the I-II loop and the II-III loop is decreased, implying their distance increases in the presence of RyR1 (Figure 4.2C and Table 3.3). In view of these significant RyR1-induced movements of cytoplasmic α_{1S} domains, it is surprising that the energy transfer between the α_{1S} N-terminus and C-terminus remains almost constant. It can be assumed that the α_{1S} C-terminus is more or less fixed by the interaction with the RyR1 in dysgenic myotubes (Lorenzon & Beam 2007). If then, the position of the

N-terminus, which most likely does not interact with the RyR1 is defined by the relocations of the RyR1-interacting domains, it is possible that the final position assumed by the N-terminus is at the same distance to the C-terminus as before (in the absence of RyR1). But how can the FRET changes between the N-terminus and the I-II loop / II-III loop be explained (Figure 4.2C and 4.4B)? As mentioned above, a movement of the two loops towards the N-terminus seems to be very likely because an orientation into the amino-terminal direction would possibly explain their increased distance to the C-terminus (Figure 4.2C and 4.4B). Whatever the exact interpretation, the II–III loop and the I-II loop are in a different microenvironment when RyR1 is present.

The model presented in Figure 4.2 and 4.4 is the first one to show potential conformational changes in the arrangement of cytoplasmic α_{1S} domains in dependence of RyR1 presence. There are portions of this model which are intentionally kept vague, paying tribute to the substantial gaps in the current knowledge about the particulars of skeletal muscle-type EC coupling. The identities of the junctional proteins postulated to be directly contacted by the α_{1S} loops have not yet been confirmed. Thus, the results of this study do not exclude other roles of α_{1S} regions which originally have been implicated in direct interactions with the RyR1 (Yang *et al.* 2007; Bleunven *et al.* 2008). Although the importance of the α_{1S} II–III loop for coupling to the RyR1 is almost universally accepted, the numerous significant changes of I_{FRET} between the α_{1S} cytoplasmic domains support the idea of multiple interacting domains during the process of EC-coupling.

The RyR1 organizes DHPRs into tetrads and the present study reports that this is accompanied by a considerable reorganization of the cytoplasmic α_{1S} interface. Amazingly, this complex possesses enough spatial reserve to accommodate the substantial additional mass of 2×27 kDa contributed by the fluorescent proteins (each of which occupies a cylindrical space 4.2 nm in height and 2.4 nm diameter (Brejc *et al.* 1997)). Moreover, if all the insertion points of the fluorophores within α_{1S} , resulting in functional subunits, are considered, a much higher mass will result which theoretically could be incorporated into the DHPR-RyR1 interface without interfering with function. Of course, it can not be excluded that the normal molecular architecture of the macromolecular complex consisting of DHPR, RyR, and of other junctional proteins is violated to some degree to allow fluorophore accommodation. Yet, such alterations associated with the

nature of these experiments appear to be tolerated by the junctions, revealing that EC coupling in skeletal muscle is a structurally well-secured process.

Unlike the cardiac RyR2, RyR1 responds only poorly to modest elevation of sarcoplasmic $[Ca^{2+}]$. The rearrangements of α_{1S} domains revealed in the present study most likely goes hand in hand with corresponding movements of RyR1 domains which activate the latter. Thus, this stringent, multilateral interaction might constitute a safety factor for the prevention of inappropriate release of the potentially detrimental calcium cation. This study provides a first basis for a further dissection of the process of skeletal muscle EC coupling. Since this study documents that it is possible to measure minimal changes in the orientation of microdomains, its applicability could be extended to allow for the observation of dynamic changes. Such could be reorientations associated with the activation of the DHPR and their transmission to the RyR1 in the process of EC coupling. Thus, one important goal of future experiments will be to confirm and to characterize the conformational changes associated with the initiation of calcium release in skeletal muscle. These experiments would mean a great advancement in the endeavor to completely understand the process of EC coupling.

4.4 Concluding remarks

It is very likely that during the EC coupling process, a combination of rotation, approximation and shifting occurs among the cytoplasmic α_{1S} domains and vice versa within the gigantic molecular RyR1 'foot' environment. The FRET technique was used to show for the first time conformational rearrangements of cytoplasmic α_{1S} loops associated with the coupling to RyR1. This study provides evidence for substantial conformational rearrangement associated with protein-protein interactions between these main components of the EC coupling apparatus.

All α_{1S} constructs which targeted correctly to junctions also formed functional Ca^{2+} channels and restored EC coupling. Significant intramolecular FRET occurs between the cytoplasmic loops of the DHPR α_{1S} subunit. Presence of RyR1 leads to significant changes in the energy transfer between defined intracellular domains. The III-IV loop of the α_{1S} seems not only to be important for the communication with the RyR1 but is also

important for DHPR targeting. Impaired targeting in dyspedic myotubes of constructs tagged within the I-II loop unmasks a supportive role of RyR1 expression in targeting. According to the results of the present study, it now appears even more likely that skeletal muscle-type EC coupling is mediated by a direct interaction between the cytoplasmic α_{1S} domains and RyR1, because this study demonstrates substantial rearrangements of the α_{1S} loops in the presence of RyR1.

4.5 Outlook

High-resolution structures of the two main players in skeletal muscle-type EC coupling, DHPR and RyR1, would be of great importance for a deeper understanding of the involvement of ion channels in various diseases linked to mutations in those channels. A better knowledge of these ion channel structures brings with it the possibility for rational drug design. Hopefully the information contained in this work will assist in advancing the understanding of EC coupling and will contribute to the multi-disciplinary research on ion channels.

Several different approaches were used to solve the 3D structure of the α_{1S} subunit but none of them has yielded a picture of the exact arrangement of the α_{1S} loops, not to mention their rearrangement in the presence of RyR1. The application of FRET to study protein interactions (e.g., during EC coupling) in combination with other imaging techniques will allow better resolution of molecular interactions at the single cell level.

Although the model shown in Figure 4.2 provides a first impression of possible mechanics of functional interaction between the cytoplasmic interface of the DHPR and the RyR1, the precise nature of communication between these two proteins remains enigmatic. Thus, the results presented in this thesis are only the beginning in the elucidation of the arrangement of α_{1S} loops and of their dynamic role in interactions with the RyR1. Additional experiments using this type of FRET measurements will help to extend our current picture of DHPR-RyR1 interactions. Conformational changes within the DHPR α_{1S} seem to be responsible for the translation of the membrane depolarization signal to the RyR1. A very important goal for the future will be to adopt the FRET technique for tracking dynamic rearrangements of cytoplasmic α_{1S} loops during the proper skeletal muscle-type EC coupling process.

Single-particle 3D reconstructions of cryo-EM images of RyR1 and the structurally similar cardiac isoform RyR2 have been already quite useful in piecing together a more detailed picture of the triad junction. A better knowledge of the α_{1S} I-II loop- β_{1A} interaction could reveal the correct orientation of DHPRs relative to the RyR1 tetramer within reconstructed tetrads. The functional nature of this interaction is an enigma that will require creative experimentation to unfold. Appropriate technologies will provide further insight into the way proteins act during EC coupling *in vivo*. The application of novel genetic systems and proteomic strategies will incrementally contribute information to our knowledge of skeletal muscle-type EC coupling. An additional important goal for future research will be to determine the detailed mechanism of the α_{1S} III-IV loop effects on L-type channel gating. It seems possible that the III-IV loop represents a region of hitherto unrecognized importance for the regulation of all the high voltage-activated channels.

5. References

- AHERN C. A., BHATTACHARYA D., MORTENSON L. & CORONADO R. (2001a) A component of excitation-contraction coupling triggered in the absence of the T671-L690 and L720-Q765 regions of the II-III loop of the dihydropyridine receptor $\alpha(1s)$ pore subunit. *Biophysical Journal*, 81, 3294-3307.
- AHERN C. A., VALLEJO P., POWERS P. A. & CORONADO R. (2001b) Recovery of excitation-contraction coupling by expression of two-domain fragments of the dihydropyridine receptor pore subunit. *Biophysical Journal*, 80, 376A.
- ARIKKATH J. & CAMPBELL K. P. (2003) Auxiliary subunits: essential components of the voltage-gated calcium channel complex. *Curr Opin Neurobiol*, 13, 298-307.
- AVILA G. & DIRKSEN R. T. (2000) Functional impact of the ryanodine receptor on the skeletal muscle L-type $\text{Ca}(2+)$ channel. *J Gen Physiol*, 115, 467-480.
- BANNISTER R. A. (2007) Bridging the myoplasmic gap: recent developments in skeletal muscle excitation-contraction coupling. *J Muscle Res Cell Motil*, 28, 275-283.
- BANNISTER R. A. & BEAM K. G. (2005) The $\alpha 1S$ N-terminus is not essential for bi-directional coupling with RyR1. *Biochem Biophys Res Commun*, 336, 134-141.
- BANNISTER R. A., GRABNER M. & BEAM K. G. (2008) The $\alpha(1S)$ III-IV loop influences 1,4-dihydropyridine receptor gating but is not directly involved in excitation-contraction coupling interactions with the type 1 ryanodine receptor. *J Biol Chem*, 283, 23217-23223.
- BANNISTER R. A., PAPADOPOULOS S., HAARMANN C. S. & BEAM K. G. (2009) Effects of inserting fluorescent proteins into the $\alpha 1S$ II-III loop: insights into excitation-contraction coupling. *J Gen Physiol*, 134, 35-51.
- BEAM K. G. & BANNISTER R. A. (2010) Looking for answers to EC coupling's persistent questions. *J Gen Physiol*, 136, 7-12.
- BEAM K. G. & FRANZINI-ARMSTRONG C. (1997) Functional and structural approaches to the study of excitation-contraction coupling. *Methods Cell Biol*, 52, 283-306.
- BEAN B. P. (1989) Classes of calcium channels in vertebrate cells. *Annu Rev Physiol*, 51, 367-384.
- BERTOCCHINI F., OVITT C. E., CONTI A., BARONE V., SCHOLER H. R., BOTTINELLI R., REGGIANI C. & SORRENTINO V. (1997) Requirement for the ryanodine receptor type 3 for efficient contraction in neonatal skeletal muscles. *EMBO J*, 16, 6956-6963.

- BLEUNVEN C., TREVES S., JINYU X., LEO E., RONJAT M., DE WAARD M., KERN G., FLUCHER B. E. & ZORZATO F. (2008) SRP-27 is a novel component of the supramolecular signalling complex involved in skeletal muscle excitation-contraction coupling. *Biochem J*, 411, 343-349.
- BLOCK B. A., IMAGAWA T., CAMPBELL K. P. & FRANZINI-ARMSTRONG C. (1988) Structural evidence for direct interaction between the molecular components of the transverse tubule/sarcoplasmic reticulum junction in skeletal muscle. *J Cell Biol*, 107, 2587-2600.
- BRAWLEY R. M. & HOSEY M. M. (1992) Identification of two distinct proteins that are immunologically related to the alpha 1 subunit of the skeletal muscle dihydropyridine-sensitive calcium channel. *J Biol Chem*, 267, 18218-18223.
- BREJC K., SIXMA T. K., KITTS P. A., KAIN S. R., TSIEN R. Y., ORMO M. & REMINGTON S. J. (1997) Structural basis for dual excitation and photoisomerization of the *Aequorea victoria* green fluorescent protein. *Proc Natl Acad Sci U S A*, 94, 2306-2311.
- BUCK E. D., NGUYEN H. T., PESSAH I. N. & ALLEN P. D. (1997) Dyspedic mouse skeletal muscle expresses major elements of the triadic junction but lacks detectable ryanodine receptor protein and function. *J Biol Chem*, 272, 7360-7367.
- CARBONNEAU L., BHATTACHARYA D., SHERIDAN D. C. & CORONADO R. (2005) Multiple loops of the dihydropyridine receptor pore subunit are required for full-scale excitation-contraction coupling in skeletal muscle. *Biophys J*, 89, 243-255.
- CATTERALL W. A. (1995) Structure and function of voltage-gated ion channels. *Annu Rev Biochem*, 64, 493-531.
- CATTERALL W. A. (2000) Structure and regulation of voltage-gated Ca²⁺ channels. *Annu Rev Cell Dev Biol*, 16, 521-555.
- CHAUDHARI N. (1992) A single nucleotide deletion in the skeletal muscle-specific calcium channel transcript of muscular dysgenesis (mdg) mice. *J Biol Chem*, 267, 25636-25639.
- CHEN Y. H., LI M. H., ZHANG Y., HE L. L., YAMADA Y., FITZMAURICE A., SHEN Y., ZHANG H., TONG L. & YANG J. (2004) Structural basis of the alpha1-beta subunit interaction of voltage-gated Ca²⁺ channels. *Nature*, 429, 675-680.
- CUI Y., TAE H. S., NORRIS N. C., KARUNASEKARA Y., POULIQUIN P., BOARD P. G., DULHUNTY A. F. & CASAROTTO M. G. (2009) A dihydropyridine receptor alpha1s loop region critical for skeletal muscle contraction is intrinsically unstructured and binds to a SPRY domain of the type 1 ryanodine receptor. *Int J Biochem Cell Biol*, 41, 677-686.
- CURTIS B. M. & CATTERALL W. A. (1984) Purification of the calcium antagonist receptor of the voltage-sensitive calcium channel from skeletal muscle transverse tubules. *Biochemistry*, 23, 2113-2118.

- DE JONGH K. S., MERRICK D. K. & CATTERALL W. A. (1989) Subunits of purified calcium channels: a 212-kDa form of alpha 1 and partial amino acid sequence of a phosphorylation site of an independent beta subunit. *Proc Natl Acad Sci U S A*, 86, 8585-8589.
- DE JONGH K. S., WARNER C., COLVIN A. A. & CATTERALL W. A. (1991) Characterization of the two size forms of the alpha 1 subunit of skeletal muscle L-type calcium channels. *Proc Natl Acad Sci U S A*, 88, 10778-10782.
- EL HAYEK R. & IKEMOTO N. (1998) Identification of the minimum essential region in the II-III loop of the dihydropyridine receptor alpha 1 subunit required for activation of skeletal muscle-type excitation-contraction coupling. *Biochemistry*, 37, 7015-7020.
- ELLIS S. B., WILLIAMS M. E., WAYS N. R., BRENNER R., SHARP A. H., LEUNG A. T., CAMPBELL K. P., MCKENNA E., KOCH W. J., HUI A. & . (1988) Sequence and expression of mRNAs encoding the alpha 1 and alpha 2 subunits of a DHP-sensitive calcium channel. *Science*, 241, 1661-1664.
- FELDER E., PROTASI F., HIRSCH R., FRANZINI-ARMSTRONG C. & ALLEN P. D. (2002) Morphology and molecular composition of sarcoplasmic reticulum surface junctions in the absence of DHPR and RyR in mouse skeletal muscle. *Biophys J*, 82, 3144-3149.
- FLUCHER B. E., ANDREWS S. B., FLEISCHER S., MARKS A. R., CASWELL A. & POWELL J. A. (1993) Triad formation: organization and function of the sarcoplasmic reticulum calcium release channel and triadin in normal and dysgenic muscle in vitro. *J Cell Biol*, 123, 1161-1174.
- FLUCHER B. E. & FRANZINI-ARMSTRONG C. (1996) Formation of junctions involved in excitation-contraction coupling in skeletal and cardiac muscle. *Proc Natl Acad Sci U S A*, 93, 8101-8106.
- FLUCHER B. E., KASIELKE N., GERSTER U., NEUHUBER B. & GRABNER M. (2000) Insertion of the full-length calcium channel alpha(1S) subunit into triads of skeletal muscle in vitro. *FEBS Lett*, 474, 93-98.
- FLUCHER B. E., WEISS R. G. & GRABNER M. (2002) Cooperation of two-domain Ca(2+) channel fragments in triad targeting and restoration of excitation-contraction coupling in skeletal muscle. *Proc Natl Acad Sci U S A*, 99, 10167-10172.
- FÖRSTER T. (1948) Zwischenmolekulare Energiewanderung und Fluoreszenz. *Ann Phys*, 2, 55-75.
- FRANZINI-ARMSTRONG C. (1970) STUDIES OF THE TRIAD : I. Structure of the Junction in Frog Twitch Fibers. *J Cell Biol*, 47, 488-499.
- FRANZINI-ARMSTRONG C. (2004) Functional implications of RyR-dHPR relationships in skeletal and cardiac muscles. *Biol Res*, 37, 507-512.
- FRANZINI-ARMSTRONG C. & KISH J. W. (1995) Alternate disposition of tetrads in peripheral couplings of skeletal muscle. *J Muscle Res Cell Motil*, 16, 319-324.

- FRANZINI-ARMSTRONG C. & NUNZI G. (1983) Junctional feet and particles in the triads of a fast-twitch muscle fibre. *J Muscle Res Cell Motil*, 4, 233-252.
- FREISE D., HELD B., WISSENBACH U., PFEIFER A., TROST C., HIMMERKUS N., SCHWEIG U., FREICHEL M., BIEL M., HOFMANN F., HOTH M. & FLOCKERZI V. (2000) Absence of the gamma subunit of the skeletal muscle dihydropyridine receptor increases L-type Ca²⁺ currents and alters channel inactivation properties. *J Biol Chem*, 275, 14476-14481.
- GARCIA J. & BEAM K. G. (1994) Calcium transients associated with the T type calcium current in myotubes. *J Gen Physiol*, 104, 1113-1128.
- GARCIA J., TANABE T. & BEAM K. G. (1994) Relationship of calcium transients to calcium currents and charge movements in myotubes expressing skeletal and cardiac dihydropyridine receptors. *J Gen Physiol*, 103, 125-147.
- GARCIA K., NABHANI T. & GARCIA J. (2008) The calcium channel alpha2/delta1 subunit is involved in extracellular signalling. *J Physiol*, 586, 727-738.
- GRABNER M., DIRKSEN R. T. & BEAM K. G. (1998) Tagging with green fluorescent protein reveals a distinct subcellular distribution of L-type and non-L-type Ca²⁺ channels expressed in dysgenic myotubes. *Proc Natl Acad Sci U S A*, 95, 1903-1908.
- GRABNER M., DIRKSEN R. T., SUDA N. & BEAM K. G. (1999) The II-III loop of the skeletal muscle dihydropyridine receptor is responsible for the Bi-directional coupling with the ryanodine receptor. *J Biol Chem*, 274, 21913-21919.
- GREGG R. G., MESSING A., STRUBE C., BEURG M., MOSS R., BEHAN M., SUKHAREVA M., HAYNES S., POWELL J. A., CORONADO R. & POWERS P. A. (1996) Absence of the beta subunit (cchb1) of the skeletal muscle dihydropyridine receptor alters expression of the alpha 1 subunit and eliminates excitation-contraction coupling. *Proc Natl Acad Sci U S A*, 93, 13961-13966.
- GURNETT C. A., DE WAARD M. & CAMPBELL K. P. (1996) Dual function of the voltage-dependent Ca²⁺ channel alpha 2 delta subunit in current stimulation and subunit interaction. *Neuron*, 16, 431-440.
- HAMILL O. P., MARTY A., NEHER E., SAKMANN B. & SIGWORTH F. J. (1981) Improved patch-clamp techniques for high-resolution current recording from cells and cell-free membrane patches. *Pflugers Arch*, 391, 85-100.
- HAMILTON S. L., SERYSHEVA I. & STRASBURG G. M. (2000) Calmodulin and Excitation-Contraction Coupling. *News Physiol Sci*, 15, 281-284.
- HESS P. (1990) Calcium channels in vertebrate cells. *Annu Rev Neurosci*, 13, 337-356.
- HOFMANN F., LACINOVA L. & KLUGBAUER N. (1999) Voltage-dependent calcium channels: from structure to function. *Rev Physiol Biochem Pharmacol*, 139, 33-87.

- HOSEY M. M., BARHANIN J., SCHMID A., VANDAELE S., PTASIENSKI J., O'CALLAHAN C., COOPER C. & LAZDUNSKI M. (1987) Photoaffinity labelling and phosphorylation of a 165 kilodalton peptide associated with dihydropyridine and phenylalkylamine-sensitive calcium channels. *Biochem Biophys Res Commun*, 147, 1137-1145.
- HUBER I., WAPPL E., HERZOG A., MITTERDORFER J., GLOSSMANN H., LANGER T. & STRIESSNIG J. (2000) Conserved Ca²⁺-antagonist-binding properties and putative folding structure of a recombinant high-affinity dihydropyridine-binding domain. *Biochem J*, 347 Pt 3, 829-836.
- HULME J. T., KONOKI K., LIN T. W., GRITSENKO M. A., CAMP D. G., BIGELOW D. J. & CATTERALL W. A. (2005) Sites of proteolytic processing and noncovalent association of the distal C-terminal domain of CaV1.1 channels in skeletal muscle. *Proc Natl Acad Sci U S A*, 102, 5274-5279.
- ITO K., KOMAZAKI S., SASAMOTO K., YOSHIDA M., NISHI M., KITAMURA K. & TAKESHIMA H. (2001) Deficiency of triad junction and contraction in mutant skeletal muscle lacking junctophilin type 1. *J Cell Biol*, 154, 1059-1067.
- JAY S. D., ELLIS S. B., MCCUE A. F., WILLIAMS M. E., VEDVICK T. S., HARPOLD M. M. & CAMPBELL K. P. (1990) Primary structure of the gamma subunit of the DHP-sensitive calcium channel from skeletal muscle. *Science*, 248, 490-492.
- JAY S. D., SHARP A. H., KAHL S. D., VEDVICK T. S., HARPOLD M. M. & CAMPBELL K. P. (1991) Structural characterization of the dihydropyridine-sensitive calcium channel alpha 2-subunit and the associated delta peptides. *J Biol Chem*, 266, 3287-3293.
- KASIELKE N., OBERMAIR G. J., KUGLER G., GRABNER M. & FLUCHER B. E. (2003) Cardiac-type EC-coupling in dysgenic myotubes restored with Ca²⁺ channel subunit isoforms alpha1C and alpha1D does not correlate with current density. *Biophys J*, 84, 3816-3828.
- KNUDSON C. M., CHAUDHARI N., SHARP A. H., POWELL J. A., BEAM K. G. & CAMPBELL K. P. (1989) Specific absence of the alpha 1 subunit of the dihydropyridine receptor in mice with muscular dysgenesis. *J Biol Chem*, 264, 1345-1348.
- KOMAZAKI S., ITO K., TAKESHIMA H. & NAKAMURA H. (2002) Deficiency of triad formation in developing skeletal muscle cells lacking junctophilin type 1. *FEBS Lett*, 524, 225-229.
- KUGLER G., GRABNER M., PLATZER J., STRIESSNIG J. & FLUCHER B. E. (2004a) The monoclonal antibody mAB 1A binds to the excitation--contraction coupling domain in the II-III loop of the skeletal muscle calcium channel alpha(1S) subunit. *Arch Biochem Biophys*, 427, 91-100.
- KUGLER G., WEISS R. G., FLUCHER B. E. & GRABNER M. (2004b) Structural requirements of the dihydropyridine receptor alpha1S II-III loop for skeletal-type excitation-contraction coupling. *J Biol Chem*, 279, 4721-4728.

- LAKOWICZ J. R., GRZYCZYNSKI I., GRZYCZYNSKI Z. & DATTELBAUM J. D. (1999) Anisotropy-based sensing with reference fluorophores. *Anal Biochem*, 267, 397-405.
- LEURANGUER V., PAPADOPOULOS S. & BEAM K. G. (2006) Organization of calcium channel beta1a subunits in triad junctions in skeletal muscle. *J Biol Chem*, 281, 3521-3527.
- LIU Z., ZHANG J., LI P., CHEN S. R. & WAGENKNECHT T. (2002) Three-dimensional reconstruction of the recombinant type 2 ryanodine receptor and localization of its divergent region 1. *J Biol Chem*, 277, 46712-46719.
- LLINAS R., SUGIMORI M., HILLMAN D. E. & CHERKSEY B. (1992) Distribution and functional significance of the P-type, voltage-dependent Ca²⁺ channels in the mammalian central nervous system. *Trends Neurosci*, 15, 351-355.
- LORENZON N. M. & BEAM K. G. (2007) Accessibility of targeted DHPR sites to streptavidin and functional effects of binding on EC coupling. *J Gen Physiol*, 130, 379-388.
- LORENZON N. M., HAARMANN C. S., NORRIS E. E., PAPADOPOULOS S. & BEAM K. G. (2004) Metabolic biotinylation as a probe of supramolecular structure of the triad junction in skeletal muscle. *J Biol Chem*, 279, 44057-44064.
- MEISSNER G. (2002) Regulation of mammalian ryanodine receptors. *Front Biosci*, 7, d2072-d2080.
- MELZER W., HERRMANN-FRANK A. & LUTTGAU H. C. (1995) The role of Ca²⁺ ions in excitation-contraction coupling of skeletal muscle fibres. *Biochim Biophys Acta*, 1241, 59-116.
- MONNIER N., PROCACCIO V., STIEGLITZ P. & LUNARDI J. (1997) Malignant-hyperthermia susceptibility is associated with a mutation of the alpha 1-subunit of the human dihydropyridine-sensitive L-type voltage-dependent calcium-channel receptor in skeletal muscle. *Am J Hum Genet*, 60, 1316-1325.
- MURATA K., NISHIMURA S., KUNIYASU A. & NAKAYAMA H. (2009) Three-dimensional structure of the {alpha}1-{beta} complex in the skeletal muscle dihydropyridine receptor by single-particle electron microscopy. *J Electron Microsc (Tokyo)*.
- NAKAI J., DIRKSEN R. T., NGUYEN H. T., PESSAH I. N., BEAM K. G. & ALLEN P. D. (1996) Enhanced dihydropyridine receptor channel activity in the presence of ryanodine receptor. *Nature*, 380, 72-75.
- NAKAI J., SEKIGUCHI N., RANDO T. A., ALLEN P. D. & BEAM K. G. (1998a) Two regions of the ryanodine receptor involved in coupling with L-type Ca²⁺ channels. *J Biol Chem*, 273, 13403-13406.
- NAKAI J., TANABE T., KONNO T., ADAMS B. & BEAM K. G. (1998b) Localization in the II-III loop of the dihydropyridine receptor of a sequence critical for excitation-contraction coupling. *J Biol Chem*, 273, 24983-24986.

- NEUHUBER B., GERSTER U., DORING F., GLOSSMANN H., TANABE T. & FLUCHER B. E. (1998a) Association of calcium channel $\alpha 1S$ and $\beta 1a$ subunits is required for the targeting of $\beta 1a$ but not of $\alpha 1S$ into skeletal muscle triads. *Proc Natl Acad Sci U S A*, 95, 5015-5020.
- NEUHUBER B., GERSTER U., MITTERDORFER J., GLOSSMANN H. & FLUCHER B. E. (1998b) Differential effects of Ca^{2+} channel $\beta 1a$ and $\beta 2a$ subunits on complex formation with $\alpha 1S$ and on current expression in tsA201 cells. *J Biol Chem*, 273, 9110-9118.
- NGUYEN A. W. & DAUGHERTY P. S. (2005) Evolutionary optimization of fluorescent proteins for intracellular FRET. *Nat Biotechnol*, 23, 355-360.
- NOWYCKY M. C., FOX A. P. & TSIEN R. W. (1985) Three types of neuronal calcium channel with different calcium agonist sensitivity. *Nature*, 316, 440-443.
- OBERMAIR G. J., KUGLER G., BAUMGARTNER S., TULUC P., GRABNER M. & FLUCHER B. E. (2005) The Ca^{2+} channel $\alpha 2\delta$ -1 subunit determines Ca^{2+} current kinetics in skeletal muscle but not targeting of $\alpha 1S$ or excitation-contraction coupling. *J Biol Chem*, 280, 2229-2237.
- OPATOWSKY Y., CHOMSKY-HECHT O. & HIRSCH J. A. (2004) Expression, purification and crystallization of a functional core of the voltage-dependent calcium channel β subunit. *Acta Crystallogr D Biol Crystallogr*, 60, 1301-1303.
- PAOLINI C., FESSENDEN J. D., PESSAH I. N. & FRANZINI-ARMSTRONG C. (2004) Evidence for conformational coupling between two calcium channels. *Proc Natl Acad Sci U S A*, 101, 12748-12752.
- PAPADOPOULOS S., LEURANGUER V., BANNISTER R. A. & BEAM K. G. (2004) Mapping sites of potential proximity between the dihydropyridine receptor and RyR1 in muscle using a cyan fluorescent protein-yellow fluorescent protein tandem as a fluorescence resonance energy transfer probe. *J Biol Chem*, 279, 44046-44056.
- PEREZ C. F., VOSS A., PESSAH I. N. & ALLEN P. D. (2003) RyR1/RyR3 chimeras reveal that multiple domains of RyR1 are involved in skeletal-type E-C coupling. *Biophys J*, 84, 2655-2663.
- PISTON D. W. & KREMERS G. J. (2007) Fluorescent protein FRET: the good, the bad and the ugly. *Trends Biochem Sci*, 32, 407-414.
- POWELL J. A., PETHERBRIDGE L. & FLUCHER B. E. (1996) Formation of triads without the dihydropyridine receptor α subunits in cell lines from dysgenic skeletal muscle. *J Cell Biol*, 134, 375-387.
- PRAGNELL M., DE WAARD M., MORI Y., TANABE T., SNUTCH T. P. & CAMPBELL K. P. (1994) Calcium channel β -subunit binds to a conserved motif in the I-II cytoplasmic linker of the $\alpha 1$ -subunit. *Nature*, 368, 67-70.
- PROENZA C., O'BRIEN J., NAKAI J., MUKHERJEE S., ALLEN P. D. & BEAM K. G. (2002) Identification of a region of RyR1 that participates in allosteric coupling with the $\alpha(1S)$ ($Ca(V)1.1$) II-III loop. *J Biol Chem*, 277, 6530-6535.

- PROENZA C., WILKENS C., LORENZON N. M. & BEAM K. G. (2000) A carboxyl-terminal region important for the expression and targeting of the skeletal muscle dihydropyridine receptor. *J Biol Chem*, 275, 23169-23174.
- PROTASI F., FRANZINI-ARMSTRONG C. & ALLEN P. D. (1998) Role of ryanodine receptors in the assembly of calcium release units in skeletal muscle. *J Cell Biol*, 140, 831-842.
- PROTASI F., FRANZINI-ARMSTRONG C. & FLUCHER B. E. (1997) Coordinated incorporation of skeletal muscle dihydropyridine receptors and ryanodine receptors in peripheral couplings of BC3H1 cells. *J Cell Biol*, 137, 859-870.
- PROTASI F., SUN X. H. & FRANZINI-ARMSTRONG C. (1996) Formation and maturation of the calcium release apparatus in developing and adult avian myocardium. *Dev Biol*, 173, 265-278.
- PROTASI F., TAKEKURA H., WANG Y., CHEN S. R., MEISSNER G., ALLEN P. D. & FRANZINI-ARMSTRONG C. (2000) RYR1 and RYR3 have different roles in the assembly of calcium release units of skeletal muscle. *Biophys J*, 79, 2494-2508.
- PROTASI F., PAOLINI C., NAKAI J., BEAM K. G., FRANZINI-ARMSTRONG C. & ALLEN P. D. (2002) Multiple regions of RyR1 mediate functional and structural interactions with alpha(1S)-dihydropyridine receptors in skeletal muscle. *Biophys J*, 83, 3230-3244.
- REUTER H. (1967) The dependence of slow inward current in Purkinje fibres on the extracellular calcium-concentration. *J Physiol*, 192, 479-492.
- REUTER H. (1979) Properties of two inward membrane currents in the heart. *Annu Rev Physiol*, 41, 413-424.
- REUTER H. (1983) Calcium channel modulation by neurotransmitters, enzymes and drugs. *Nature*, 301, 569-574.
- REUTER J. E., MCCORMACK J., INVEST C. F. & BROSE M. O. (1979) Cementation failures. *J Am Dent Assoc*, 98, 173.
- RUTH P., ROHRKASTEN A., BIEL M., BOSSE E., REGULLA S., MEYER H. E., FLOCKERZI V. & HOFMANN F. (1989) Primary structure of the beta subunit of the DHP-sensitive calcium channel from skeletal muscle. *Science*, 245, 1115-1118.
- SAMBROOK, J., FRITSCH, E. F. AND MANIATIS, T. (1989) Molecular Cloning: A Laboratory Manual. *Cold Spring Harbor Laboratory Press*, New York.
- SAMBROOK J. & RUSSEL D. W. (2001) Molecular Cloning: A Laboratory Manual. *Cold Spring Harbor Laboratory Press*, New York
- SAMSO M. & WAGENKNECHT T. (2002) Apocalmodulin and Ca²⁺-calmodulin bind to neighboring locations on the ryanodine receptor. *J Biol Chem*, 277, 1349-1353.

- SAMSO M., WAGENKNECHT T. & ALLEN P. D. (2005) Internal structure and visualization of transmembrane domains of the RyR1 calcium release channel by cryo-EM. *Nat Struct Mol Biol*, 12, 539-544.
- SCHNEIDER M. F. & CHANDLER W. K. (1973) Voltage dependent charge movement of skeletal muscle: a possible step in excitation-contraction coupling. *Nature*, 242, 244-246.
- SCHREDELSEKER J., DI B., V, OBERMAIR G. J., FELDER E. T., FLUCHER B. E., FRANZINI-ARMSTRONG C. & GRABNER M. (2005) The beta 1a subunit is essential for the assembly of dihydropyridine-receptor arrays in skeletal muscle. *Proc Natl Acad Sci U S A*, 102, 17219-17224.
- SERYSHEVA I. I. (2004) Structural insights into excitation-contraction coupling by electron cryomicroscopy. *Biochemistry (Mosc)*, 69, 1226-1232.
- SHERIDAN D. C., TAKEKURA H., FRANZINI-ARMSTRONG C., BEAM K. G., ALLEN P. D. & PEREZ C. F. (2006) Bidirectional signaling between calcium channels of skeletal muscle requires multiple direct and indirect interactions. *Proc Natl Acad Sci U S A*, 103, 19760-19765.
- STRUBE C., BEURG M., POWERS P. A., GREGG R. G. & CORONADO R. (1996) Reduced Ca²⁺ current, charge movement, and absence of Ca²⁺ transients in skeletal muscle deficient in dihydropyridine receptor beta 1 subunit. *Biophys J*, 71, 2531-2543.
- SUN X. H., PROTASI F., TAKAHASHI M., TAKESHIMA H., FERGUSON D. G. & FRANZINI-ARMSTRONG C. (1995) Molecular architecture of membranes involved in excitation-contraction coupling of cardiac muscle. *J Cell Biol*, 129, 659-671.
- TAE H. S., NORRIS N. C., CUI Y., KARUNASEKARA Y., BOARD P. G., DULHUNTY A. F. & CASAROTTO M. G. (2009) Molecular recognition of the disordered dihydropyridine receptor II-III loop by a conserved spry domain of the type 1 ryanodine receptor. *Clin Exp Pharmacol Physiol*, 36, 346-349.
- TAKAHASHI M., SEAGAR M. J., JONES J. F., REBER B. F. & CATTERALL W. A. (1987) Subunit structure of dihydropyridine-sensitive calcium channels from skeletal muscle. *Proc Natl Acad Sci U S A*, 84, 5478-5482.
- TAKEKURA H., BENNETT L., TANABE T., BEAM K. G. & FRANZINI-ARMSTRONG C. (1994) Restoration of junctional tetrads in dysgenic myotubes by dihydropyridine receptor cDNA. *Biophys J*, 67, 793-803.
- TAKEKURA H., NISHI M., NODA T., TAKESHIMA H. & FRANZINI-ARMSTRONG C. (1995) Abnormal junctions between surface membrane and sarcoplasmic reticulum in skeletal muscle with a mutation targeted to the ryanodine receptor. *Proc Natl Acad Sci U S A*, 92, 3381-3385.
- TAKEKURA H. & FRANZINI-ARMSTRONG C. (1999) Correct targeting of dihydropyridine receptors and triadin in dyspedic mouse skeletal muscle in vivo. *Dev Dyn*, 214, 372-380.

- TAKEKURA H., PAOLINI C., FRANZINI-ARMSTRONG C., KUGLER G., GRABNER M. & FLUCHER B. E. (2004) Differential contribution of skeletal and cardiac II-III loop sequences to the assembly of dihydropyridine-receptor arrays in skeletal muscle. *Mol Biol Cell*, 15, 5408-5419.
- TAKESHIMA H. (1993) Primary structure and expression from cDNAs of the ryanodine receptor. *Ann N Y Acad Sci*, 707, 165-177.
- TAKESHIMA H., IINO M., TAKEKURA H., NISHI M., KUNO J., MINOWA O., TAKANO H. & NODA T. (1994) Excitation-contraction uncoupling and muscular degeneration in mice lacking functional skeletal muscle ryanodine-receptor gene. *Nature*, 369, 556-559.
- TAKESHIMA H., YAMAZAWA T., IKEMOTO T., TAKEKURA H., NISHI M., NODA T. & IINO M. (1995) Ca²⁺-induced Ca²⁺ release in myocytes from dyspedic mice lacking the type-1 ryanodine receptor. *EMBO J*, 14, 2999-3006.
- TANABE T., BEAM K. G., ADAMS B. A., NIIDOME T. & NUMA S. (1990a) Regions of the skeletal muscle dihydropyridine receptor critical for excitation-contraction coupling. *Nature*, 346, 567-569.
- TANABE T., BEAM K. G., POWELL J. A. & NUMA S. (1988) Restoration of excitation-contraction coupling and slow calcium current in dysgenic muscle by dihydropyridine receptor complementary DNA. *Nature*, 336, 134-139.
- TANABE T., MIKAMI A., NUMA S. & BEAM K. G. (1990b) Cardiac-type excitation-contraction coupling in dysgenic skeletal muscle injected with cardiac dihydropyridine receptor cDNA. *Nature*, 344, 451-453.
- TREVES S., VUKCEVIC M., MAJ M., THURNHEER R., MOSCA B. & ZORZATO F. (2009) Minor sarcoplasmic reticulum membrane components that modulate excitation-contraction coupling in striated muscles. *J Physiol*, 587, 3071-3079.
- TRUETT G. E., HEEGER P., MYNATT R. L., TRUETT A. A., WALKER J. A. & WARMAN M. L. (2000) Preparation of PCR-quality mouse genomic DNA with hot sodium hydroxide and tris (HotSHOT). *Biotechniques*, 29, 52, 54.
- TSIEN R. W., LIPSCOMBE D., MADISON D. V., BLEY K. R. & FOX A. P. (1988) Multiple types of neuronal calcium channels and their selective modulation. *Trends Neurosci*, 11, 431-438.
- TSIEN R. Y. (1998) The green fluorescent protein. *Annu Rev Biochem*, 67, 509-544.
- UCHINOUMI H., YANO M., SUETOMI T., ONO M., XU X., TATEISHI H., ODA T., OKUDA S., DOI M., KOBAYASHI S., YAMAMOTO T., IKEDA Y., OHKUSA T., IKEMOTO N. & MATSUZAKI M. (2010) Catecholaminergic polymorphic ventricular tachycardia is caused by mutation-linked defective conformational regulation of the ryanodine receptor. *Circ Res*, 106, 1413-1424.
- VAN PETEGEM F., CLARK K. A., CHATELAIN F. C. & MINOR D. L., JR. (2004) Structure of a complex between a voltage-gated calcium channel beta-subunit and an alpha-subunit domain. *Nature*, 429, 671-675.

- WAGENKNECHT T. & RADERMACHER M. (1997) Ryanodine receptors: structure and macromolecular interactions. *Curr Opin Struct Biol*, 7, 258-265.
- WANG Y., SHYY J. Y. & CHIEN S. (2008) Fluorescence proteins, live-cell imaging, and mechanobiology: seeing is believing. *Annu Rev Biomed Eng*, 10, 1-38.
- WEISS R. G., O'CONNELL K. M., FLUCHER B. E., ALLEN P. D., GRABNER M. & DIRKSEN R. T. (2004) Functional analysis of the R1086H malignant hyperthermia mutation in the DHPR reveals an unexpected influence of the III-IV loop on skeletal muscle EC coupling. *Am J Physiol Cell Physiol*, 287, C1094-C1102.
- WILKENS C. M., GRABNER M. & BEAM K. G. (2001a) Potentiation of the cardiac L-type Ca(2+) channel (alpha(1C)) by dihydropyridine agonist and strong depolarization occur via distinct mechanisms. *J Gen Physiol*, 118, 495-508.
- WILKENS C. M., KASIELKE N., FLUCHER B. E., BEAM K. G. & GRABNER M. (2001b) Excitation-contraction coupling is unaffected by drastic alteration of the sequence surrounding residues L720-L764 of the alpha 1S II-III loop. *Proc Natl Acad Sci U S A*, 98, 5892-5897.
- WOLF M., EBERHART A., GLOSSMANN H., STRIESSNIG J. & GRIGORIEFF N. (2003) Visualization of the domain structure of an L-type Ca²⁺ channel using electron cryo-microscopy. *J Mol Biol*, 332, 171-182.
- YANG T., SUHAIL Y., DALTON S., KERNAN T. & COLECRAFT H. M. (2007) Genetically encoded molecules for inducibly inactivating CaV channels. *Nat Chem Biol*, 3, 795-804.
- ZHANG J., LIU Z., MASUMIYA H., WANG R., JIANG D., LI F., WAGENKNECHT T. & CHEN S. R. (2003) Three-dimensional localization of divergent region 3 of the ryanodine receptor to the clamp-shaped structures adjacent to the FKBP binding sites. *J Biol Chem*, 278, 14211-14218.

6. Abbreviations

I	first (of the four repeated) transmembrane domain of α_{1S}
II	second (of the four repeated) transmembrane domain of α_{1S}
III	third (of the four repeated) transmembrane domain of α_{1S}
IV	fourth (of the four repeated) transmembrane domain of α_{1S}
2D	two-dimensional
3D	three-dimensional
α_{1C}	alpha 1 subunit of the cardiac L-type calcium channel
α_{1S}	alpha 1 subunit of the skeletal L-type calcium channel
β_{1A}	beta 1A subunit of the skeletal L-type calcium channel
γ	gamma subunit of the skeletal L-type calcium channel
$\alpha_{2\delta}$	alpha 2 delta subunit of the skeletal L-type calcium channel
μl	microliter
μg	microgram
μM	micromol
μm	micrometer
∞	infinite

A

\AA	angstrom
AID	alpha interaction domain

B

BA	band pass
Ba^{2+}	barium
BaCl_2	barium chloride
bp	basepairs
BSA	bovine serum albumin

C

$^{\circ}\text{C}$	Celsius (degree temperature)
C	carboxyl terminus
Ca^{2+}	calcium
CaCl_2	calcium chloride
CaM	Ca^{2+} -calmodulin
Ca_v	voltage-dependent L type calcium channel
cDNA	complementary deoxyribonucleic acid
CFP	cyan fluorescent protein
CIP	calf intestinal alkaline phosphatase
cm	centimeter
CMF	calcium-magnesium-free
CO_2	carbon dioxide

CRU	calcium release unit
cryo	cryogenic
Cs ₂ EGTA	carbon disulfide ethylene glycol tetraacetic acid
CsAsp	Cesium aspartate
CsOH	Cesium hydroxide
CyPet	cyan fluorescent protein for energy transfer

D

Da	Dalton
dd H ₂ O	double-distilled water
DHP	dihydropyridine
DHPR	dihydropyridine rezeptor
DM	dichroic mirror
DMEM	Dulbecco's modified eagle medium
DNA	desoxyribonucleic acid
dNTP	deoxyribonucleoside triphosphate
dys	dyspedic

E

<i>E.coli</i>	<i>Escherichia coli</i>
EC	excitation-contraction
ECACC	European Collection of Cell Cultures
ECFP	enhanced cyan fluorescent protein
ECL	entactin-collagen IV-laminin
EDTA	ethylene diamine triacetic acid
e.g.	exempli gratia (for example)
EGFP	enhanced green fluorescent protein
EM	electron microscopy
Eq	equation
et al.	et alii (and others)
EYFP	enhanced yellow fluorescent protein

F

FBS	fetal bovine serum
FP	fluorescent protein(s)
FRET	fluorescence resonance energy transfer
fw	forward

G

<i>g</i>	gravitational force
----------	---------------------

H

h	hour(s)
HEK	human embryonic kidney
HF	high fidelity
HS	horse serum

I

I	intensity
i.e.	id est (that is)

J

JP	junctional protein
----	--------------------

K

KCl	potassium chloride
kDa	kilodalton

L

l	liter
LB	Luria Bertani
LUT	look up table

M

M	molar
MCS	multiple cloning site
MDa	megadalton
mdg	muscular dysgenesis
Mg ²⁺	magnesium
MgCl ₂	magnesium chloride
MgSO ₄	magnesium sulphate
MH	malignant hyperthermia
min	minute(s)
ml	milliliter
mm	millimeter
mM	millimolar
MΩ	megaohm
ms	milliseconds
mV	millivolt

N

N	Adenine or Cytosine or Guanine or Thymine
N	amino terminus
n	nucleus
NA	numerical aperture
Na ⁺	sodium
NaCl	sodium chloride
NaOH	sodium hydroxide
NEB	New England Biolabs
ng	nanogram
nm	nanometer

O

OD ₆₀₀	Optical Density at 600 nanometer
-------------------	----------------------------------

P

pA	picoampere
PCR	Polymerase chain reaction
Pen/Strep	benzylpenicillin procaine / dihydrostreptomycine
pF	picofarat
<i>Pfu</i>	<i>Pyrococcus furiosus</i>
pH	negative logarithm of H ₃ O ⁺ ion concentration (mol/l)
PH	pinhole
PMT	photomultiplier tube
pos.	position

Q

QC	quikchange
----	------------

R

R	Adenine or Guanine
rev	reverse
RNase	ribonuclease
ROI	region of interest
rpm	rounds per minute
RyR1	type 1 ryanodine receptor (isoform of skeletal muscle)
RyR2	type 2 ryanodine receptor (isoform of myocardium)
RyR3	type 3 ryanodine receptor

S

S.D.	standard deviation
sec	seconds
sm	silent mutation
SR	sarcoplasmic reticulum

T

<i>Taq</i>	<i>Thermus aquaticus</i>
TEACl	tetraethylammonium chloride
TEAOH	tetraethylammonium hydroxide
TFB	transformation buffer
tt	transverse tubules

U

UV	ultraviolet
----	-------------

V

V	Volt
VGCC	voltage-gated Ca ²⁺ channel
v/v	volume/volume

W

W Adenine or Thymine
wt wildtype
w/v weight/volume

X

XPet CyPet or YPet

Y

YFP yellow fluorescent protein
YPet yellow fluorescent protein for energy transfer

7. List of figures and tables

	Page
Figure 1.1. The skeletal muscle fibre.....	2
Figure 1.2. Topography of voltage-gated Ca ²⁺ Channels (VGCCs).....	3
Figure 1.3. Location of Calcium release units in skeletal muscle.	8
Figure 1.4. Ordered arrangement of DHPR and RyR1 in junctions of skeletal muscle.....	9
Figure 1.5. Schematic representation of the DHPR α_{1S} subunit with ascribed (patho-) physiological roles listed for every cytoplasmic domain, after Bannister (2007), modified.	13
Figure 1.6. 3D structure of DHPR obtained by cryo-EM and single particle reconstruction (Serysheva <i>et al.</i> 2004).....	16
Figure 1.7. Model of DHPR by Wolf <i>et al.</i> (2003), modified.	17
Figure 1.8. 3D reconstruction of the DHPR structure and of the α_1 - β complex of Murata <i>et al.</i> (2009), modified.	17
Figure 1.9. Excitation and emission spectra of the FRET pair CyPet and YPet.	20
Figure 2.1. O'GeneRulerTM 1 kb DNA Ladder, <i>ready to use</i> (Fermentas).	30
Figure 2.2. Schematic illustration of the CyPet- and YPet-tagged α_{1S} FRET constructs.....	36
Figure 2.3. pECFP-C1 & pECFP-N1.	37
Figure 2.4. Different α_{1S} C-terminus variants.	38
Figure 2.5. Introducing YPet or CyPet into the α_{1S} I-II loop (A), II-III loop (B) and III-IV loop (C).....	41
Figure 2.6. Location of the introduction sites for YPet and CyPet within cytoplasmic α_{1S} domains.....	42
Figure 2.7. Schemes of doubly tagged α_{1S} tandem constructs serving as 'no-FRET' controls.	43
Figure 2.8. Spectra of CyPet/YPet excitation and emission.....	51
Figure 2.9. Optical path diagram.	52
Figure 2.10. FRET between CyPet and YPet.	53
Figure 2.11. Background correction and ROI definition.....	55
Figure 2.12. Detection of cellular autofluorescence.....	57
Figure 2.13. Defining a binary mask to measure FRET efficiencies exclusively within fluorescent foci.....	58
Figure 2.14. Intensity profile & raw data.	59
Figure 2.15. Generation of I_{FRET}	59

Figure 3.1.	Location of DHPRs in junctions of myotubes.	62
Figure 3.2.	Targeting of single tagged α_{1S}	64
Figure 3.3.	Targeting deficiency of α_{1S} with YPet inserted upstream the AID in dyspedic myotubes.	65
Figure 3.4.	Proteolytic cleavage of $\alpha_{1S}(1666)$ -XPet in dyspedic myotubes.	67
Figure 3.5.	Prevention of proteolytic cleavage of the fluorophore C-terminally attached at α_{1S} position 1636.	68
Figure 3.6.	Comparison of the FRET ratio of ‘no-FRET’ control constructs with the FRET ratios between CyPet and YPet after attachment to different cytoplasmic domains within one α_{1S} subunit expressed in the same myotube type.	74
Figure 3.7.	Comparison of I_{FRET} ratios between CyPet and YPet after attachment to the cytoplasmic α_{1S} domains expressed under varying conditions.	76
Figure 4.1.	Model of the DHPR-RyR complex by Wolf <i>et al.</i> (2003), modified.	79
Figure 4.2.	Schematic model of the relative orientations of cytoplasmic α_{1S} domains and of their possible rearrangement in the presence of RyR1 (α_{1S} is shown in oblique view from the cytoplasmic site).	80
Figure 4.3.	Model of the involvement of α_{1S} II-III loop subregions in interactions with junctional partners - most likely the RyR1 - in the process of EC coupling, after Bannister & Beam (2010), modified.	85
Figure 4.4.	Model of the potential transition cytoplasmic α_{1S} domains experience in the presence of RyR1. View from the cytoplasmic side.	87
Table 1.1.	Subunit composition and function of voltage-gated Ca^{2+} channel (VGCC) sub-types (Catterall 2000).	5
Table 1.2	FRET pair properties.	19
Table 2.1.	Restriction endonucleases (RE) used in this work.	25
Table 2.2.	Primer-oligonucleotides used in this work.	26
Table 3.1.	Schematic illustration of single tagged α_{1S} constructs including their targeting and electrophysiological properties.	63
Table 3.2.	Schematic display of all CyPet- AND YPet-tagged α_{1S} constructs used for FRET analysis in this study including their targeting and electrophysiological properties.	70
Table 3.3.	Schematic display of all CyPet- AND YPet-tagged α_{1S} constructs used for FRET analysis in this study including the I_{FRET} ratios and RyR1 induced changes of the FRET partners attached to different cytoplasmic sites of the DHPR α_{1S}	73

8. Acknowledgements

Though only my name appears on the cover of this dissertation, a great many people have contributed to its production. I owe my gratitude to all those people who have made this dissertation possible and because of whom my graduate experience has been one that I will cherish forever. In fact, because of the dissertation submission process, I now feel much more prepared to face many of the events that lie in my academic future.

My deepest gratitude is to my advisor, Prof. Dr. Symeon Papadopoulos. I have been amazingly fortunate to have an advisor who gave me the freedom to explore on my own and at the same time the guidance to recover when my steps faltered. Simon taught me how to question thoughts and express ideas. He provided me with a tremendous graduate education and I hope that one day I would become as good an advisor to my students as Simon has been to me.

I am very grateful to Prof. Dr. Gerolf Gros for his professional knowledge, his invaluable support and many helpful discussions.

I would like to acknowledge Prof. Dr. Kurt G. Beam, Drs. Roger A. Bannister and Joshua D. Ohrtman for numerous helpful discussions on related topics that helped me improve my EC coupling knowledge throughout my research.

I am also very thankful to Dr. Alfred T. Welzel for encouraging the use of correct grammar and consistent notation in my writings and for carefully reading and commenting of this dissertation.

I am grateful to the following former or current staff in the Department of Vegetative Physiology at Medical School Hannover for their various forms of support and great cooperation during my graduate study - Steffi Reuß, Dr. Nina Hanke, Dr. Volker Endeward, Samer Al-Samir, Sahar Pourebrahim, Ulrike Fuhrmann, Dr. Barbara Ritter and Fabi anTenne - my thanks for making my stay a pleasant one.

Many friends have helped me stay sane through these difficult years. Their support and care helped me overcome setbacks and stay focused on my graduate study. I greatly value their friendship and I deeply appreciate their belief in me. Special thanks go to Steffi, Heiko, Merle and Hans-Martin to share my free time and to crack a beer at just the right time have been greatly appreciated.

Thanks Pia, your support during the last months has been an invaluable asset - priceless.

9. Erklärung zur Dissertation:

Hiermit versichere ich, dass ich meine Dissertation mit dem Titel „FRET Reveals Substantial Reorientation of the Cytoplasmic Interface of the Skeletal Muscle DHPR in the Presence of RyR1“ selbstständig verfasst habe und dass ich sie nicht schon als Diplom- oder ähnliche Prüfungsarbeit verwendet habe. Es wurden keine anderen als die angegebenen Quellen und Hilfsmittel verwendet.

Hannover, 2011

Alexander Polster

10. Curriculum vitae

Name: Alexander Polster
 Adresse: Höninger Weg 196

50969 Köln
 Geburtsdatum: 20.12.1978
 Geburtsort: Georgsmarienhütte
 Familienstand: ledig
 Staatsangehörigkeit: deutsch

Schulbildung:

1985 – 1989 Grundschule Bad Essen / Lintorf
 1989 – 1991 Orientierungsstufe Bad Essen
 1991 – 1999 Gymnasium Bad Essen
 Abschluss mit Abitur / Allg. Hochschulreife

07/1999 – 07/2000 Zivildienst (Paracelsus Berghofklinik Bad Essen)

Studium:

WS 2000 - SS2003 Studium der Biologie „Bachelor of Science“ & „Diplom-Biologie“ an der Universität Osnabrück

SS 2003 Bachelorarbeit im Institut für Spezielle Botanik an der Universität Osnabrück

WS 2003 - SS2005 Studium der Biologie „Master of Science“ & „Diplom-Biologie“ an der Universität Osnabrück

SS 2005 Masterarbeit im Institut für Spezielle Botanik, Universität Osnabrück

WS2005/SS2006 Studium der Biologie „Diplom-Biologie“, Universität Osnabrück

07/2006 -01/2010 Wissenschaftlicher Mitarbeiter im Institut für Vegetative Physiologie der Medizinischen Hochschule Hannover

seit 02/2010 Wissenschaftlicher Mitarbeiter im Institut für Vegetative Physiologie des Uniklinikums der Universität zu Köln

11. List of scientific publications

Abstracts / Poster

- 2010 **A. Polster**, S. Papadopoulos
 “Association of the α_{1S} I/II loop peptide with β_{1A} results in translocation of the complex to the cell surface and in clustering”, Biophysical Society Meeting. Biophysical Journal
- 2009 J. D. Ohrtman, S. Papadopoulos, **A. Polster**, and K.G. Beam
 “Voltage- and calcium-dependent inactivation of $\alpha 1C$ is suppressed in muscle cells and this suppression does not appear to be a consequence of insertion into triad junctions“, Gordon Research Conference
- 2008 **A. Polster**, S. Papadopoulos
 “Evidence for a close spatial arrangement of intracellular domains of the skeletal muscle DHPR using measurements of fluorescence resonance energy transfer (FRET) between CyPet and YPet in a non-destructive measuring variant”, Biophysical Society Meeting. Biophysical Journal
- 2007 K. Mummenhoff, A. Mühlhausen, **A. Polster**, D. Lobbes, and G. Theißen
 “Comparative analysis of fruit dehiscence / indehiscence in Brassicaceae”, Plant Biology
- 2005 **A. Polster**, K. Mummenhoff
 “The role of lignification patterns in dehiscent and indehiscent fruits in Brassicaceae: A comparative anatomical approach“, XVII International Botanical Congress

Journal articles

- 2010 A. Mühlhausen, **A. Polster**, G. Theissen, and K. Mummenhoff
 “Evolution of Fruit Dehiscence in Brassicaceae – Examples from *Aethionema* and *Lepidium*“ Hansen M (ed.). Proceedings of the Vth. International Symposium on Brassicas & XVIth. Crucifer Genetics Workshop, Lillehammer. Acta Horticulturae Vol 867, International Society for Horticultural Science, Leuven, pp. 207-219.
- 2009 K. Mummenhoff, **A. Polster**, A. Mühlhausen, and G. Theissen
 “*Lepidium* as a model system for studying the evolution of fruit development in Brassicaceae” Journal of Experimental Botany 60(5):1503-1513
- 2008 J. D. Ohrtman, B. Ritter, **A. Polster**, K. G. Beam, and S. Papadopoulos
 “Sequence differences in the IQ motifs of CaV1.1 and CaV1.2 strongly impact calmodulin binding and calcium-dependent inactivation” The Journal of Biological Chemistry, 283, 29301-29311.